THESIS SUBMITTED FOR Ph.D.

Three level spectroscopic technique applied to collision rate and line shape determinations in a plasma.

GEOFFREY KOLBE

IMPERIAL COLLEGE OF SCIENCE AND TECHNOLOGY

兵法一曰度二曰量
三曰數四曰称五曰胜

ACKNOWLEDGEMENTS

I would like to express my gratitude and deep appreciation to David Burgess, Professor of Spectroscopy at Imperial College, without whose patience, forsight and perseverence, this thesis might have been written, but not by me.

I would also like to thank the other members of the Spectroscopy Group for their help down the years, particularly Dick Learner and Ann Thorne for their interest and intellectual sustenance and Pete Ruthven who was ever ready to take my thoughts and scribblings and with his skills turn dumb metal into reality.

Others who must be mentioned are Nick Jackson, who, with his camera, is surely the best to be found to breathe life into the instruments with which we work. Dave Yarwood is, alas, now dead. But while he was alive he was the man who ground, cut, polished and cleaned the quartz tubes within my lasers.

Also, thanks to my friend Ding, (who inscribed the chinese text from 'the Art of War' by Sun Tzu, circa 500BC, for me). My memory of Ding will always be a warm and smiling one.

Last but by no means least, my dear mother, who has been a constant source of encouragement and who typed this thesis for me.

ABSTRACT

The normal techniques of absorption and emission spectroscopy used in the determination of lineshapes and collision rates in a plasma, have inherent limitations, in that only two levels of the test atom are involved. This thesis examines the way in which laser based three level techniques can be used to overcome some of these limitations.

A three level lineshape technique which could discriminate against impurity contributions, was used to measure the Balmer Beta lineshape of Hydrogen whose central 'dip' has been a subject of controversy for many years - being experimentally less than predicted by theory for an electron density $10^{15} cm^{-3}$.

Using a three level laser based technique, an experiment was performed to determine if a molecular impurity transition was filling in the central dip. No evidence of any impurity was found. However, a feature was found on the red wing of the H-Beta profile for an electron density of $5 \times 10^{14} cm^{-3}$. This was found to be an impurity but the species could not be identified.

The determination of collision rates out of atomic excited states in a plasma, by laser fluorescence,

methods, is a well known technique. However, such techniques are limited to collision rate coefficients less than about $10^{9}sec^{-1}$, due to the inability of currently available detectors and data recorders, to respond to transients faster than $10^{-9}sec$.

This limitation can be overcome by the use of laser based three level technique. This technique is demonstrated by measuring the rate out of the n=4 level of the He II ion in a plasma.

LIST of CONTENTS

CHAPTER 3.

APPARATUS and EXPERIMENTAL METHOD

Section 1 : Apparatus

Section 2

Section 3 : Three Level Lineshape of H-Beta

LIST of FIGURES

CHAPTER 1.

CHAPTER 2.

CHAPTER 5.

APPENDIX I

LIST of TABLES

CHAPTER 1.

INTRODUCTION

This thesis describes two experiments. One to measure the collision rate coefficient out of the n=4 level of the He II ion in a Helium plasma. The other was to measure the lineshape of Balmer Beta in a Hydrogen plasma.

The technique used to measure the lineshape of H-Beta, discriminated against any possible impurity contribution, by using three levels of the Hydrogen atom instead of two, as with the usual techniques of emission or absorption spectroscopy. The measurement of the collision rate co - efficient from n=4 in He II also involved the use of a three level technique.

In Chapter 2, a critical analysis of the three level techniques used for the two experiments, will be presented. Also, there will be a comparison between these techniques and other possible methods.

Chapter 3 will describe the experimental layout for the two experiments.

Chapters 4 and 5 will present the analysis of the experimental results.

The remainder of this chapter will give the scientific background to the experiments performed and place them in context with other work in the same field.

1.1 PLASMA SPECTROSCOPY

The observed shapes and strengths of atomic transitions have long been used to gain information regarding the temperature and densities of the electrons, atoms and ions in a plasma. A considerable body of literature exists which attempts to link the basic plasma parameters of particle density and temperature to the observed spectral information. The literature falls broadly into two categories - Lineshapes and Collision Rates (cross sections).

Both categories attempt to deal with the way in which the free space eigen functions of the emitter are perturbed by the plasma environment.

In the case of lineshapes, the perturbation is due, predominantly, to the adiabatic collisions between the emitter, electrons and ions, whereas studies of collision rates or cross sections, deal with the excitation or de-excitation of the emitter, due to an inelastic or super-elastic collision between the emitter, electrons and ions.

1.2 LINE BROADENING. (LOW DENSITY PLASMAS)

The background to some of today's topical problems for the low density 'ideal' plasmas, (i.e. those with many particles per Debye sphere), will be briefly discussed, particularly where pertinent to the work in this thesis.

The number of charged particles per Debye sphere is given by N_D where

$$N_D = \frac{4\pi}{3}\left(\frac{\epsilon_0 KT}{e^2}\right)^{3/2} \frac{\left(N_e + \sum_i N_i\right)}{\left(N_e + \sum_i z^2 N_i\right)^{3/2}} \qquad 1.1$$

and where

Ne is the electron density.

Ni is the ion density of the i'th ion stage.

Z is the charge on the i'th ion stage.

See Mihalas (1978)

For Hydrogen this reduces to

$$N_D = \left(\frac{T^3}{Ne}\right)^{1/2} \times 10^6 \quad m^{-3} \qquad 1.2$$

For example in a Hydrogen plasma, having T=1eV and Ne=$10^{15}cm^{-3}$, there will be about 30 charged particles within a radius of, and so interacting with, a radiating atom. Outside this Debye radius, the atom is screened from the effects of any individual electron or ion.

Much work has also been done recently on dense, non ideal, (less than one particle per Debye sphere) plasmas, particularly laser produced plasmas. See, for example, Lee (1981) However, there will be no further discussion on this topic, here.

The theory of line broadening has been developing throughout this century, since the classical impact 'interruption' theory of Lorentz (1906). However, modern line broadening calculation techniques, may be said to have their roots in papers by Baranger (1958) and Kolb and Griem (1958) - when the problem was treated quantum mechanically and non-adiabatic (inelastic) collisions were included for the first time.

By 1969, the theory of the broadening of Hydrogen lines was thought to be largely completed. Stark broadening, due to ions, was described by the 'static' approximation, first proposed by Holtzmark (1919) and the electron broadening

was described by elaborate 'unified' theories due to Voslamber (1969) and Vidal, Cooper and Smith (1969) or the modified impact theory of Kepple and Griem (1968)

1.2a ION DYNAMICS

Similar techniques were used to describe the astrophysically important He I transition $2^3P - 4^3D$ ($\lambda = 4471$ Å) and its optically forbidden companion $2^3P - 4^3F$ ($\lambda = 4470$ Å) see Barnard, Cooper and shamey (1969) and Griem (1968) However Burgess and Cairns (1970 and 1971) determined the lineshape of the 4471Å pair experimentally and showed that there was substantial disagreement in the peak intensity of both the allowed and forbidden components. Burgess (1970) laid the blame for the disagreement on the treatment of the ions as being static and proposed that 'ion dynamics' should be accounted for. Lee (1972) showed that the inclusion of ion dynamics would indeed account for the experimental discrepancy.

Meanwhile, in 1971, Hill et al, showed experimentally, that the central dip of Balmer Beta in neutral Hydrogen was much less pronounced than theory predicted; the failure of the static ion approximation being one of the two possible explanations put forward. This was reinforced by an experiment by Burgess and Mahon (1972), which showed that for $Ne=10^{15} cm^{-3}$ and Te=1eV the dip was less than 5% (of the peak height), whereas theory (Vidal, Cooper and Smith 1970), predicted a dip at the line core of about 30%. Burgess and Mahon also concluded that the most reasonable explanation for the lack of agreement was use of the static ion approx-

imation.

Using a formalism due to Dufty (1970), Lee (1973) showed that ion motion effects may be important for the Hydrogen line cores. Also, a series of experiments by, for example, Kelleher and Wiese (1973), Wiese et al (1975) and more recently, Ehrich and Kelleher (1980) and Fleurier et al (1980), showed the dependence of the H-Beta dip on the emitter-perturber ion reduced mass. This appeared to be good evidence that ion dynamics were indeed important.

Agreement on this point has been by no means universal however. Experimentally, Ramette and Drawin (1976) showed evidence that the dip in their H-Beta profiles was being filled in by what they interpreted as ion satellites. They also observed satellites on both wings of the line-shape corresponding to the electron plasma wavelength away from line centre. But Drawin (1981) showed that many observed 'plasma satellites' were in fact more likely due to strong molecular transitions, Piel (1981) also showed how strong molecular transitions can fill in the central dip of H-Beta. Thus, at the date of the present experimental work, an element of uncertainty remained in the comparison of theory with experiment.

Theoretically, Peach (1981) argued that the problem was not due to the static ion approximation at all, but due to approximations, generally made, which under estimate the effects of electron broadening at the line core. Also, the most popular method used today to overcome the problems of including ion dynamics, is the 'Model Microfield Method', (see for example, Dufty (1981)), in which ion

dynamics is included naturally in the formalism.

Despite its success in accounting for most of the inconsistency between experiment and theory, however, the Model Microfield Method is treated with some circumspection by many lineshape theorists, in that it is hard to get estimates of validity criteria for the M.M.M. or to connect it to the standard collisional lineshape theories. See, for example, Dufty (1981).

However, even attempts to include ion dynamics in lineshape calculations using the M.M.M. (Brissaud and Mazure, 1976, Siedel 1977, Mazure, Goldback and Nollez 1981) have not been entirely successful. For example, for $Ne=10^{15} cm^{-3}$ and $Te=Ti=10^{4}$ K, the theories cited above predict dips of between 3% and 7%, whereas both Burgess and Mahon and Fleurier et al, show experimental profiles for these conditions which have no observable dip.

Given a lack of complete confidence in the results produced, using the M.M.M. technique to include ion dynamics into lineshape calculations and also the indications that experiments on measuring the H-Beta dip may have been influenced by the unsuspected presence of H_2 contributions to the lineshape; it would appear apposite to determine if indeed, under the experimental conditions of Burgess and Mahon (1973), there was any impurity contribution to the H-Beta. The classic methods of absorption and emission spectroscopy do not differentiate between the lineshape contributions from the test atom and that due to any impurity that may be present, as only two levels of the test atom are used in the observation -which do not define the atom uniquely.

1.2b LINESHAPES OBSERVED via THREE LEVEL SPECTROSCOPY

The relationship between three levels of a test atom will almost certainly be unique to that atom and not be shared by any impurity. Thus an impurity-free lineshape may be obtained by methods which make use of the relative separation of three levels of the atom instead of two, as for instance, in standard emission or absorption spectroscopy. In general, these three level techniques use a laser which pumps a transition in the test atom and then another transition, usually having a level common with the pumped transition, is observed in absorption (with a probe laser) or in emission.

Since it is the amount by which the levels of the observed transition are perturbed which is measured. Impurities can have no effect on the result in lineshape. These techniques are discussed in detail in Chapter 2.

This general technique, that is irradiating one transition of a test atom and observing the consequences on another transition having the same lower (or upper) state, is generally refered to as Double Resonance Spectroscopy. This however is a loose assignation which is more properly confined to that class of experiment originated by Brossel and Bitter (1952). They revealed the hyper-fine structure of an excited state in Mercury, by the use of a polarised light source and a tunable microwave source to selectively excite the hyper-fine levels of interest. See fig. 1.1. In this thesis then, the general technique as outlined above will be refered to as Three Level Spectroscopy.

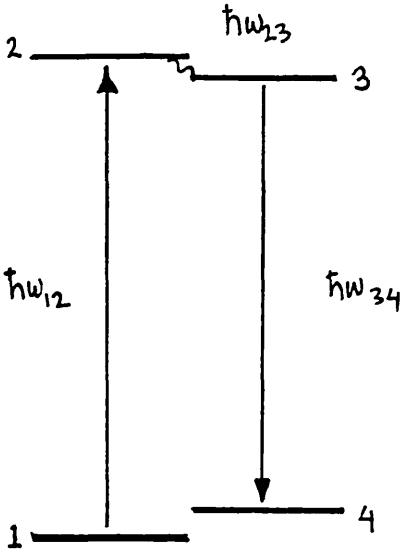

Fig. 1.1

LEVEL DIAGRAM of DOUBLE RESONANCE TECHNIQUE
used by BROSSEL and BITTER

Visible photons having energy $\hbar\omega_{12}$ excite the atom (or molecule) from level 1 to level 2. Microwave radiation puts the atom into level 3 where it decays by spontaneous emission to level 4

In such experiments, level 3 is usually a member of the sublevel set of level 2. Using this technique, the sub-level set can be investigated without the problems of Doppler broadening that would make direct visible observations impossible.

Although double resonance spectroscopy and other three level spectroscopy is a common technique when working with neutral vapours, the problems of working with plasmas are such that examples of laser spectroscopy, (let alone three level spectroscopy), are rare.

Due to the broadening of the transition lines by ion stark broadening and electron pressure broadening and due to the high electron collision rates, much higher laser powers (typically, megawatts per cm^2 for plasmas, as opposed to a few watts per cm^2 for neutral vapours) are required to perturb level populations significantly. See Burgess (1979) for a detailed discussion of this problem. In fact there is only one example, prior to the present work, in which a three level technique was used to determine a lineshape in a plasma, that of Kunze (1981) in which the plasma satellites to the forbidden 2^3P-4^3F ($\lambda = 4470$ Å) transition in He I were revealed by induced laser fluorescence on the 4^3D-2^3P ($\lambda = 4471$ Å) transition. The 4^3F population was enhanced by laser photon plus plasmon excitation. The 4^3D population was then enhanced by virtue of the strong mixing between the 4^3D and 4^3F levels. See Fig.1.2 and 1.3.

THREE LEVEL LINESHAPE OF H-BETA

This thesis will then, in part, discuss in detail an experiment in which the core of the H-Beta transition was examined using a three level technique to assertain, whether or not, there was an impurity contribution which is filling in the 'dip' at line centre.

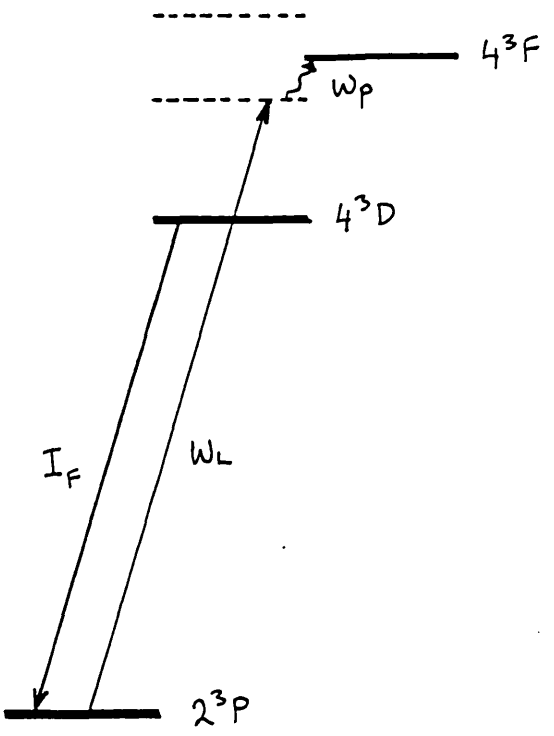

Fig. 1.2

TERM SCHEME of KUNZE'S EXPERIMENT on 4471Å

A tunable laser, frequency W_L, pumped atoms out of 2^3P. The laser could pump the 4^3D transition direct; also 4^3F is weakly coupled to 4^3D due to the plasma field so the laser will pump 4^3D if tuned to the 2^3P-4^3F transition. The laser can also pump 4^3F directly by a two photon transition using a plasmon, W_p, as the other photon.

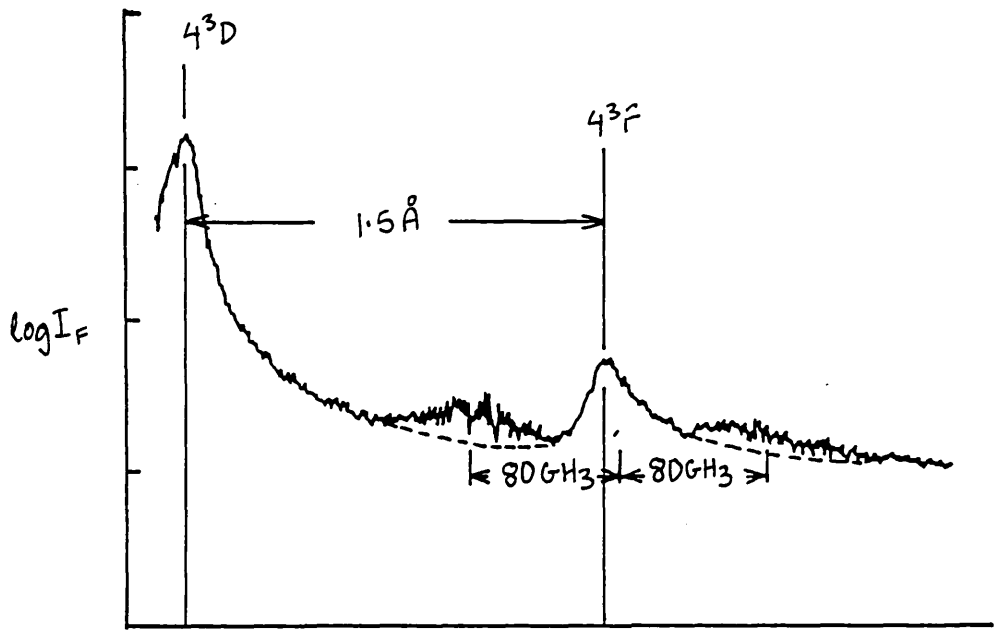

Fig. 1.3

SPECTRUM from KUNZE'S EXPERIMENT on 4471Å

Spectrum from Kunze's experiment showing the plasma satellites either side of the forbidden component of the Helium 4471Å transition. The laser was tuned through the frequency band shown and enhanced fluorescence, I_F, on 4^3D-2^3P was observed.

1.3 ELECTRON COLLISION CROSS SECTIONS

The observed relative intensities of emission lines are a function of the population densities of the upper state of the observed transition, and the A value of that transition.

The population density for any state in the plasma will be a function of collisional and radiative rates into and out of that state; i.e.

$$Na = \frac{Ca}{Da} \qquad 1.1$$

Where Na is the population density of level a, Ca are the sum total of rates into levela and Da is the total rate coefficiént out of level a.

The population densities of the various states in a system may generally be described by a Collisional Radiative Model (C.R.M.), in which the rate coefficients between the n levels of the system, are used to create a set of n simultaneous linear equations which are solved to find the population densities of the discrete states. This form of model is generally attributed to Bates Kingston and McWhirter (1962) but for a clear, detailed exposition of C.R.M.s , see Hess and Burrell (1979).

In the limit, where the electron density is high, such that the excitation and de-excitation rates are dominated by collisional, rather than radiative rates, the population densities will be in equilibrium with the free electron density (Local Thermodynamic Equilibrium, L.T.E.) and can be described by the Saha-Boltzmann equation. See, for example, Mihalas (1978) for a discussion of L.T.E.

All that is required to deduce the population densities of the excited states of an atom or ion, when conditions of L.T.E. are valid, is a knowledge of the electron temperature, Te, and electron density Ne.

In seeking to use the absolute or relative intensities of spectral lines as a diagnostic of the electron density and temperature in a plasma, particularly in an astrophysical context, it is usually necessary to use a C.R.M. where the density and / or temperature are it erated until a fit to the spectral data is found. (Since L.T.E. is not usually valid). This requires a detailed knowledge of the rate coefficients between individual levels and much effort has been spent in trying to measure or compute the collision rates for elements of astrophysical interest, e.g. H, He, Fe. When not measured directly, collision rate coefficients are normally obtained from cross sections.

For a transition between levels a and b the collision rate coefficient Rab is related to cross section $\sigma_{ab}(v)$ by

$$R_{ab} = \int_0^\infty \sigma_{ab}(v)\, v\, f(v)\, dv \qquad 1.2$$

Where v is the electron velocity and f(v) is the normalised electron velocity destribution; usually assumed to be Maxwell Boltzmann. for plasmas greater than 1% ionized. (See Shoub, 1977).

To date, direct measurement of electron collision cross sections, using colliding atomic and electron beams, are confined to excitations from the ground state, or metastable states. See for example, Fite and Brackman (1958)

for 1s - 2s and 1s - 2p in Hydrogen. Van Raan et al (1971) for transitions from the ground state of He. Dolder and Peart (1973) for 1s - 2s in He^+.

In very low density, high temperature plasmas, direct excitation from the ground state is often the dominant mechanism controlling level populations.

In consequence, much theoretical effort has been spent in computing these experimentally tractable ground state cross sections. See, for example, a review by Bely and Van Regemorter (1970).

By comparison the experimental data for transitions between excited states is much scarcer and less reliable and relatively little theoretical work has been done on such transitions.

Experimentally, indirect means have been used for determining cross sections between excited states. For example an experiment by Johnson and Hinnov (1969) used variable-parameter empirical cross sections in a C.R.M. for Helium and it eratively varied the parameters so that the population densities predicted by the C.R.M. would agree with those measured in a plasma (whose Ne and Te were independently known) by calibrated emission spectroscopy.

This experiment formed the basis of a set of empirical cross section and collision rate coefficient formulae developed by Johnson (1972) for Hydrogen and which, until recently, were regarded as the best available set of data for Hydrogen.

With the development of tunable dye lasers, however, it became possible to perturb the populations of individual discrete levels in Hydrogen and so deduce, from the characteristic relaxation times of these level populations, total depopulation rates and individual transfer rates. The first applicstions of such a technique was on a Helium plasma by Burrel and Kunze (1972).

Burgess and Skinner (1974) showed that by using a laser of high enough power, a transient spike could be produced at the leading edge of the fluorescence signal, from which additional information could be obtained. See Fig. 1.4. This was followed by similar experiments on a Hydrogen plasma by Himmel and Pinnekamp (1977) and Burgess, Myerscough, Skinner and Ward (1980). Burgess, Kolbe and Ward used, what will be called a three level absorption technique to study the rates out of n=2 in Hydrogen. See Fig. 1.5.

The conclusion of these experiments, and those of Delpech et al (1977) and Devos et al (1979) on the (hydrogenic) excited states of a Helium plasma, showed Johnson's empirical cross sections to be too high near threshold. As a result, Vriens and Smeets (1980) produced a new set of empirical formulae for cross sections and collision rates between excited states of one electron atom. The rate coefficients of Vriens and Smeets appear to give good agreement with experiments for levels $n > 6$. See Himmel and Sava (1983)

However, the results of Burgess et al (1978 and 1980) are still not explained by the lower rate coefficients of Vriens and Smeets -which still seem too high for the plasma conditions used by Burgess.

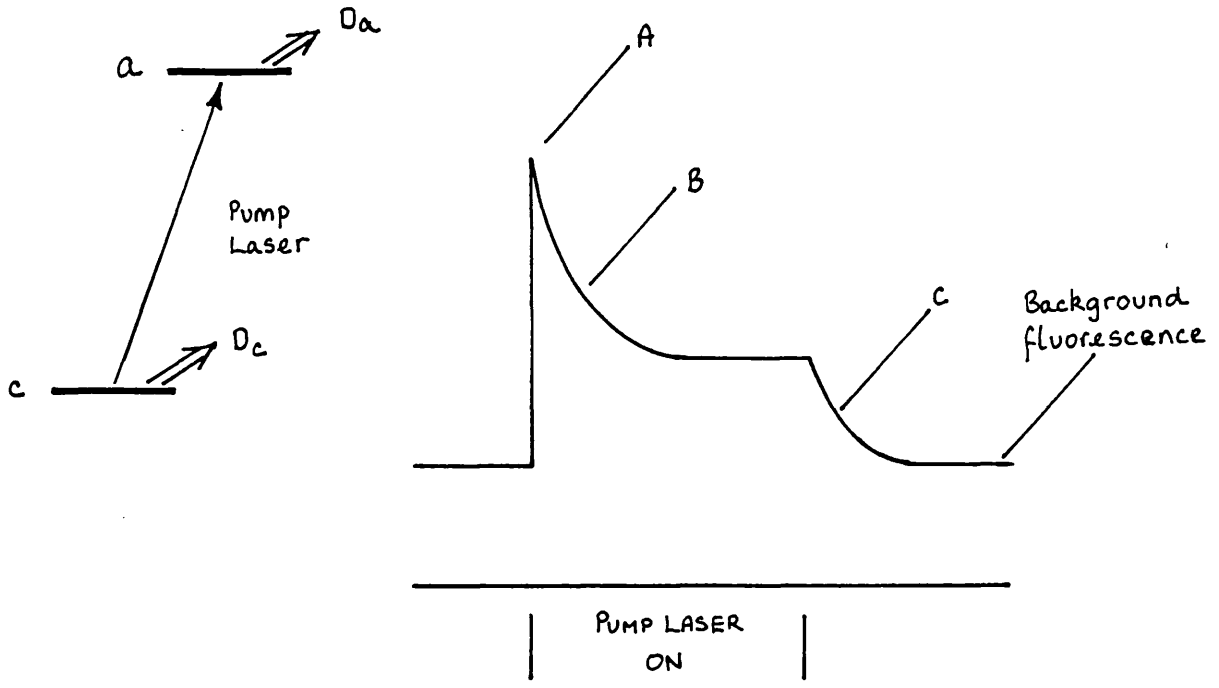

Fig. 1.4

LASER FLUORESCENCE TECHNIQUE FOR OBSERVING DE-EXCITATION RATE COEFFICIENTS

The dynamics of the level n=a are observed in fluorescence while the transition n=c to n=a is irradiated with a laser having a fast rise and fall time.

A. Initial equalization of populations of n=c and n=a.

B. Relaxation of populations of locked pumped levels to a new equilibrium on a $1/\ell$ timescale $1/(Da + Dc)$. Da and Dc are the total rate coefficients out of levels n=a and n=c, but not including Aac.

C. Laser now off. Level a now decoupled from level c. Level a relaxes back to its original population in a $1/\ell$ time of $1/Da$.

Power required to cause transient 'spike' at A, is

$$P \gtrsim \frac{g_a 8\pi h\nu^3 \Delta\nu\, Da}{g_c c^2 \quad Aac} \quad W m^{-2}$$

where $\Delta\nu$ is the equivalent width of the pumped transition, the laser rise time must be $\ll 1/(Da + Dc)$

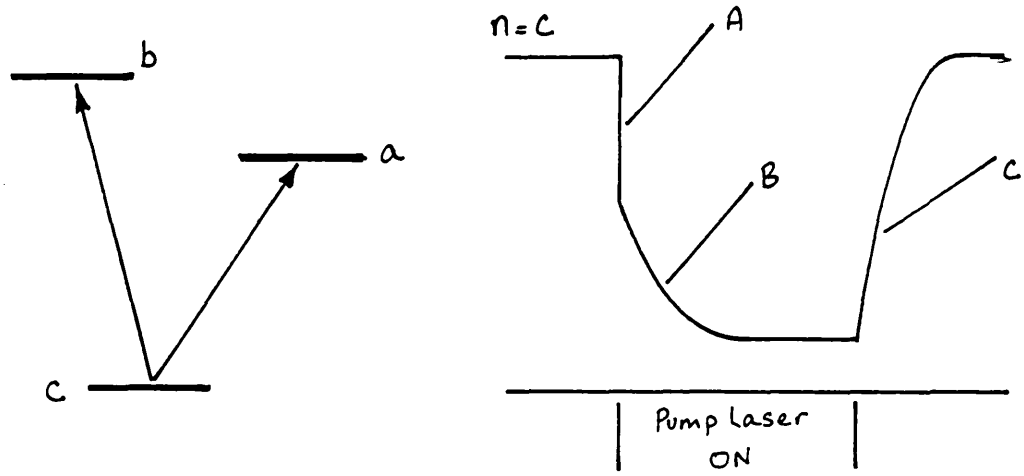

Fig. 1.5

THREE LEVEL ABSORPTION TECHNIQUE

for observing

DE-EXCITATION RATE COEFFICIENTS

The Dynamics of the level n=c are observed in absorption by a probe light source on the n=c to n=b transition.

A. As in Fig. 1.4.

B. As in Fig. 1.4.

C. Laser now off. Level c now decoupled from Level a. Level c relaxes back to its original population in a $1/e$ time of $1/Dc$.

The pump laser should have enough power to cause significant depletion in n=c.

$$P \gtrsim \frac{g_a 8\pi h\nu^3 \Delta\nu\, Dc}{g_c\, c^2 \quad A_{ac}} \qquad W\, m^{-2}$$

Given this history of disagreement between experiment and theory for neutral Hydrogen, it was thought worthwhile to investigate experimentally, the collision rate coefficient using a laser based technique for He^+. If agreement with theory could be achieved, then this would show:

a. The experimental method of using a laser based technique to measure rate coefficients was sound and the laser did not contribute an unknown rate of its own.

b. The theory for calculating collision cross sections between excited states, was basically correct (for ions at least)

CROSS SECTIONS and COLLISION RATES for IONS

Electron Collision Rates between excited states of positive ions, have been measured, almost exclusively using calibrated emission techniques, on well diagnosed, hot, laboratory (Hydrogen) plasmas, into which the element of interest is introduced as an impurity. The method is described in detail in a review article by Kunze (1972), but is basically that of Johnson and Hinnov (1969) where a C.R.M. is used with variable parameter cross section expressions as described above.

The use of lasers to observe collision rates by watching the relaxation of perturbed level population, (in the manner of Burgess et al and others) is more difficult for ions than for neutral atoms, because the collision rates for visible transitions are higher for ions than for neutrals

Take for example neutral Hydrogen and the hydrogenic ions. The Bohr radius R for the n^{th} excited state is

$$R = \frac{\hbar^2 \varepsilon_0 n^2}{\pi m z e^2} \qquad 1.3$$

The cross section σ is given by

$$\sigma \approx \pi R^2 \propto \frac{\pi n^4}{z} \qquad 1.4$$

The visible transitions in the ions, are between the n = ~~s~~p and ~~s~~q levels. For instance Balmer Alpha in neutral Hydrogen is between p = 3 and q = 2 levels where λ = 6563Å. For He II the transition n = 6 to n = 4 has λ = 6560Å. The collision cross sections for the levels associated with visible transitions, then goes as

$$\sigma_z \propto \frac{(zn)^4}{z} \qquad 1.5$$

The collision rates into and out of levels associated with visible transition in He II will thus be about on order of magnitude larger than the equivalent levels for neutral Hydrogen (for the same Te and Ne)

Burgess (1981) shows how, even for neutral Hydrogen in a plasma, laser powers of the order of 1MW and detection equipment, having temporal resolution of the order of 1 nsec. are required to monitor the dynamics of the level population under laser irradiation (i.e. n = 3,4,5,and 6)

For the Ions then, laser power of many mega watts and detectors and data recorders of subnanosecond response times would be required.

A THREE LEVEL LASER TECHNIQUE TO OBSERVE COLLISION RATES

To overcome the requirements of using lasers with subnanosecond risetimes, powers of many MW and detection equipment with subnanosecond response times, it is possible to use the laser to perturb the level population in a relatively time- stationary fashion and so deduce the depopulation rate from a knowledge of the relative population change of the observed level and the known laser rate. This technique is discussed in detail in Chapter 2, sections 2.6,and 2.7.

Figure 1.6 shows a diagram of the scheme. The population of level a is governed by the ratio of the populating rate Ca and the de-populating rate coefficient Da. By adding a new known laser rate out of level a and observing the change in population of level a, it is possible to determine Da.

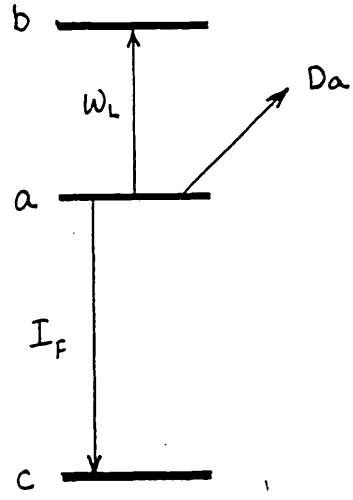

Fig. 1.6

TERM SCHEME of THREE LEVEL TECHNIQUE
to MEASURE COLLISION RATES

The laser is tuned to the a to c transition. The net laser rate out of level a, adds to the other rates out of level a, so depleting the population of level a. By knowing the laser rate and the relative depletion of level a, the magnitude of the other rates can be estimated.

REFERENCES

Baranger,M., Phys. Rev., 111, 494, (1958)

Barnard A.J., Cooper J., Shamey L.T., Astron. Astrophys., 1, 28, (1969)

Bates D.R., Kingston A.E., McWhirter R.W.P., Proc. Roy. Soc. 267, 297, (1962)

Bely O., van Regemorter H., Ann. Rev. Astr. Ap. 8, 329, (1970)

Brissaud A., Mazure A., Private Communication. (1976)

Brossel J., Bitter F., Phys. Rev. 86, 308, (1952)

Burgess D.D., J.Phys.B., 3, L70, (1970)

Burgess D.D., Cairns C.J., J.Phys.B, 4, 1364, (1971) and 3, L67, (1970)

Burgess D.D., Mahon R., J.Phys.B., 5, 1756, (1972)

Burgess D.D., Kolbe G., Ward J.M., J.Phys.B. 11, 2765, (1978)

Burgess D.D., Skinner C.H., J.Phys.B. 7, L297, (1974)

Burgess D.D., Myerscough V.P., Skinner C.H., Ward J.M., J.Phys.B. 13, 1675, (1980)

Burrell F., Kunze H.J., Phys. Rev. Lett. 28, 1, (1972)

Delpech J.F., Boulmer J., Devos F., Phys.Rev. Lett. 39, 1400, (1977)

Dolder K.T., Peart B., J.Phys.B. 6, 2415, (1973)

Drawin H.W., 'Spectral Line Shapes', p.527.
Ed., B.Wende, Pub., Walter de Gruyter. New York (1981)

Dufty J.W., Phys rev. A. 2, 534, (1970)

Dufty J.W. 'Spectral Line Shapes', p.41, Ed. B.Wende.
Pub. W.de Gruyter, New York, (1981)

Ehrich H., Kelleher D.E., 21, 319, (1980)

Fite W.L., Brackman R.T., Phys. Rev. 112, 1141, (1958)

Fleurier C., Couland G., Ranson., Phys Rev.A. 21
861, (1980)

Hess R., Burrell., J.Quant. Spectrosc. Radiat. Transfer.
21, 23, (1971)

Hill R.A., Gerardo J.B., Kepple P., Phys.Rev.A.
3, 855, (1971)

Himmel G., Pinnekamp F., J.Phys.B. 10, 1457, (1977)

Himmel g., Sowa L., J.Quant. Spectrosc. Rad. Trans.
30, 357, (1983)

Holtzmark J., Ann. Physik., 58, 577, (1919)

Johnson L.C., Hinnov E., Phys.Rev. 187, 143, (1969)

Johnson L.C. Ap.J. 174, 227, (1972)

Kelleher D.E., Wiese W.L., Phys. Rev. Lett. 31,
1431, (1973)

Kepple P., Griem H., Phys. Rev. 173, 317, (1968)

Kolb A.C., Griem H., Phys. Rev., 111, 514, (1958)

Kunze H.J. Space Sci. Rev. 13, 565, (1972)

Kunze H.J. 'Spectral Line Shapes'. p.517.
Ed. B.Wende. Pub. W.de Gruyter. New York. (1981)

Lee R.W., J.Phys.B. 5, L23, (1972)

Lee R.W., J.Phys.B. 6, 1044, (1973)

Lee R.W., 'Spectral Line Shapes' p.333, Ed. B.Wende.
Pub. W. de Gruyter. New York. (1981)

Lorentz H.A., Proc. Roy. Acad. Sci. (Amsterdam) 8, 591, (1906)

Mazure A., Goldbach C., Nollez G., (See Esrom H., Helbig V.) 'Spectral Line Shapes', p.135. Ed. B.Wende. Pub.W.de Gruyter. New York. (1981)

Mihalas D., 'Stellar Atmospheres'., 2nd Edit.
Pub. Freeman. San Francisco. (1978)

Peach G., 'Spectral Line Shapes' p.91. Ed. B.Wende.
Pub. Walter de Gruyter. New York. (1981)

Piel A., 'Spectral Line Shapes' p.135. Ed B.Wende.
Pub. Walter de Gruyter. New York. (1981)

Ramette J., Drawin H.W., Z. Naturforsch. 31a, 401, (1976)

Seidel J., Z. Naturforsch. 32a, 1207, (1977)

Shoub E., Astrophys.J.Supp. 34, 259, (1977)

van Raan A.F.J., de Jongh J.P., van Eck J., Heideman H.G.M.
Physica. 53, 45, (1971)

Vidal C.R., Cooper J., Smith E.W.,
J.Quant.Spectrosc.Radiat.Transfer. 10, 1011, (1970)

Vriens L., Smeets A.H.M., Phys. Rev.A. 22, 940, (1980)

Voslamber D., Z. Naturforsch., 24a, 1458, (1969)

Chapter 2.

DETAILED EXAMINATION OF THREE LEVEL SPECTROSCOPIC TECHNIQUES

SUMMARY

This chapter gives the theoretical background to the Three Level Spectroscopic Techniques used and described in this thesis. This chapter will be presented in three basic parts.

Firstly, the general theory of the depletion of atomic level populations due to laser irradiation will be discussed, using the rate equation formulation.

Secondly, the application of these techniques to the measurements of collision rate coefficients will be described.

Thirdly, the application of these techniques to the measurement of impurity-free line shapes will be described.

2.1 THE RATE EQUATION FORMALISM

For any ensemble of atoms, the rate at which the population density N_a of any given level a, changes will be equal to the difference of the rates into that level from the rest of the system, C_a, and the rates out of that level to the rest of the system, $N_a D_a$:-

$$\frac{d}{dt} N_a = C_a - N_a D_a \qquad 2.1$$

(D_a is the total rate coefficient for all the rates out of level a,)

If the system is time stationary, then

$$\frac{d}{dt} N_a = 0 \quad ; \quad N_a = \frac{C_a}{D_a} \qquad 2.2$$

Since C_a and D_a are sums, we may rewrite eqn. 2.1 as

$$\frac{d}{dt} N_a = \sum_{n \neq a} C_{na} - N_a \sum_{n \neq a} D_{an} \qquad 2.3$$

Where, for example, Cna is the rate from level n to level a.

In general these rates will be radiative rates, collisionally induced rates or the sum of collisionally induced and radiative rates.

2.2 COLLISIONAL RATES

Non radiative excitation or de-excitation can take place between levels due to inelastic collisions between the test atom and other atoms, ions or electrons.

The reaction (for example, electrons) is of the form

$$A^* + e^-[v] \rightleftharpoons A + e^-[v + (2\hbar\omega/m)^{1/2}] \qquad 2.4$$

where * denotes an atom in an excited state. Here, an electron, velocity v takes off the excitation energy $\hbar\omega$ from the excited atom in a superelastic collision.

If the cross section for the reaction is $\sigma_{ab}(v)$ for, say, excitation from level a to level b then the rate will be,

$$R_{ab} = N_e \int_v \sigma_{ab}(v)\, v\, f(v)\, dv \qquad 2.5$$

where f(v) is the normalised electron velocity distribution such that,

$$\int_v f(v)\, dv = 1 \qquad 2.6$$

and Ne is the electron density.

The electron velocity distribution is usually taken to be that described by Maxwell-Boltzmann statistics so that

$$f(v) = 4\pi \left(\frac{m_e}{2\pi K T_e}\right)^{3/2} v^2 \exp - m_e v^2/2KT_e \qquad 2.7$$

This will be valid for any thermal, fully ionised, plasma. (Spitzer 1949). Though where the ionisation is less than about 1%, the high velocity tail of the distribution may be modified, due to the superelastic collisions of electrons off atoms in excited states, see for example Shoub (1977)

2.3 RADIATIVE RATES

In general, the radiative rates may be described by the Einstein coefficients for absorption, stimulated emission and spontaneous emission. For two levels, a and b, (a having a lower energy than b), the absorption rate may be written as:-

$$N_a \int_\nu B_{ab} \rho(\nu) \Phi(\nu) \, d\nu \quad \text{sec}^{-1} \qquad 2.8$$

Where

N_a = Population density of level a.

B_{ab} = Einstein absorption coefficient.

$\rho(\nu)$ = Radiation density per Hz.

$\Phi(\nu)$ = The normalised line shape function.

i.e. $$\int_\nu \Phi(\nu) \, d\nu = 1$$

Similarly, the stimulated emission rate from level b to a can be expressed as:-

$$N_b \int_\nu B_{ba} \rho(\nu) \Phi(\nu) \, d\nu \quad \text{sec}^{-1} \qquad 2.9$$

Where B_{ba} is the Einstein stimulated emission coefficient.

The Spontaneous emission rate is expressed as:-

$$N_b A_{ba} \quad \text{sec}^{-1} \qquad 2.10$$

Where A_{ba} is the Einstein spontaneous emission coefficient

The coefficients are related by the expressions

$$B_{ab} = \frac{g_b}{g_a} B_{ba} \qquad 2.11$$

Where g_a is the statistical weight of level a.

$$A_{ba} = \frac{8\pi h\nu^3}{c^3} B_{ba} \qquad 2.12$$

In addition, the absorption oscillator strength f_{ab} of the transition is related to the A value by:-

$$A_{ba} = \frac{8\pi^2 e^2 \nu^2 f_{ab}}{c^3 m} \frac{g_a}{g_b} \qquad 2.13$$

2.4 LASER INDUCED RATES

To consider the radiative rates induced by laser radiation, the laser power per unit frequency $P(\nu)$, may be related to the total laser power P, by

$$P(\nu) = P\psi(\nu) \qquad 2.14$$

Where $\psi(\nu)$ is the normalised line shape function of the laser. $P(\nu)$ is related to the radiation density $\rho(\nu)$ by

$$P(\nu) = c\rho(\nu) \qquad 2.15$$

If Lab is the laser pumping rate from level a to level b then

$$L_{ab} = \frac{N_a B_{ab} P}{c} \int_\nu \psi(\nu) \phi(\nu) d\nu \qquad 2.16$$

If the laser linewidth is large compared to that of the irradiated line, then, $\psi(\nu)$ can be considered constant across the line shape profile and eqn. 2.16 can be written

$$L_{ab} = \frac{N_a B_{ab} P}{c} \psi(\nu') \int_\nu \phi(\nu) d\nu \qquad 2.17$$

Where ν' is the line centre frequency of the transition.

If ν'' is the line centre frequency of the laser, then eqn. 2.16 can be written as

$$L_{ab} = \frac{N_a B_{ab} P}{c \Delta\nu_L} \left(\frac{\psi(\nu')}{\psi(\nu'')} \right) \qquad 2.18$$

where $\Delta\nu_L$ is the equivalent linewidth of the laser. such that

$$\Delta\nu_L = \frac{1}{\psi(\nu'')} \int_\nu \psi(\nu)\, d\nu \qquad 2.19$$

Similarly, if the laser linewidth is narrow compared to that of the transition, eqn. 2.16 may be written

$$L_{ab} = \frac{N_a B_{ab} P}{c \Delta\nu_T} \left(\frac{\Phi(\nu'')}{\Phi(\nu')} \right) \qquad 2.20$$

where $\Delta\nu_T$ is the equivalent width of the transition, such that

$$\Delta\nu_T = \frac{1}{\Phi(\nu')} \int_\nu \Phi(\nu)\, d\nu \qquad 2.21$$

If the linewidth of the laser and the transition are comparable, then the integral in eqn. 2.16 will have to be calculated explicitly.

However, theintegral in eqn. 2.16 may be expressed as a general 'equivalent width' such that

$$\int_\nu \Phi(\nu)\, \psi(\nu)\, d\nu = \frac{1}{\Delta\nu} \qquad 2.22$$

So that in general eqn. 2.16 may be written

$$L_{ab} = \frac{N_a B_{ab} P}{c \Delta\nu} \qquad 2.23$$

For the case where $\Phi(\nu)$ and $\psi(\nu)$ are both Gaussians and where $\nu' = \nu''$ then figure 2.1 shows how $\Delta\nu$, (normalised to $\Delta\nu_T$), varies as a function of $\Delta\nu_L / \Delta\nu_T$

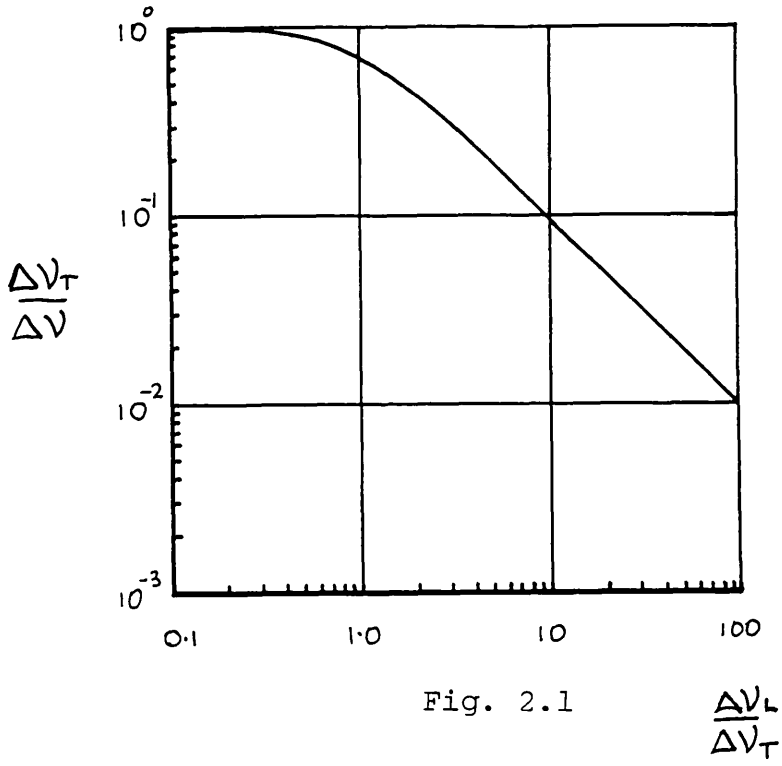

Fig. 2.1

GENERAL EQUIVALENT WIDTH PLOT

This plot shows how the general equivalent width $\Delta\nu$ used in eqn 2.23, normalised to the transition linewidth $\Delta\nu_T$, varies as a function of laser linewidth $\Delta\nu_L$ also normalised to $\Delta\nu_T$

2.4a HOMOGENEOUS and INHOMOGENEOUS BROADENING

In concluding this section, it is worth mentioning that eqn 2.16 is completely general and applies, whether the irradiated transition broadening is homogeneous (e.g. electron pressure broadening or natural broadening) or inhomogeneous (e.g. Doppler broadening).

To see this, consider the case of homogeneous broadening. Consider a narrow bandwidth laser pumping a relatively broad transition having a normalised lineshape function $\phi(\nu)$. Wherever the laser is tuned over the transition, the laser will be pumping all the atoms that are in level a. The degree or strength with which the laser will couple to the transition will depend upon where it is tuned in the line. Obviously the coupling strength will be greater if it is tuned to line centre than if it is tuned to some point in the farline wing.

The laser induced rate can then be written

$$L_{ab} = \frac{N_a B_{ab} P}{c} \int_\nu \psi(\nu)\phi(\nu)\,d\nu \qquad 2.24$$

In the case of a narrow laser tuned to some point in a relatively broad inhomogeneously broadened line, say, a Doppler broadened line, the laser will only be pumping that small subset of atoms having the same frequency as the laser. The number of atoms radiating between ν and $\nu + d\nu$ will be $N_a(\nu)\,d\nu$ where

$$N_a(\nu)\,d\nu = N_a \mathcal{P}(\nu)\,d\nu \qquad 2.25$$

Here $\mathcal{P}(\nu)$ is the normalised lineshape function of the inhomogeneously broadened line.

The laser rate will now be

$$L_{ab} = \frac{B_{ab} P}{c} \int_{\nu} N_a(\nu) \psi(\nu) \, d\nu \qquad 2.26$$

However, substituting from eqn.2.25, then

$$L_{ab} = \frac{N_a B_{ab} P}{c} \int_{\nu} \psi(\nu) P(\nu) \, d\nu \qquad 2.27$$

Now eqn. 2.27 is formally equivalent to eqn. 2.24 so showing that the laser rate will be independent of the broadening mechanism of the line.

2.5 THE VALIDITY OF THE RATE EQUATION FORMALISM

In describing interactions between matter and intense electromagnetic fields, e.g. laser beams, only the density matrix formalism is exactly correct.
The density matrix formalism takes coherent interactions between atomic states into account which the rate equation formalism does not. In the long term, the effect of collisions and radiative decay cause a dephasing of the wave functions of the atoms with respect to each other, so that coherent effects become unimportant and the density matrix formalism becomes well approximated by the rate equation approach. Where rapid transients in the time evolution of an atomic state are being considered due to laser pumping, (i.e. a sudden change if the population density) and these transients are on a timescale small compared to the mean period between dephasing events, (collisions or radiative decay) then the rate equation approach is not valid and the density matrix formalism

should be followed. McIlrath and Carsten (1975) and Daily (1977) have analysed the regions of validity of the rate equation formalism in detail and what follows here is a general summary of their findings.

Considering a two level atom being pumped by a monochromatic laser, then in general the rate equation formalism becomes invalid when

a. The time the laser power density takes to rise to saturating levels is small compared to the mean dephasing period of the atoms.

b. The Rabi oscillation period is small compared to the mean dephasing period of the atoms.

Here, 'saturation' power densities have the usual definition that the laser power is higher than that required to induce a stimulated emission rate that is equal to the spontaneous emission rate. That is

$$P \geq \frac{A_{ba} c \Delta\nu_T}{B_{ba}} \qquad 2.28$$

These sort of power levels are required to significantly perturb the level populations.

For plasmas such as are being considered in this thesis where $N_e \simeq 5\times10^{14} cm^{-3}$ and $T_e \simeq 1eV$ the important dephasing events are listed below.

EVENT TYPE	TYPICAL PERIOD BETWEEN EVENTS
Radiative Decay. Typical A value for visible transitions is about 10^8 sec^{-1}	10^{-8} sec.
Inelastic Collisions. For Neutral Hydrogen, the collision rate out of n=3 is about $10^8 sec^{-1}$ for the above plasma conditions. See Vriens and Smeets (1980)	10^{-8} sec.
'Elastic' Adiabatic Collisions. These give rise to the broadening of the line. For the above conditions, the line width of H-Alpha is 0.6Å. (Vidal, Cooper and Smith. 1973) this leads to a collision frequency of about 10^{11} sec^{-1} via the uncertainty principle.	10^{-11} sec.

The Rabi period is a function of the interaction of the Atom-radiation system, which is given by the interaction operator $\underline{d}_{ab} \cdot \underline{E}'$ and is the cyclic period over which the population of the pumped levels changes.

$\underline{d}_{ab}$ is the atomic dipole operator for the transition

$\underline{E}' = \underline{E} \cos(2\pi\nu t)$, the laser field (monochromatic)

The interaction energy is related to the Rabi period, T, by

$$\underline{d}_{ab} \cdot \underline{E}' = \frac{h}{T} \qquad 2.29$$

$\underline{E}$ is related to the laser power density via the Poynting vector, so for a monochromatic laser field

$$E = \left(\frac{2P}{c\varepsilon_o}\right)^{1/2}$$

The Rabi period can then be written as

$$T = \left|\frac{a_o e}{d_{ab}}\right| \left[\frac{h}{a_o e}\left(\frac{c\varepsilon_o}{2}\right)^{1/2}\right] \frac{1}{P^{1/2}}$$

$$\simeq 3.14 \times 10^{-6} \left|\frac{a_o e}{d_{ab}}\right| \frac{1}{P^{1/2}} \qquad 2.30$$

For times longer than the dephasing period of the atom, the Rabi oscillations will be damped and the rate equation formalism becomes valid.

2.5a THE VALIDITY of the RATE EQUATION FORMALISM WHEN IRRADIATING BALMER ALPHA

Both the He II collision rate experiment and the H-Beta lineshape experiment, described in this thesis, require laser powers high enough to saturate the irradiated transition. To test for the validity of the rate equation formalism used to describe the experiments, the case of a laser pumping the H-Alpha transition in the H-Beta lineshape experiment will now be considered.

At $Ne=10^{15}$ and Te=1eV, the F.W.H.M. half width of H-Alpha is 0.8Å. (Vidal, Cooper and Smith, 1973). This corresponds to a mean dephasing time of 2×10^{-11}sec. The dipole moment for any level n in hydrogen is

$$d \approx n^2 a_0 e$$

So for a transition from level a to level b

$$d_{ab} = (b^2 - a^2) a_0 e$$

For H-Alpha then $d_{23} \approx 5 a_0 e$. Using this in eqn 2.27 it would require a laser power density of about 1 MW cm^{-2} to achieve a Rabi period of 2×10^{-11}sec.

Laser power densities of this magnitude were used, but for the rate equation formalism to become invalid the laser would have had to reach these intensities in a time less than 10^{-11}sec. Also, the rate equation formalism would only be non valid for a period of $\simeq 2 \times 10^{-11}$sec. In fact, the rise time of the laser was $\simeq 10^{-8}$seconds, so it seems certain that at no time was the rate equation formalism invalid.

2.6 DE-EXCITATION RATES MEASURED, USING A THREE LEVEL EMISSION TECHNIQUE

Fig. 2.2 shows the level scheme for this technique. From eqn 2.2, the population of level a will be

$$N_a = \frac{C_a}{D_a}$$

A laser, tuned to the n=a to n=b transition adds a new, known, rate out of n=a. As a result the population of n=a will be depleted to a new population N_a^L where

$$N_a^L = \frac{C_a^L}{D_a + L} \qquad 2.31$$

C_a^L is the new rate into level a due to the laser rate from level b and the perturbed populations of other levels collisionally or radiatively coupled to level b.

Since the collision rates out of level n go roughly as n^2, the relatively higher collision rates out of level b mean that N_b will not be significantly perturbed and only Na will be driven significantly out of equilibrium by the laser. For laser powers well below that required to saturate the transition, then, it is possible to make the approximation $C_a^L = C_a$. Then eqn 2.31 can be rearranged t give

$$\frac{N_a^L}{N_a} = \frac{D_a}{D_a + L_{ab}} \qquad 2.32$$

or

$$D_a = \frac{L_{ab}}{1 - N_a^L/N_a} \qquad 2.33$$

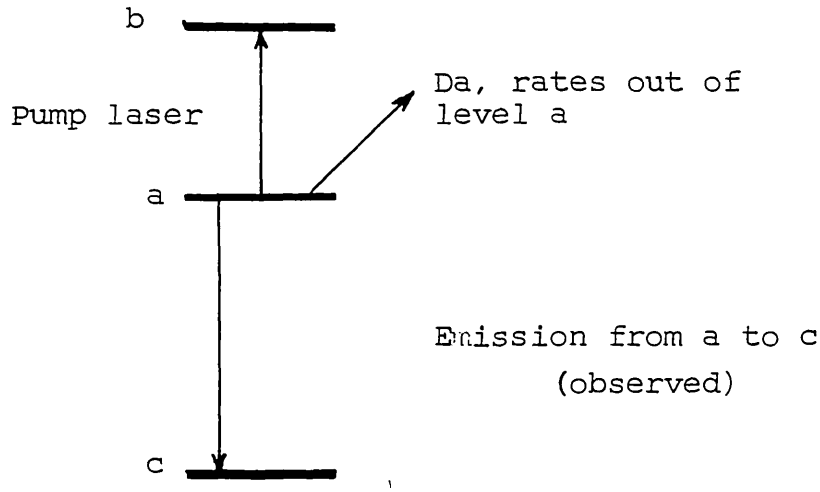

Fig. 2.2

THREE LEVEL EMISSION SCHEME

FOR

MEASUREMENT OF DE-EXCITATION RATES

The population of level a is depleted by using a laser to pump atoms up to level b, The relative depletion of level a, (observed in emission on the n=a to n=c transition) will be a function of the known laser rate and the other rates out of n=a, Da.

Given the relative depletion of level a, observed by watching the change in emission from level a to level c, and the known laser rate L_{ab}, Da can be deduced. In practice, this model will usually lead to an over-estimate of Da, since $Ca^L > Ca$ in general.

2.6b A TWO LEVEL MODEL TO DESCRIBE THE DEPLETION OF THE OBSERVED LEVEL.

The one level model described by eqn 2.32 is improved by setting $Ca^L = Ca$ for all laser powers and putting in the rates to and from level b explicitly. N_b is fixed at its long term equilibrium value for laser power densities well above saturation values. This will make Na^L correct for those high laser powers. The laser rates from level b are not important for laser power densities well below saturation values, so Na^L will also be correct for low laser powers despite N_b being incorrect at these powers. Then

$$Na^L = \frac{L_{ba} + D_a N_a}{L_{ab} + D_a} \qquad 2.34$$

Using eqn 2.23

$$2.35 \qquad Na^L = \left[\frac{N_b B_{ba} P}{c\Delta\nu} + D_a N_a \right] \Big/ \left[\frac{B_{ab} P}{c\Delta\nu} + D_a \right]$$

Let K be a constant, where

$$K = \frac{D_a N_a c \Delta\nu}{N_b B_{ba}} \qquad 2.36$$

Then

$$\frac{Na^L}{Na} = \frac{g_a N_b (P + K)}{g_b N_a P + g_a N_b K} \qquad 2.37$$

Now let $Na^L(Sat)$ be the asymptotic value of Na^L for laser powers $P \gg K$, then

$$Na^L(Sat) = \frac{Nb\, g_a}{g_b} \qquad 2.38$$

Substituting 2.38 into 2.37 and dividing top and bottom by Na, then

$$\frac{Na^L}{Na} = \left[\frac{Na^L(Sat)}{Na}\right](P+K) \Big/ \left[P + \left(\frac{Na^L(Sat)}{Na}\right)K\right] \qquad 2.39a$$

Fig. 2.3 shows plots of eqn 2.39 for various values of $\left[\frac{Na^L(Sat)}{Na}\right]$. Note that now one extra piece of information is required over the one level model of eqn 2.32, namely the value of Na^L / Na when $P \gg K$, in other words the value of $\left[\frac{Na^L(Sat)}{Na}\right]$.

This model should now be correct for $P \ll K$, (like in eqn 2.32) and also $P \gg K$. Comparison of this model with results obtained with a full collisional radiative model show good agreement for $P \approx K$ as well. (Section 4.4, Chapter 4). This is because the effects of having Nb fixed (Na^L being higher than it should be) will be partially offset by having Ca fixed. (Which pushes Na^L lower than it should be)

Having obtained a value of K and $\left[\frac{Na^L(Sat)}{Na}\right]$ by fitting eqn 2.39 to the data, Da may be recovered, using eqns 2.36 and 2.38.

$$Da = \frac{K\, B_{ba}\, g_b}{c\, \Delta\nu\, g_a}\left[\frac{Na^L(Sat)}{Na}\right] \qquad 2.39b$$

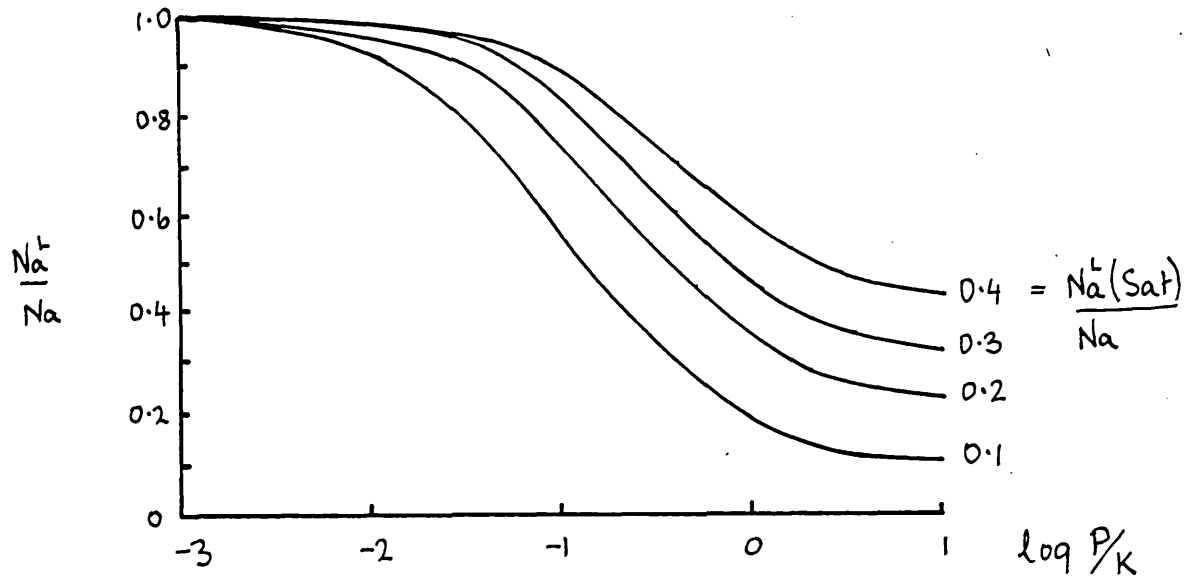

Fig. 2.3

Plots of Two level model for various values of $Na^{L}(Sat)/Na$.

2.6c OPTIMUM DEPLETION LEVELS

Although the depletion is larger for larger laser powers, so making it easier to measure, it is also true that $\frac{d}{dp}\left(\frac{Na^L}{Na}\right)$ is also decreasing with P so making the measurement less sensitive.

The optimim depletion to work at then, is when the product $\Delta Na \frac{d}{dP}(\Delta Na)$ is maximised; where

$$\Delta Na = 1 - \frac{Na^L}{Na}$$

This occurs when

$$\frac{Na^L}{Na} = \left[\left(\frac{Na^L(Sat)}{Na}\right) + 1\right]/2 \qquad 2.40$$

2.6d COMPARISON OF ONE LEVEL and TWO LEVEL DEPLETION MODELS

The one level model can be recovered from eqn 2.39 by removing the stimulated emission term. Then

$$\frac{Na^L}{Na} = K\left[\frac{Na^L(Sat)}{Na}\right]\Big/\left[P + K\left(\frac{Na^L(Sat)}{Na}\right)\right] \qquad 2.41$$

Fig. 2.4 shows comparisons of the one level model with the two level model. In general the one level model follows the two level model more closely for low values of $\frac{Na^L(Sat)}{Na}$. In the worst case shown, when $\frac{Na^L(Sat)}{Na} = 0.4$, the values of P when $Na^L/Na = 0.5$ differ for the two models by a factor of 5. The values of Da derived, using the one level model , would then be a factor of 5 too high. Where $\frac{Na^L(Sat)}{Na} = 0.1$ however, the error would only be 30%. The errors incurred using the one level model could be quite severe despite its attraction that a knowledge of $\frac{Na^L(Sat)}{Na}$ is not required.

A laser capable of powers high enough to find $\frac{Na^L(Sat)}{Na}$ experimentally would need to be about two orders of magnitude more powerful than that needed to work at the optimum depletion (eqn 2.40) for best sensitivity.

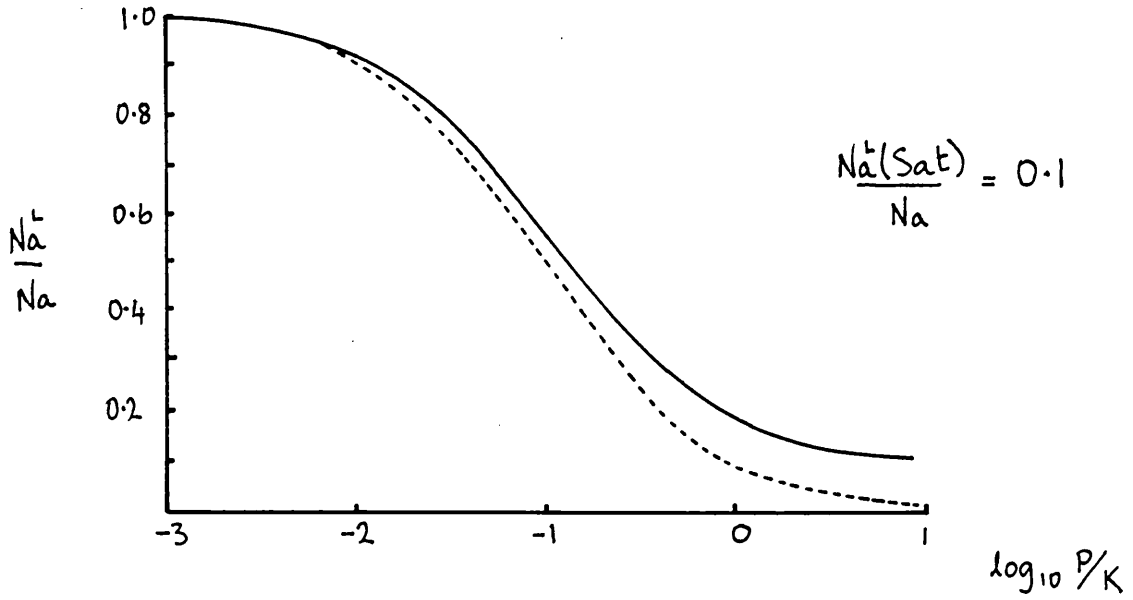

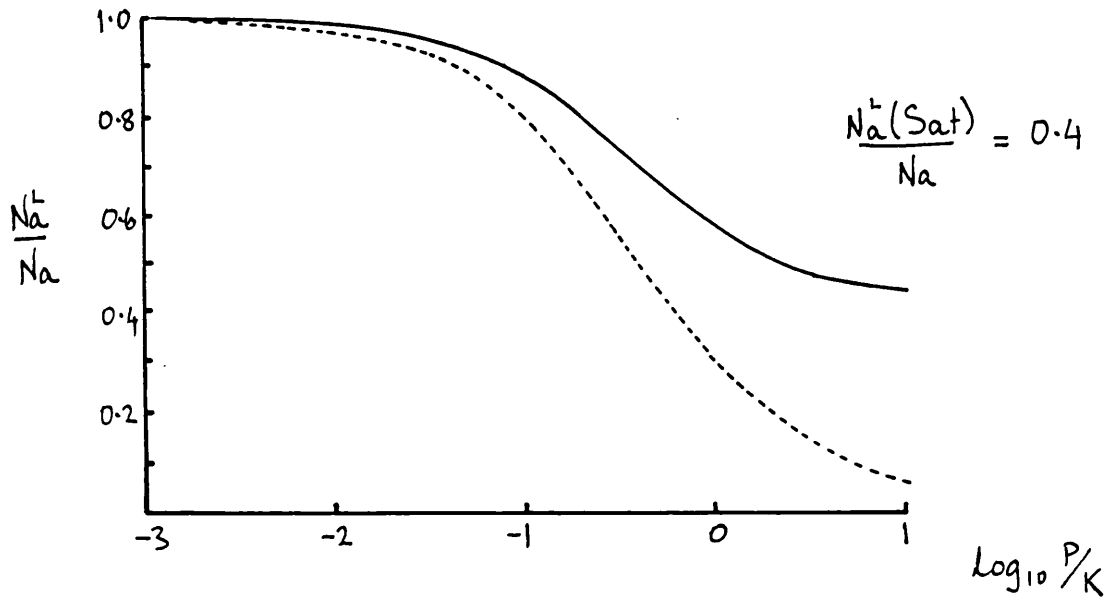

Fig. 2.4

COMPARISONS OF ONE LEVEL AND

TWO LEVEL MODELS

——— Two level model

..... One level model

2.6e COLLISIONAL RADIATIVE MODELS

A COLLISIONAL RADIATIVE MODEL, (C.R.M.), is generally described and defined in section 1.3a and described in detail in appendix 1. By using a C.R.M. for the test atom in a plasma of given Ne and Te it is, in principle, possible to model the dynamics of the level of interest under laser irradiation without any approximations being made. However, in comparing the model predictions with experiment, it is then only possible to comment on the correctness of the model. If the model does not predict the behaviour of Na correctly as a function of P, it is difficult to know how to change the many parameters of such a model to make it correct and so deduce the rates out of level a.

However, a 10 level C.R.M. for He II was constructed and a detailed description of it is also given in appendix 1.

It was found that, in fact, use of the simple two level model, outlined in sections 2.6a and 2.6b, seemed, together with the C.R.M., to be the best approach for the analysis of the He II collision rate experiment.

2.7 LASER REQUIREMENTS FOR THE He II COLLISION RATE EXPERIMENT

This section deals with the requirements of the laser or how the parameters of laser beam homogeneity, pulse length or beam diameter could affect the resulting observed depletion of Na.

2.7a THE EFFECTS OF VARIATIONS IN POWER DENSITY ACROSS THE BEAM.

In the experiment on He II, the n = 4 population was observed by monitoring the change in emission at 4686Å. (n=4 to n=3). The observation was made at right angles to the laser beam. Inhomogeneity in the power density across the beam diameter could lead to variations in N_4^L across the sample volume of plasma. The observed N_4^L will then differ from that expected from the average power density due to the non linear relationship between these two parameters.

An analysis will now be performed using eqn 2.39a The power density for which Na^L/Na is most non linear will be determined. A worst case analysis will then be given to show the effects of variations in power density across the laser beam for the power density derived above.

From eqn 2.39a for laser powers much higher than saturation, i.e. $P \gg K$, then Na^L becomes independent of P. Variation in laser power density across the beam (Provided the power density at any point is well above saturation) will then have no effect on Na^L.

Similarly for laser powers much lower than saturation, i.e. $P \ll K$, the depletion in Na is linear with power density. The average depletion observed will then be that expected from the average power density. The region where $P \simeq K$ then, is the region where Na is sensitive to

variations in power density across the beam.

At the high power limit where $P \gg K$, eqn 2.39a reduces to

$$\frac{Na^L}{Na} = \frac{Na^L(Sat)}{Na} \qquad 2.42$$

At the low power limit, where $P \ll K$, the depletion is linear with P. Let the depletion be ΔNa where

$$\Delta Na = Na - Na^L = Na\left(1 - \frac{Na^L}{Na}\right) \qquad 2.43$$

Then

$$\Delta Na = \frac{Na\, P\left[1 - \left(\frac{Na^L(Sat)}{Na}\right)\right]}{P + K\left(\frac{Na^L(Sat)}{Na}\right)} \qquad 2.44$$

At low powers eqn 2.44 reduces to

$$\Delta Na \simeq \frac{P}{K} Na\left[\frac{Na}{Na^L(Sat)} - 1\right] \qquad 2.45$$

i.e. Na is a linear function of P. Rearranging eqn 2.45

$$\frac{Na^L}{Na} = 1 - \frac{P}{K}\left[\frac{Na}{Na^L(Sat)} - 1\right] \qquad 2.46$$

Fig. 2.5 shows plots of 2.37, 2.42 and 2.46 for various values of $\frac{Na^L(Sat)}{Na}$

The plots of eqn 2.42 and 2.46 show models which are insensitive to variations in power density. Therefore, the power density at which eqn 2.37 deviates most from these models will be the power at which Na^L is most sensitive to variations in power density across the beam diameter. This occurs when

$$\frac{P}{K} = \frac{Na^L(Sat)}{Na} \qquad 2.47$$

More formally, eqn 2.47 may be obtained as the root of the second differential of eqn 2.39 with respect to P, giving the power at which the gradient changes most

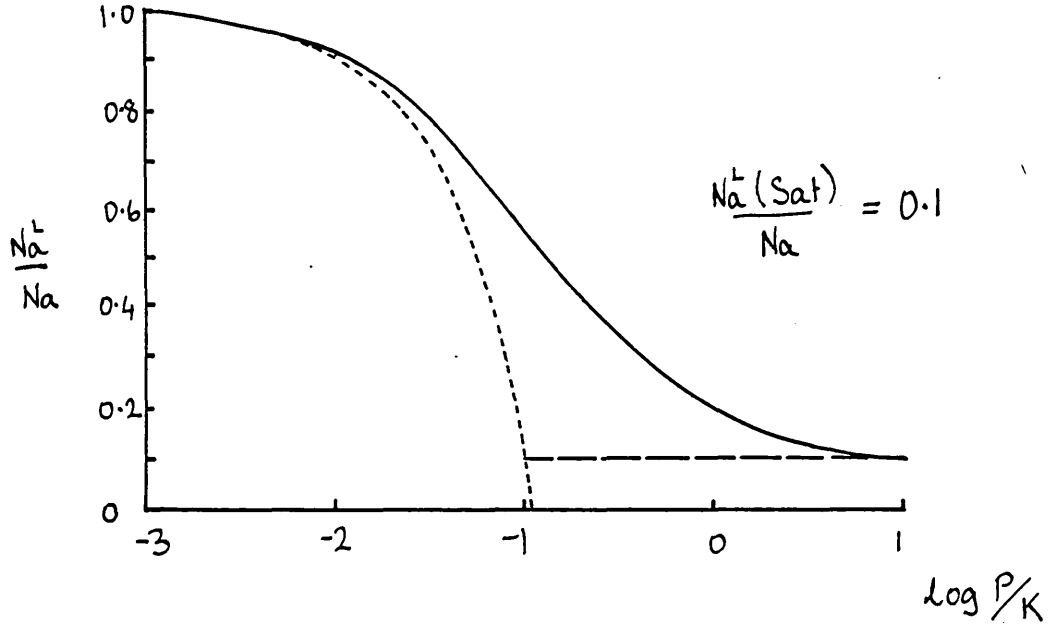

——— eqn 2.37

..... eqn 2.42

– – – – eqn 2.46

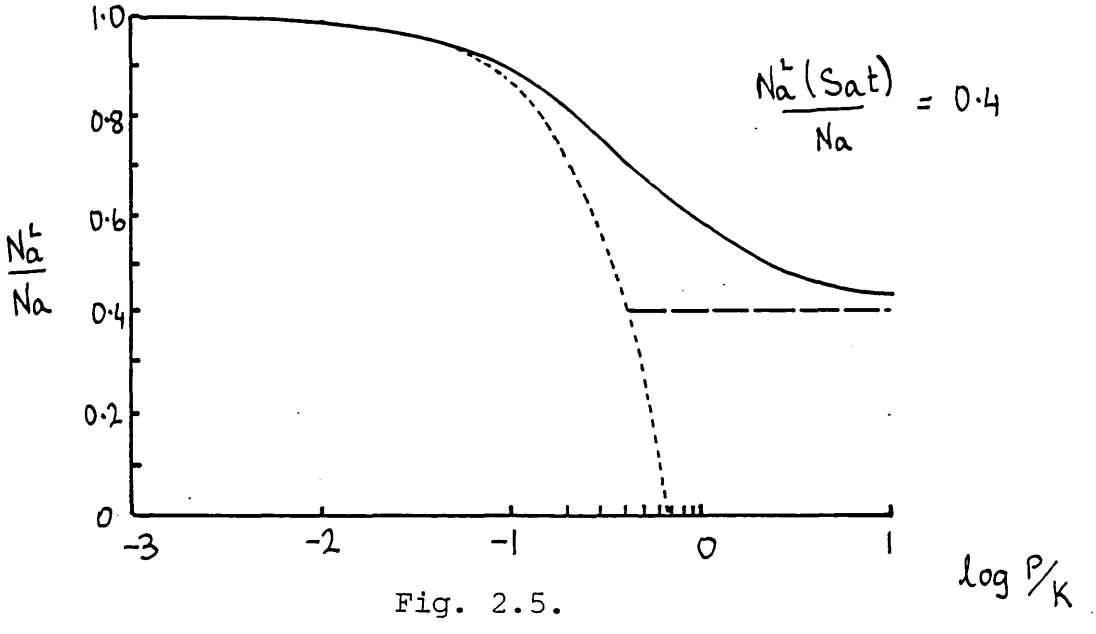

Fig. 2.5.

Comparison of Two Level Model with models showing the two extremes of sensitivity to laser power.

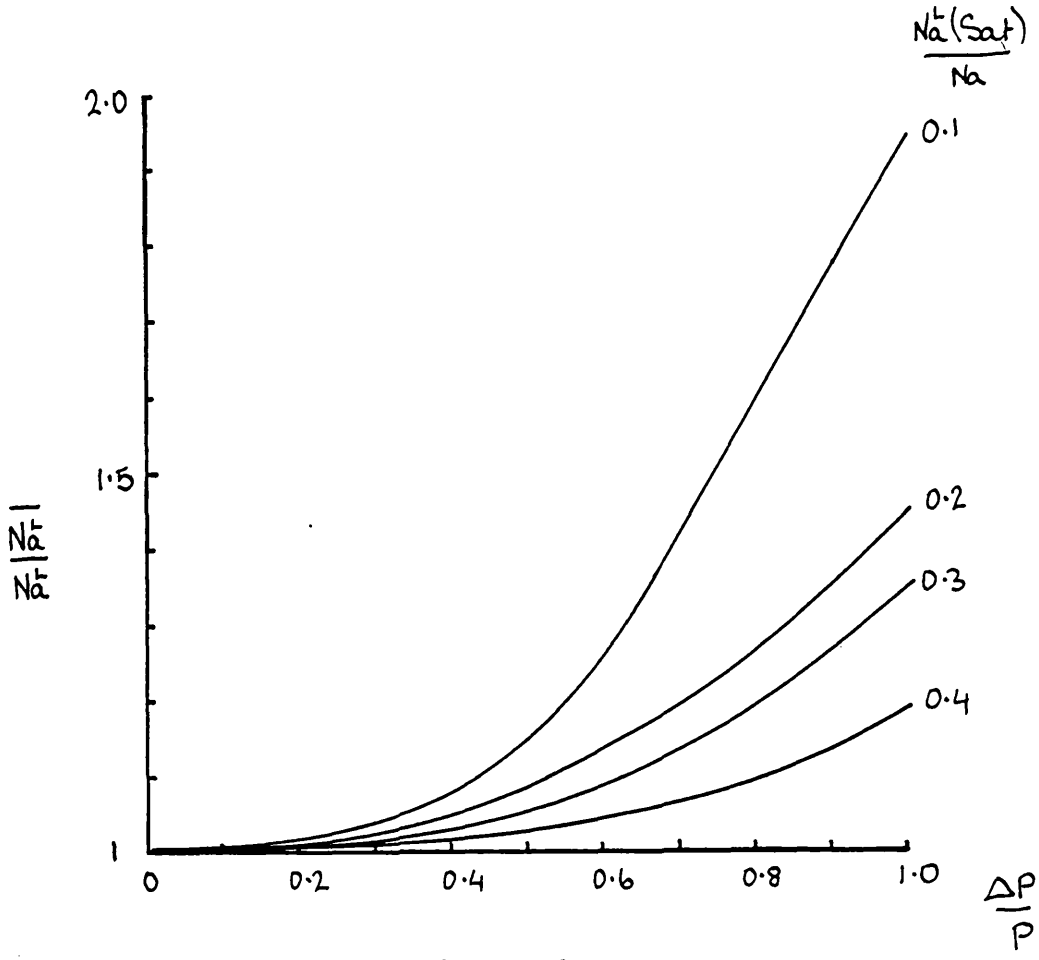

Fig. 2.6

ERROR in OBSERVED POPULATION due to NON UNIFORM LASER BEAM

Na^L is the population density due to laser power P.

If half the laser beam has power $P + \Delta P$ and the other half $P - \Delta P$, the resulting population density observed will be $\overline{N_a^L}$

(or is most non linear) with P.

A 'non uniform laser beam' can be modelled by assuming a laser beam where the mean power density is P, but where half the beam has a power density $P + \Delta P$ and half a power density $P - \Delta P$. The detector will now see an average population density, $\overline{Na^L}$, due to irradiation from the two power densities. In Figure 2.6 the ratio $\overline{Na^L}/Na^L$ is plotted against $\Delta P/P$ for various values of $\frac{Na^L(Sat)}{Na}$. In general it can be seen that a variation in power density of up to 30% only changes the depletion seen in level a by the order of 1%. Also, the lower the depletion at high powers, the greater the effects of variations in power density across the beam diameter will be.

2.7b DURATION OF LASER PULSE

To measure Na^L with the pump laser on, it is necessary that Na^L has reached equilibrium along with the other levels coupled to level a. It is also necessary then, that the laser should be on for a time exceeding this equilibrium period.

Initially, the response of Na to the laser pulse can be written

$$\frac{dNa^L}{dt} = -Na^L(Da + L_{ab}) + Ca \qquad 2.48$$

(Here it is assumed $Ca^L \approx Ca$)

For a step function laser profile, then eqn 2.37 has the solution.

$$N_a^L(t) \approx \frac{N_a}{D_a + L_{ab}} \left(L_{ab} \exp -(D_a + L_{ab})t + \frac{C_a}{N_a} \right) \quad 2.49$$

In general then $Na^L(t)$ will change in a time scale of the order

$$1/(D_a + L_{ab})$$

For high laser powers, i.e. $P \gtrsim K$, then Na and Nb will be redistributed between the two levels in a time scale of about 1/Lab according to their statistical weights. Then

$$N_a^L + \frac{g_a}{g_b} N_b^L = N_a + N_b \quad 2.50$$

Burgess and Skinner (1974) showed that after this, the two laser-locked levels will relax to a new equilibrium in a time scale of about 1/Db, where, in general, Db > Da when level b is higher than level a.

So for low laser powers, $P < K$, the laser should have a pulse length greater than 1/Da. For high laser powers, $P \gtrsim K$, the pulse length should be greater than 1/Db. The measurement of Na^L should be taken after these time periods when Na^L is at an equilibrium.

For the He II collision rate experiment, rate coefficients of the order of 10^9 for D4 were expected.

Since the coaxial flashlamp pumped laser used for the experiment had a rise time 10^{-8} sec and a pulse length 3×10^{-7} sec, it is safe to assume that a condition of dynamic equilibrium will be valid.

2.7c A COMPARISON of the THREE LEVEL TECHNIQUE. WITH OTHER METHODS of MEASURING DE-EXCITATION RATE COEFFICIENTS

The fluorescence technique of Burgess and Skinner (1974) may be considered complimentary to the three level emission technique discussed in sections 2.6 and 2.7, in that, the three level technique may be used to obtain the rate coefficient out of the lower level of a laser pumped transition, whereas, the fluorescence technique may be used for the upper level. The three level absorption technique used by Burgess, Kolbe and Ward (1978) is similar to the emission technique, in that it is the lower level of the laser pumped transition that is observed. The three level absorption technique has the advantage, that (in principle) the information can be obtained in one shot. However, the plasma volume has to be homogeneous over the optical path length required to make the probe transition optically deep. By comparison, the three level emission technique only requires relatively small test volumes of plasma.

Where a laser can be tuned to two transitions which have the level of interest as an upper level or as a lower level, there will be a choice between using the Fluorescence or three level method, For example, He II, n=4 to n=3 at 4686Å, the rate coefficient out of n=4 could be studied using the fluorescence technique. Or n=4 to n=8 at 4859Å, the laser could be tuned to this transition and the three level emission technique used to study n=4. The advantage of the fluorescence technique, is that only one shot is required to get the information.

The disadvantage is that the laser pulse has to have a rise time to saturating powers small compared to the characteristic relaxation period of the level studied. If the level n=a is being studied, the relaxation of level a to equilibrium (see figure 1.4) will take place in a time 1/Da, the laser rise time T must thus be $T < 1/Da$.

The Detector must also be capable of responding on a time scale faster than 1/Da. If the laser pulse is shaped with a pockels cell to give it a fast rise time, then this limits T to about one nanosecond, which, in turn, sets an upper limit on the rate coefficient Da that can be measured so that $Da \lesssim 10^9$.

The three level emission technique, whilst requiring several shots to aquire the data, does not require a fast detector. The laser pulse must have a life time greater than 1/Da or the response time of the photo detector - whichever is the slower. The measurable limit on the rate coefficient is set only by the available power density. The laser then must be capable of power densities

$$P \gtrsim \frac{Da\, C\, \Delta\nu}{Bab} \quad Wm^{-2}$$

The three level technique can be used then to look at rate coefficients in conditions of high density and temperature, where the rate coefficient will be greater than about $10^9 sec^{-1}$.

TECHNIQUE	ADVANTAGES	DISADVANTAGES	POWER REQUIRED Wm^{-2}
LASER FLUORESCENCE	Results obtained in one shot. Small test volume.	Difficult to measure rate coefficients $> 10^9 sec^{-1}$ Fast risetime laser required. Fast detectors required	$P \geq \frac{g_a 8\pi h\nu^3 \Delta\nu\, D_a}{g_c\, c^2 \qquad A_{ac}}$
THREE LEVEL EMISSION TECHNIQUE	Small test volume Do not need fast risetime laser. Do not need fast detectors Measurable rate coefficients only limited by laser power.	Several shots required Need uniform laser beam	$P \geq \frac{g_a 8\pi h\nu^3 \Delta\nu\, D_{ac}}{g_c\, c^2 \qquad A_{ac}}$
THREE LEVEL ABSORPTION TECHNIQUE	Results obtained in one shot	Uniform pump laser needed Large plasma volume required (for optically deep probe transition)	$P \geq \frac{g_a 8\pi h\nu^3 \Delta\nu\, D_c}{g_c\, c^2 \qquad A_{ac}}$

Table 2.1

Summary of advantages and disadvantages for the three techniques compared in Section 2.7. See Fig.1.4 and Fig.1.5 for the level schemes corresponding to the 'power required' formulae.

2.8 LINESHAPES OBSERVED VIA THREE LEVEL SPECTROSCOPIC TECHNIQUES.

As described in Chapter 1, measuring lineshapes using three (or more) levels of an atom offers a way of aquiring a lineshape free of any impurities. There are basically three ways in which an impurity free lineshape may be obtained. These are summarised in figs 2.7.

Fig 2.7a shows a method where the lineshape of interest is obtained in absorption in the usual way. The absorption lineshape is then obtained again, but this time, while another transition, having a common lower level, is saturated with a high power dye laser. If there is no impurity contribution the two lineshapes so obtained, should be the same, except that the optical depth in the second case is reduced across the profile, due to the action of the pump laser depleting the common lower level.

If there is an impurity contribution, its optical depth will not be reduced by the pump laser, so then, by suitably normalising the two profiles and taking one from the other, the line shape of the impurity will be revealed. This can then be taken from the first straight absorption profile, so leaving an impurity free profile. This technique will here be called Saturated Three Level Absorption Spectroscopy S.T.L.A.S.

Fig. 2.7b shows a method where a pump laser of known power density, is now tuned through the lineshape of interest and the resulting depletion of the lower state is monitored by a probe laser tuned to another transition, having a common lower level.

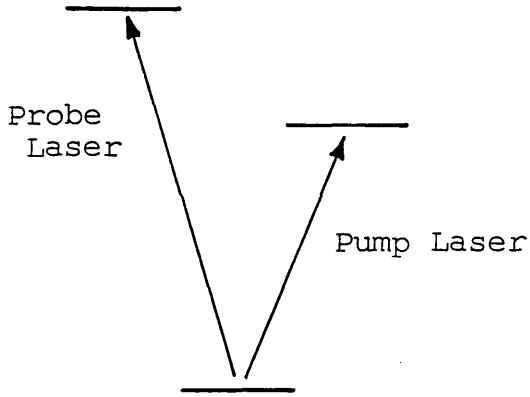

Fig. 2.7a

SATURATED

THREE LEVEL ABSORPTION

SPECTROSCOPY

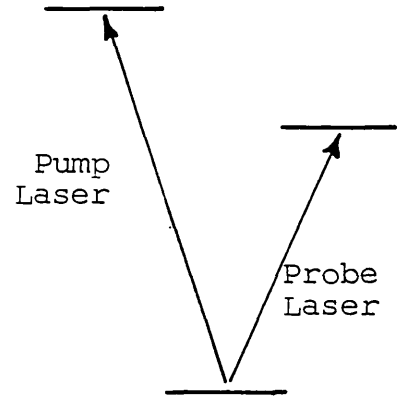

Fig.2.7b

NON SATURATED THREE LEVEL

ABSORPTION SPECTROSCOPY

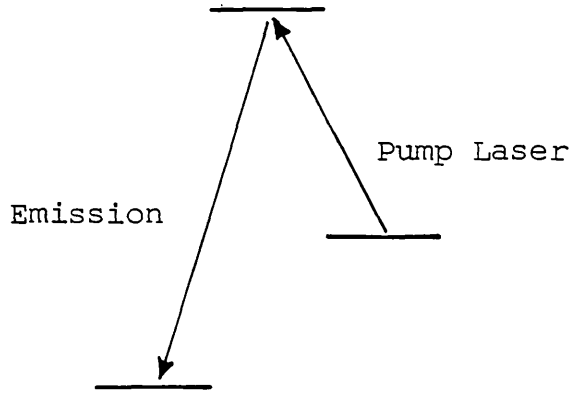

Fig.2.7c

SATURATED THREE LEVEL

EMISSION SPECTROSCOPY

SCHEMES for THREE LEVEL LINESHAPE SPECTROSCOPY

The depletion of the lower level will be a function of the pump laser power and the value of the line shape function at the pump laser frequency. The lineshape so produced will be independent of any impurities having transitions at the same frequency. This technique will be called Non Saturated Three Level Absorption Spectroscopy. - N.S.T.L.A.S.

Figure 2.7c shows a method where the lineshape of interest is observed in emission in the usual way. The lineshape is then observed again when the population of the upper level is perturbed by irradiating another transition, which has the upper level as one of the laser pumped levels. The two profiles should again be the same, if there is no impurity, but the emission strength in the second case will have changed across the profile.

As with the first absorption method described above, the lineshape of any impurity will be revealed by suitably normalising the two profiles and taking one from the other. This technique will be called Saturated Three Level Emission Spectroscopy. S.T.L.E.S.

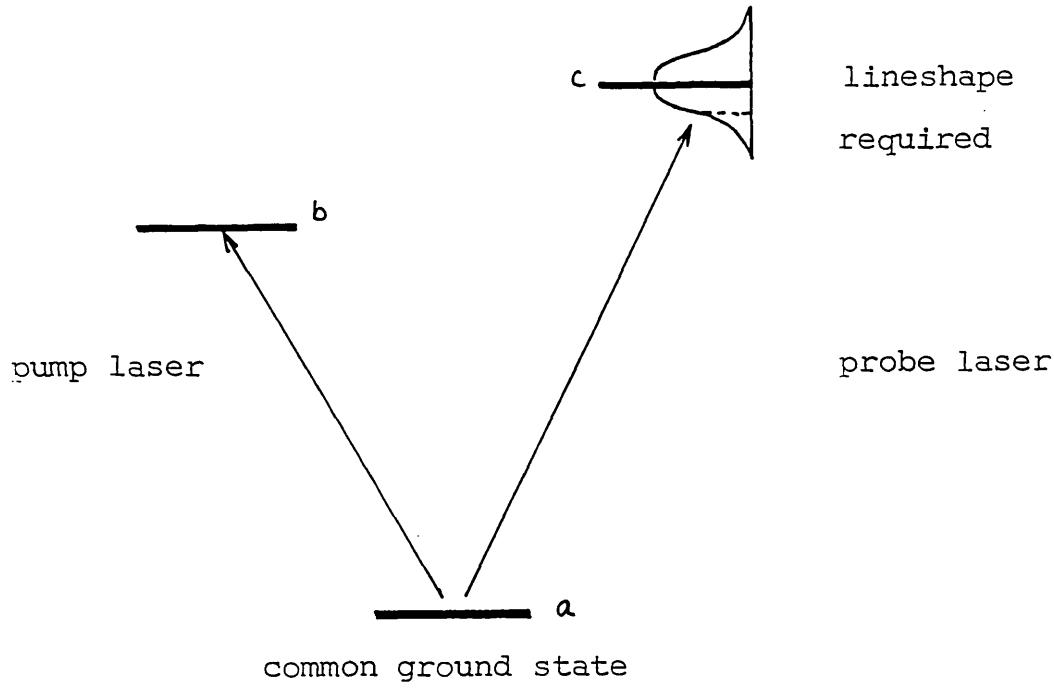

Fig. 2.8

LEVEL SCHEME for SATURABLE

THREE LEVEL ABSORPTION SPECTROSCOPY

The lineshape of the a to c transition is obtained twice - once by straight forward absorption, then again by absorption, but this time, depleting level a by pumping on the a to b transition with a dye laser.

2.9 SATURATED THREE LEVEL ABSORPTION SPECTROSCOPY - (S.T.L.A.S.)

Figure 2.8 shows the scheme for S.T.L.A.S. The lineshape is obtained twice. Firstly, an orthodox absorption profile is obtained using a probe laser. Secondly, an absorption profile is obtained, again in the same basic way, but this time the lower level of the transition is depleted by saturating another transition, having a common lower level. This second absorption profile will have a lower optical depth for any given frequency than the first profile. The optical depth of any impurity will, however, remain unchanged. If the two profiles are suitably normalised and one taken from the other, then the lineshape of the impurity will be revealed.

If $\tau(\nu)$ is the optical depth of the transition of interest at frequency ν, then $\tau(\nu)$ is a function of the population of the lower level Na.

Let $\tau(\nu)_L$ be the optical depth whilst the laser, (tuned to another transition of the same series,) is on. Let F be the normalising factor such that

$$F\,\tau(\nu) = \tau(\nu)_L \qquad 2.51$$

Let $I(\nu)$ be the impurity optical depth at frequency ν When the normalised lineshapes are removed from each other, let $R(\nu)$ be the remainder, then

$$R(\nu) = F\left[\tau(\nu) + I(\nu)\right] - \left[\tau(\nu)_L + I(\nu)\right]$$

$$= I(\nu)\left(F - 1\right) \qquad 2.52$$

From eqn 2.52 it can be seen that the sensitivity of the experiment is a function of F, which is a measure of the depletion of the lower level. It is then desirable to have as large a change in the lower level as possible for maximum sensitivity.

2.9a LASER REPRODUCIBILITY

To achieve maximum depletion, it is seen from eqn2.37, that laser power densities, greater than saturation, are required i.e. $P \gg K$. Using high laser powers is also an advantage, since then the depletion becomes independent of laser power. Thus shot to shot fluctuations in power and beam inhomogeneity are not a problem and the laser need not be monitored, even if it were not of high quality (in terms of beam homogeneity or reproducibility).
In Section 2.7a it was shown that even for a worst case analysis, where $P \simeq K$, the variation in the Na^L due to laser beam in homogeneity, would be quite small. This would be especially so at high laser powers where $P \gg K$. Laser irreproducibility is another matter though.

At high power densities the radiative rates between level a and level b will dominate the rates for level a.
The population of level a will then be, (from eqn 2.37)

$$N_a^L = \frac{g_a N_b (P+K)}{g_b P} \qquad 2.53$$

The uncertainty in Na, due to irreproducibility of the laser, may be written

$$N_a^L + \Delta N_a^L = \frac{g_a N_b \left((P + \Delta P) + K \right)}{g_b (P + \Delta P)} \qquad 2.54$$

Multiply top and bottom by $(P - \Delta P)$ and ignore all terms in ΔP^2, then

$$\Delta N_a^L = \frac{g_a N_b K}{g_b P} \left(\frac{\Delta P}{P} \right) \qquad 2.55$$

At high laser powers

$$N_a^L \approx \frac{g_a}{g_b} N_b$$

Eqn 2.55 can be written

$$\frac{\Delta N_a^L}{N_a^L} = \frac{K}{P} \left(\frac{\Delta P}{P} \right) \qquad 2.56$$

The error in Na^L is then proportional to the error in P, but is reduced by a factor K/P.

For example then, if the reproducibility in the laser is 20%, then, to ensure the consequent error in Na^L is less than 1%, the laser power should be 20 times the saturation power.

For laser powers lower than this, it would be necessary to account in some way for the laser irreproducibility. The laser power would have to be monitored on a shot to shot basis and then the data could be corrected for consequent variations in Na^L by reference to a previously prepared Plot of Na^L versus P, obtained experimentally.

2.9b PUMP LASER PULSE LENGTH and PROBE LASER TIMING

Section 2.7b showed how the pulse length of the pump laser should be at least 1/Db and preferably longer, so that Na^L came into equilibrium. It is also necessary that the new optical depth be determined only after this time. So if the probe laser were a pulsed laser, it should be triggered only after the pump laser has been on for a time $\simeq$ 1/Db. The probe laser should also turn off before the pump laser does.

2.10 NON SATURATED THREE LEVEL SPECTROSCOPY

Figure 2.9 shows the scheme for N.S.T.L.A.S.. The pump laser is tuned through the transition of interest. The resulting depletion of the lower level population is measured using the probe laser which monitors the change in opacity on another transition of the same series. The change in opacity on the probe transition will then be a function of the pump laser power and the value of the line-shape function at the pump laser frequency. (It is assumed here that the pump laser bandwidth is small compared to that of the transition.). Since the opacity of any impurity will remain unchanged by the action of the pump laser, the resulting profile will be free of any impurities.

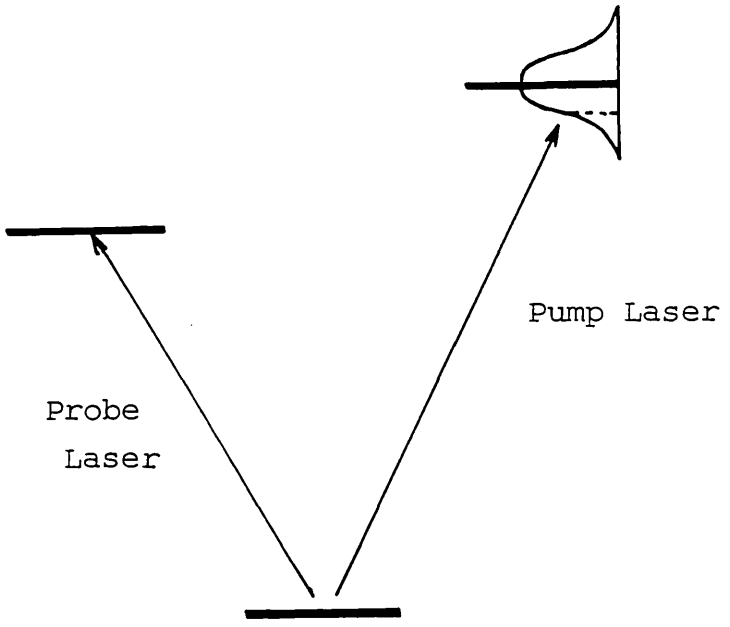

Fig. 2.9

LEVEL SCHEME FOR NON SATURATING

THREE LEVEL SPECTROSCOPY

The pump laser is tuned through the transition of interest on a shot to shot basis. The depletion of the lower level, monitored by the probe laser, will be a function of the laser power and the transition line strength at the pump laser frequency.

There are two possible methods of approach to this technique. One is to keep the pump laser power density low enough that changes in Na will be a linear function of the laser power density and the lineshape function. i.e.

$$\frac{\Delta Na}{Na} = W\phi(\nu)\,P(\nu) \qquad 2.57$$

Where $P(\nu)$ is power density of the pump laser tuned to frequency ν and W is a constant. In this approach the laser power density may be kept the same whilst tuning through the transition and then $\phi(\nu)$ will be proportional to ΔNa, which is observed as a change in opacity on another transition with a common lower level.

The other approach is to increase the power density so that (the now larger) ΔNa is not linear with $P(\nu)$. Now, however, ΔNa is kept fixed and $\phi(\nu)$ is inversely proportional to $P(\nu)$.

Both the above approaches will now be analysed in detail.

2.10a LINEAR N.S.T.L.A.S.

The linear N.S.T.L.A.S. approach is when the pump laser power density is low so that the depletion in Na is a linear function of the laser power density, i.e. eqn 2.43 may be said to apply. Figure 2.10 shows the percentage departure of eqn 2.43 from the 'correct' model of eqn 2.34 as a function of P/K for various values of Nb.

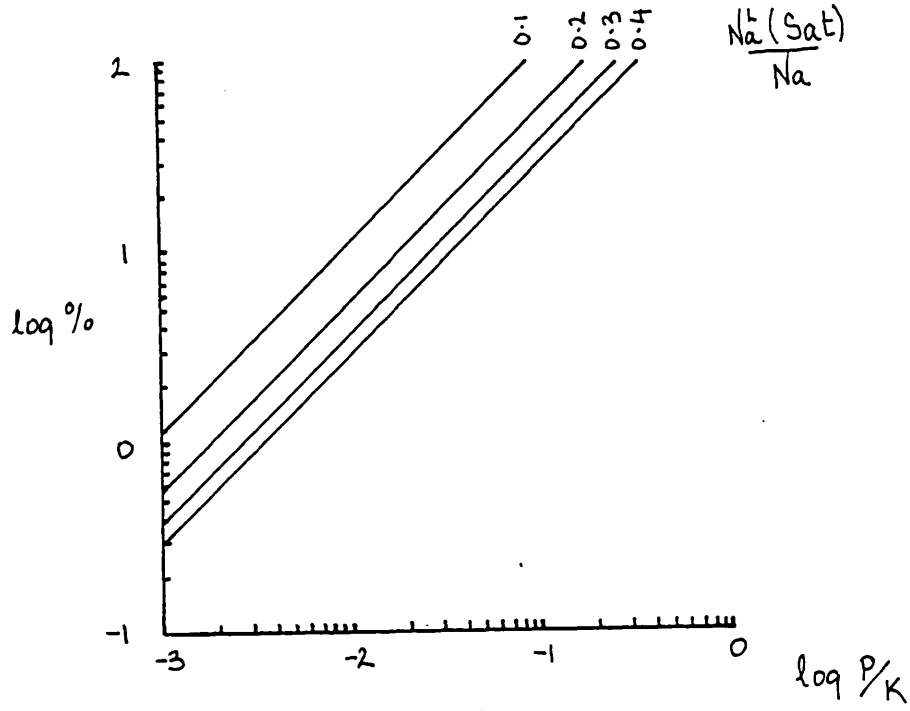

Fig. 2.10

Percentage departure from linearity with laser power for the two level model of eqn 2.39a

This plot shows how the two level model of eqn 2.39a deviates from the linear low power model of eqn 2.46 as a function laser power normalised to P.

In general it can be seen that to keep Δ Na linear with $P(\nu)$ to better than 1%, then the pump laser power density must be kept to less than one thousandth that required to saturate the transition. Also the depletions induced must be kept to less than 1%.

This places quite severe constraints on the accuracy of the detection apparatus which, to obtain an accuracy of 1% in measuring Δ Na, must be able to measure Na^L to one part in 10^4 or better.

The beam quality of the pump laser would not be a problem with linear N.S.T.L.A.S. for reasons given in section 2.7a. Since the laser power would be constantly monitored, reproducibility would also not be a problem.

Where the optical depth at the pump laser frequency is significant, then the pump laser power density will decrease exponentially down the test column. This can be corrected for, by determining the average power density and using this in eqn 2.57 to calculate the lineshape function from the observed average Δ Na.

If $P(\nu)$ is the input power density, then the average power density along the column length will be $\overline{P(\nu)}$ where

$$\overline{P(\nu)} = P(\nu)\left(\frac{1 - e^{-\tau(\nu)}}{\tau(\nu)}\right) \qquad 2.58$$

$\tau(\nu)$ is the optical depth at frequency ν.

2.10b NON LINEAR N.S.T.L.A.S.

The non linear approach outlined below, allows the depletion of Na to be increased by increasing $P(\nu)$ so that the depletion is no longer linear with $P(\nu)$. When tuning through the transition, then, it is required to find the value of $P(\nu)$ that will give a set depletion in Na. $\phi(\nu)$ will then be inversely proportional to that value of $P(\nu)$.

Although Δ Na is increased by increasing $P(\nu)$, so making it easier to measure, it is also true that $\frac{d}{dP}\Delta Na$ is also decreasing with $P(\nu)$ so making the measurement less sensitive. The optimum depletion to work at then is that where the product $\Delta Na \frac{d}{dP} \Delta Na$ is maximised. This occurs when

$$\frac{Na^L}{Na} = \frac{\left(\frac{Na^L(Sat)}{Na} + 1\right)}{2} \qquad 2.59$$

or when

$$\frac{P}{K} = \frac{Na^L(Sat)}{Na} \qquad 2.60$$

This depletion however is (as might be expected) the point where Na^L is most sensitive to inhomogeneities in the pump laser beam. The effects of variations in the power density across the pump laser beam are discussed in Section 2.7a.

When working in this non linear mode however, it is essential that the transition be optically thin at the pump laser frequency or the pump laser intensity will vary down the sample column in a manner which will be difficult to predict. As a general rule this technique should not be used where the optical depth is greater that 0.01, say if an accuracy in $\phi(\nu)$ of better than 1% is required.

2.10c THE REQUIREMENTS FOR THE PROBE LASER.

The probe laser measures the change in Na by monitoring the change in opacity on the probe transition. The optical depth of the probe transition is measured by taking the log of the ratio of the input and output intensity of the probe laser, so that

$$\ln \frac{P(\nu)}{\dot{P}(\nu)} = \tau(\nu)$$

$$\text{or} \quad \dot{P}(\nu) = P(\nu)\, e^{-\tau(\nu)} \qquad 2.61$$

Where $P(\nu)$ and $\dot{P}(\nu)$ are the input and output power densities of the probe laser tuned to frequency ν.

The change in the optical depth $\Delta\tau(\nu)$ is found by measuring the change in laser power density $\Delta\dot{P}(\nu)$. In the linear mode the change in optical depth will be a linear function of the change Na, or

$$\frac{\Delta\tau(\nu)}{\tau(\nu)} = \frac{\Delta Na}{Na} \qquad 2.62$$

In the non linear mode, the stimulated emission rate from the upper level of the pumped transition will mean $\Delta\tau(\nu)$ and ΔNa are not linearl y related, however, since ΔNa and hence $\Delta\tau$, would be kept a constant, in this mode this should not matter.

The relationship between $\Delta\tau$ and $\Delta\dot{P}(\nu)$ is found from eqn 2.56.

$$\dot{P}(\nu) + \Delta\dot{P}(\nu) = P(\nu)\, e^{-\tau(\nu)}\, e^{-\Delta\tau(\nu)} \qquad 2.63$$

$$\text{then} \quad \frac{\Delta P(\nu)}{\dot{P}(\nu)} = \exp -\left[\left(\frac{\Delta\tau(\nu)}{\tau(\nu)}\right)\tau(\nu)\right] - 1 \qquad 2.64$$

$$\text{or} \quad \frac{\Delta\tau(\nu)}{\tau(\nu)} = \frac{1}{\tau(\nu)} \ln\left[\frac{\dot{P}(\nu)}{\dot{P}(\nu)+\Delta P(\nu)}\right] \qquad 2.65$$

Eqn 2.65 shows that for any given change in Na and hence change in optical depth, the fractional change in the intensity of the probe laser will be a function of the optical depth.

Figure 2.11 shows how $\Delta\dot{P}(\nu)$ varies with $\tau(\nu)$ for a 1% and a 5% variation in Na.

For maximum sensitivity then, the probe laser should be tuned to the highest optical depth possible whilst maintaining accuracy in the measurement of $\dot{P}(\nu)$.

In practice this should only be limited by photon shot noise. For example, if an accuracy of 1% was required in the measurement of $\dot{P}(\nu)$ then 10^4 detected photons are required during the integrating period of the detection system to achieve a signal to noise ratio of 100. Assuming the detector has a quantum efficiency of 10% then 10^5 photons are required.

Assume the probe laser is a CW dye laser and the pump laser is a flashlamp pumped dye laser with a pulse length of 300nsec. The integrating period is then 300nsec. A photon flux of 3×10^{11} photons/sec is then required for $\dot{P}(\nu)$ CW dye lasers are capable of 300mw power which is a photon flux of 10^{18} photons/sec at 5000Å for $P(\nu)$

Now

$$\ln\frac{\dot{P}(\nu)}{P(\nu)} = \ln\frac{10^{18}}{3\times10^{11}} = 15.02 = \tau(\nu)$$

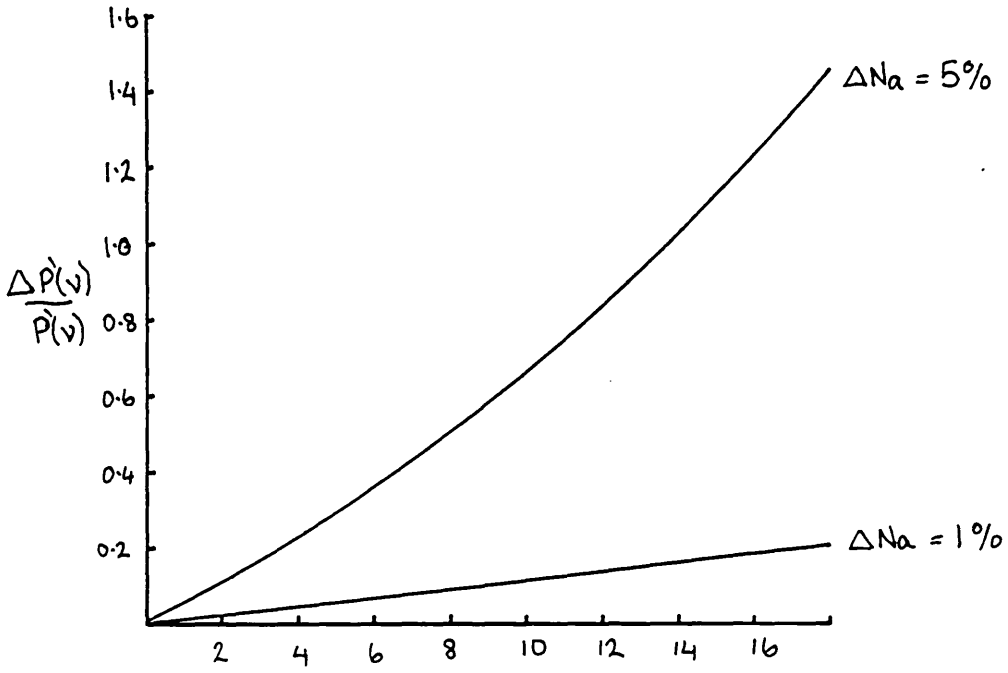

Fig. 2.11

Variation of laser output intensity with optical depth for a given change in Na.

This plot shows how a probe laser intensity will vary for given changes in Na as a function of optical depth.

For such a system it should then be possible to achieve an increase in the sensitivity of the measurement of $\Delta Na/Na$ by a factor of 15 or more, (see fig. 2.11) by tuning the probe laser to a point in the probe transition where the optical depth is 15.

This overcomes to some extent, the objection to the use of the linear N.S.T.L.A.S. that only small values of $\Delta Na/Na$ could be tolerated; since a one percent change in Na registers as a 15% change in $P'(\nu)$ (fig. 2.11) which would be relatively easy to measure and would reduce the accuracy requirements on the measurement of $P'(\nu)$ by a factor 16 over measuring the same change at optical depth one.

2.10d WHEN TO USE S.T.L.A.S.

S.T.L.A.S. is most useful when the optical depth of the probe transition (the transition of interest) is high. Thus it is useful for looking at the cores of lines but becomes progressively less sensitive as the change in the intensity of the probe laser due to the transition opacity approaches the error in measuring that intensity.

Thus, in the line wing where the line becomes optically thin, S.T.L.A.S. might not be as suitable as N.S.T.L.A.S.

2.11 SATURATED THREE LEVEL EMISSION SPECTROSCOPY

Figure 2.12.shows a schematic diagram of the method. The lineshape of the transition of interest, b to c, is obtained in emission, in the normal way. The emission profile is then taken again, but this time another transition, a to b, sharing the same upper level, b, as the transition of interest is irradiated. The b to c emission will be enhanced for this second lineshape profile, but the lineshape should otherwise remain the same.

If there are any impurity contributions to the b to c lineshape, these will not be enhanced by the action of the laser on the a to b transition. When the two profiles are suitably normalised and one is taken from the other, the lineshape of any impurity contribution will be revealed.

As shown in figure 2.13, the upper level of the transition of interest, need not be the same as one of the levels of the pumped transition. They may be two close lying levels, b and c, which are strongly coupled by ordinary plasma processes, either by spontaneous radiation or collisionally.

Clearly, the sensitivity of this technique depends on the degree of enhancement obtained for the upper level. For maximum enhancement it is necessary to saturate the pumped transition.

Comments similar to those made in section 2.9a for S.T.L.A.S. can be made here, regarding the pump laser reproducability and beam inhomogeneity.

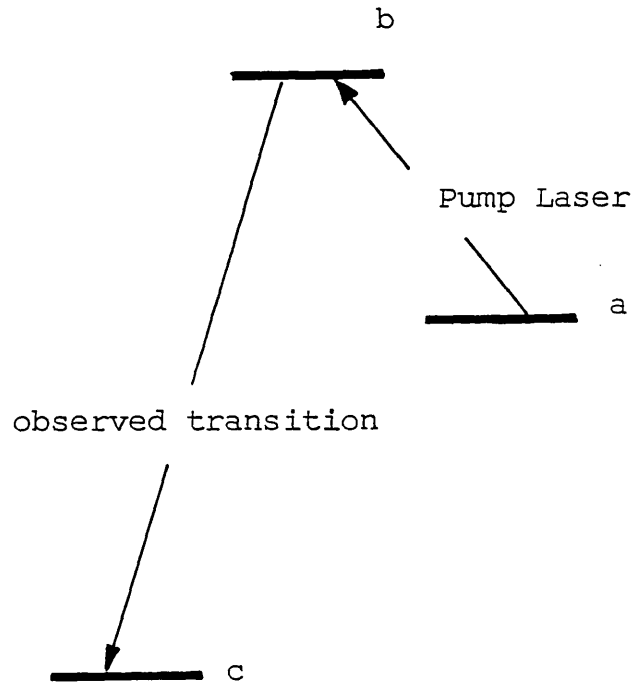

Fig. 2.12

THE LEVEL SCHEME for S.T.L.E.S.

The intensity of the emission profile on the observed transition is increased by using it as the upper level of a laser pumped transition. The relative increase will be the same for any point in the profile.

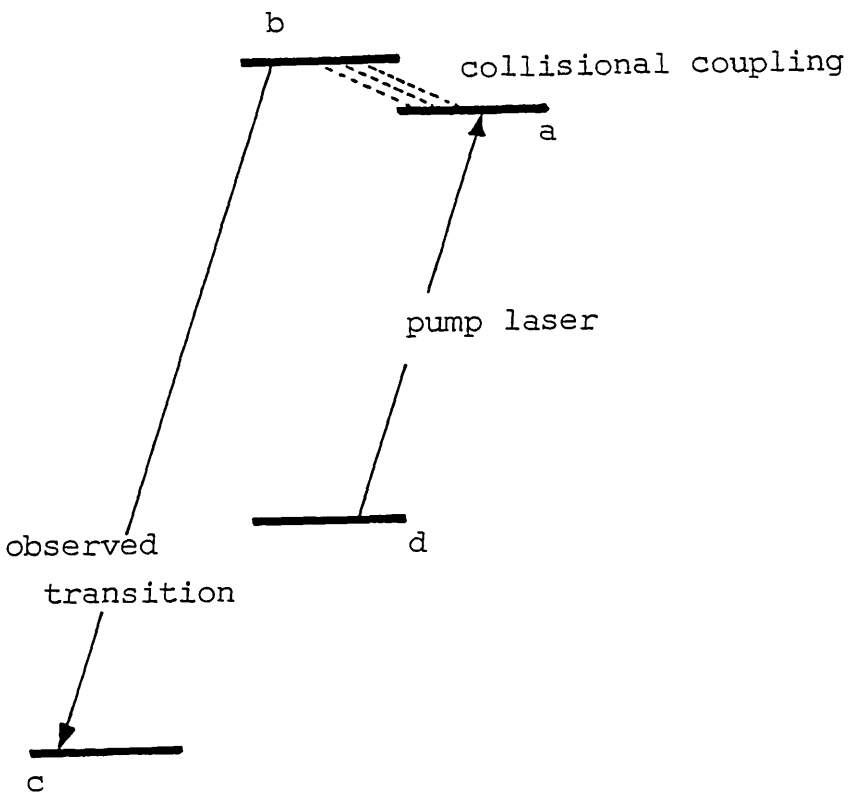

Fig, 2.13

ALTERNATE LEVEL SCHEME

FOR

S.T.L.E.S.

As for Fig. 2.12., but the upper level of the observed transition is now enhanced by collisional coupling to the upper level of the laser pumped transition.

2.11a ENHANCEMENT OF THE UPPER LEVEL IN S.T.L.E.S.

As explained in section 2.6a, in a plasma, the upper level of the pumped transition should tend to relax back to very near the population density that existed before the laser was turned on. This is due to the rates out of the upper level being generally much higher than those out of the lower level of the pumped transition. Burgess et al (1980) showed that for Hydrogen, this was not necessarily the case. For a hydrogen plasma, where $0.3eV < T_e < 0.8eV$ and $2\times10^{14}cm^{-3} < N_e < 1.2\times10^{15}cm^{-3}$ it was found, the enhancement was, in general, about 6 times greater than expected for n=3 when H-Alpha was pumped and about 12 times greater for n=4 when pumped.

The enhancements observed by Burgess et al (1980) were, in fact, about a factor of two instead of 10% as expected. Similar anomalous enhancements were seen by Huang, Kolbe and Burgess (in preparation) for Helium. No consistent reason for this anomalous enhancement has as yet been given.

The Short time enhancement that occurs soon after the laser turns on, is due to the rapid equalization of populations of the upper and lower levels. This enhancement is much greater than the long term enhancement discussed above, however, accurate measurements of this 'spike' would be difficult due to its transient nature.

Fig. 2.13 shows a scheme which makes use of sensitised fluorescenceto enhance the upper level of the transition of interest. An estimate of the amount of enhancement to be expected can be obtained in the following way.

2.11b LEVEL ENHANCEMENT EXPECTED due to SENSITIZED FLUORESCENCE.

For a time stationary system in the absence of any laser pumping, the rate equation for level b, may be written (from eqn 2.2)

$$D_b N_b = C_b$$

With the laser turned on, there is an enhanced population in level a, which in turn leads to an increase in the collisonal rate from level a to levelb. The new rate equations for level b may be written

$$\frac{dN_b(t)}{dt} = - D_b N_b(t) + C_b + D_{ba} \Delta N_a \qquad 2.66$$

Strictly speaking, Cb does not remain constant, since the populations of other levels collisionally (or radiatively) coupled to level a, will also be affected, so affecting their rates into level b. However, it is assumed, level b is tightly coupled to a. Solving for Nb(t).

$$N_b(t) = N_b(t=0) + \frac{\Delta N_a D_{ab}}{D_b} \left(1 - e^{-D_b t}\right) \qquad 2.67$$

for $t \to \infty$,

$$\Delta N_b = N_b(t) - N_b(t=0) = \frac{\Delta N_a D_{ab}}{D_b} \qquad 2.68$$

$$\frac{\Delta N_b}{N_b} = \frac{\Delta N_a D_{ab}}{C_b} \qquad 2.69.$$

The relative increase in Nb is proportional to the relative increase in the total rate into level b, which is a function of the rate coefficient Dab.

Burgess et al. (1980) looked at the sensitized fluorescence of H-Beta and H-Gamma while pumping H-Alpha. A summary of their results is given below in Table 2.2.

$N_e\,(cm^{-3})$		9×10^{14}	4×10^{14}	2×10^{14}
$T_e\,(eV)$		0·7	0·45	0·37
$\frac{\Delta N_4}{N_4}$	theory	0·02	0·08	0·33
	exp.	0·4	0·85	0·73
$\frac{\Delta N_5}{N_5}$	theory	0·00	0·02	—
	exp.	0·2	0·42	—

Table 2.2

The experimental enhancements given in Table 2.2, show the level of enhancement that may be expected from sensitized fluorescence - generally less than a factor of 2. Eqn 2.62 shows that the time scale over which the change in population takes place is of the order of 1/Db. As explained above, however, the change in Na does not take place instantaneously, but in a time scale of the order 1/Da. (Burgess and Skinner, 1974).

For the plasma conditions set out in Table 2.1

$$5\times10^{-8}\,\text{sec} > 1/D_3 > 10^{-8}\,\text{sec} \quad \text{and} \quad 1/D_{45} \lesssim 10^{-8}\,\text{sec}$$

The pump laser should be on for periods longer than 1/Da or 1/Db, whichever is the longer.

2.12 A COMPARISON OF THREE LEVEL LINESHAPE TECHNIQUES.

In the preceeding sections of this chapter, three techniques have been analysed, by which an impurity free lineshape may be obtained. For all three techniques the sensitivity and hence efficacy of the technique depends upon the relative change in the observed parameter induced by the perturbing laser.

S.T.L.A.S. may be used where the transition of interest has a high optical depth. It will thus be generally restricted to use for looking at the line core. Practically, its use is restricted to optical depths greater than 0.01.

N.S.T.L.A.S. on the other hand, when used in the non linear mode, is restricted to use where the optical depth of the transition of interest is below 0.01. If the probe transition has high optical depth (i.e. $\gtrsim 10$), then the sensitivity of N.S.T.L.A.S. can be very good. S.T.L.A.S. and N.S.T.L.A.S. are seen to be complimentary then in their use across a complete line profile.

Where $\tau(\nu) >$ 0.01, N.S.T.L.A.S. can only be used in its linear mode, but this reduces the sensitivity of the technique severely, even if high optical depth is available on the probe transition. S.T.L.A.S. is therefore to be prefered over linear N.S.L.A.S. at the line core. S.T.L.A.S. is also to be prefered over S.T.L.E.S., the emission technique, for reasons of sensitivity. The induced depletions in S.T.L.A.S. are of the order of 10, whereas the enhancements in S.T.L.E.S. will normally only be of the order of 2 or less.

Also for S.T.L.E.S. the emission observed, is generally not from the laser pumped region alone, which lessens still further the observed enhancement due to laser pumping. In general then, S.T.L.A.S. is about 5 or more times more sensitive than S.T.L.E.S.

S.T.L.A.S. and N.S.T.L.A.S. are confined, in general, to series where the pumped and probed transitions are in the visible or near visible. Using frequency doubling or tripling techniques, it is possible to extend these techniques to the U.V. or even V.U.V. but tunable laser powers in these regions presently do not exceed a few tens of kilowatts. S.T.L.E.S. on the other hand can be used with far greater flexibility over the entire spectrum.

2.12a THE CHOICE OF TECHNIQUE FOR THE H-BETA LINESHAPE EXPERIMENT

The purpose of the H-Beta lineshape experiment, was to look for possible impurity contributions at the core of the line in the region of the central dip. The optical depth of the centre of H-Beta, for the Z-pinch plasma source used, was about 1.5. This immediately restricts the choice to the use of S.T.L.A.S. and so this was the chosen technique.

REFERENCES

Burgess D.D.,Kolbe G.,Ward J.M., J.Phys.B. 11, 2765, (1978).

Burgess D.D.,Myerscough V.P.,Skinner C.H.,Ward., J.Phys.B. 13, 1675, (1980)

Burgess D.D.,Skinner C.H., J.Phys.B. 7, L297, (1974)

Daily J.W., App.Op. 16, 2322, (1977)

McIlrath T.J.,Carsten J.L., Phys.Rev.A. 6, 1091, (1975).

Shoub E., Astrophys.J.Supp. 34, 259, (1977).

Spitzer L.,'The Physics of Ionizer Gases'. (1949)

Vidal C.R.,Cooper J.,Smith E.W.,J.Quant.Spectrosc. Radiat.Transfer. 10, 1011, (1970)

Vriens L.,Smeets A.H.M., Phys.Rev.A. 22, 940, (1980)

CHAPTER 3.

APPARATUS and EXPERIMENTAL METHOD

SECTION 1 : APPARATUS

3.1.1. PLASMA SOURCE

The plasma source used in all the experiments described in this thesis, was the afterglow phase of a 70cm linear Z pinch. The construction of the plasma vessel and the associated vacuum, plumbing and electrical circuitry, were practically identical to another device used for a number of lineshape and collision rate experiments in this laboratory. See e.g. Burgess and Cairns (1970 and 1971), Burgess and Mahon (1972), and Burgess, Myerscough, Skinner and Ward (1980).

The Plasma vessel is shown in Fig. 3.1 and consisted of a 70cm long pyrex tube of internal diameter 4.5cm. The hollow ring electrodes which support the tube at each end allow an uninterupted view down the central axis of the vessel. The vessel was rendered vacuum tight by means of 'O' ring seals between the electrodes and the pyrex tube: the quartz windows on the ends of the vessel similarly had 'O' ring seals. The six earth return bars were placed on a radius of 7cm around the pyrex tube.

The filling gas was flowed continuously through the vessel, by a rotary pump, which exhausted the gas at one end while the gas input was via a needle valve at the other end. The needle valve was used to control the pressure, which was measured using a McCleod gauge. A liquid nitrogen cold trap was placed in the exhaust line to prevent oil fumes from the rotary pump con-

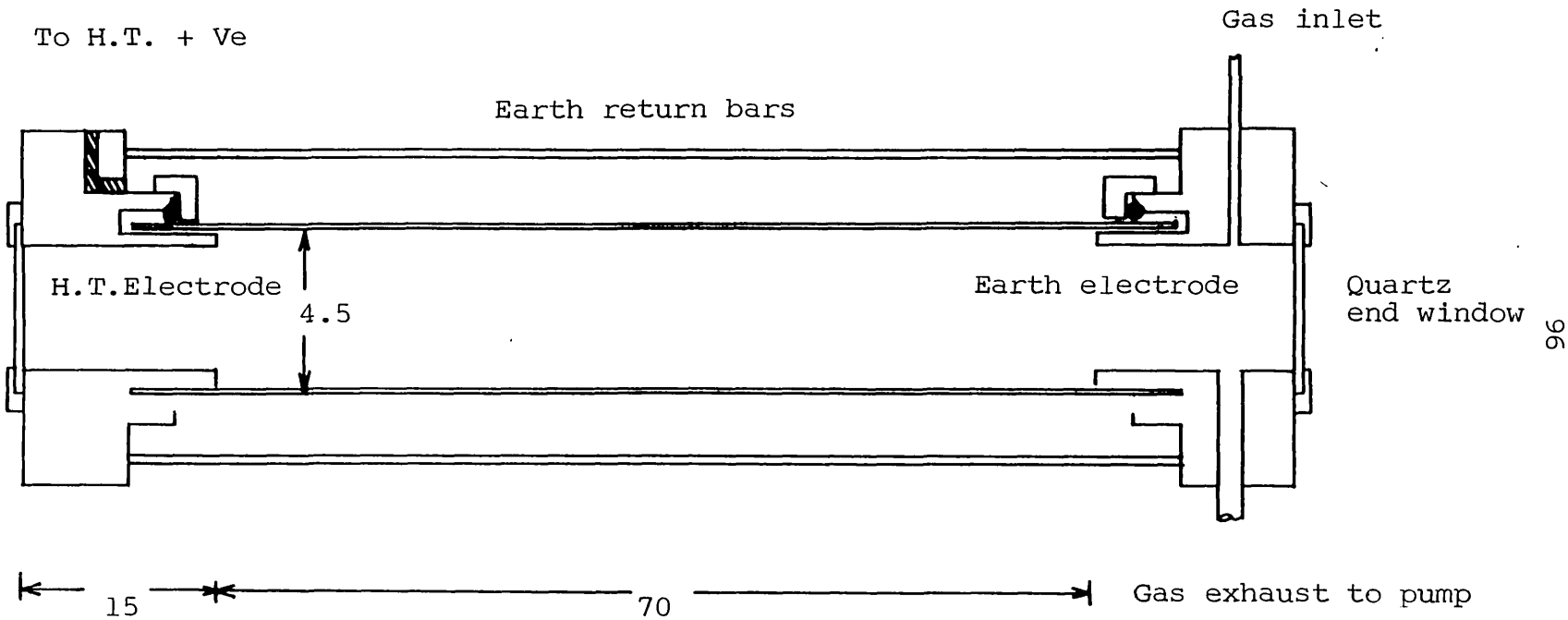

Fig. 3.1

DIAGRAM of LINEAR Z PINCH. (not to scale)

taminating the vacuum vessel.

The electrical circuit is shown in Fig. 3.2. It consisted of a 0.5m.f.d. rapid discharge capacitor, which was charged to 20 KV and discharged into the plasma vessel via the spark gap. A 3ohm damping resistor was used to prevent ringing.

3.1.2. ELECTRON DENSITY

This was measured, using an interferometric technique due to Ashby and Jephcott (1963). The experimental method was similar to that used by Mahon (1973) and will not be described in detail here.

Each fringe on the resulting interferogram represented a change in the electron density of Δ Ne, where

$$\Delta N_e = \frac{m_e \varepsilon_0 8\pi^2 c^2}{e^2 L \lambda} \quad m^{-3} \qquad 3.1$$

Where L is the length of the plasma column and λ is the laser wavelength.

Figs 3.3 and 3.4 show plots of electron density versus time after peak current for Hydrogen and Helium respectively.

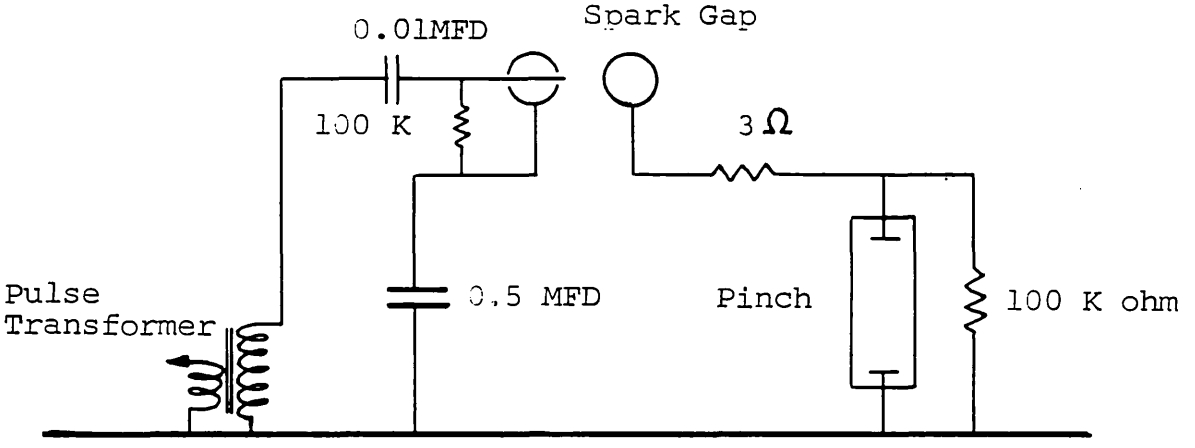

Fig. 3.2

ELECTRICAL CIRCUIT of Z PINCH

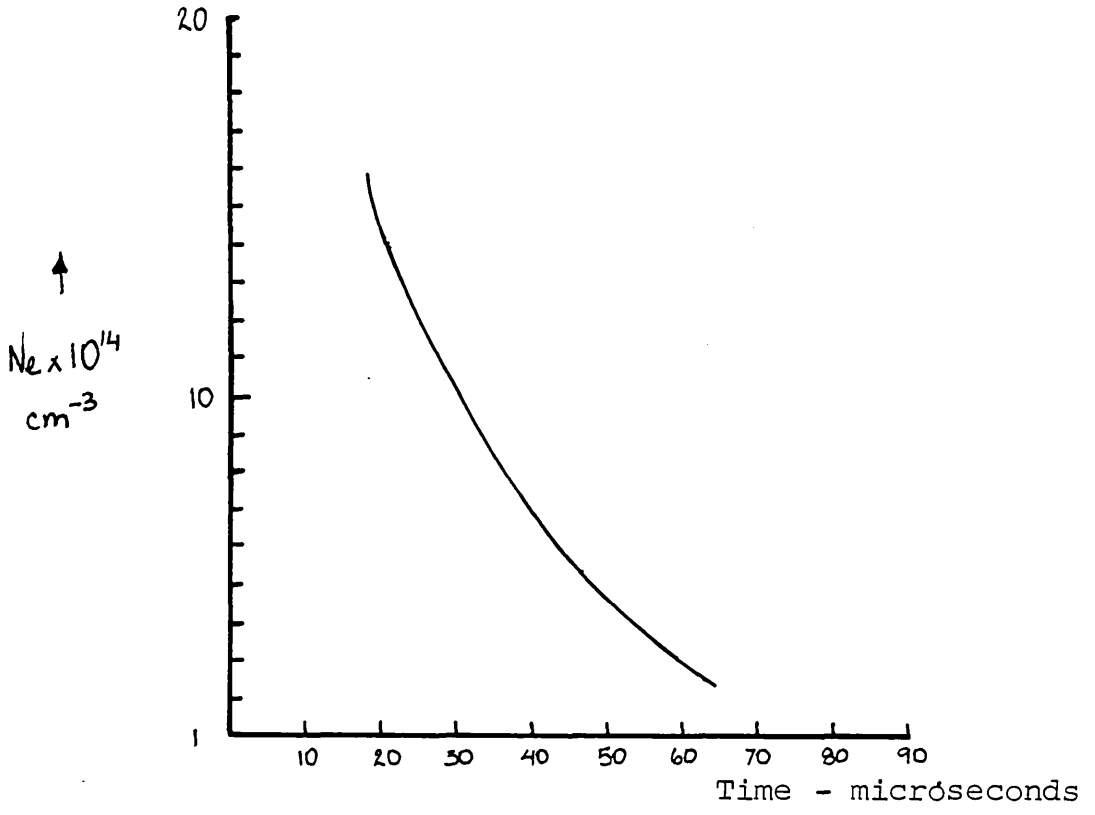

Fig.3.3

ELECTRON DENSITY for HYDROGEN

AFTERGLOW PLASMA

Filling pressure was 0.450 Torr

Charging voltage was 20 KV.

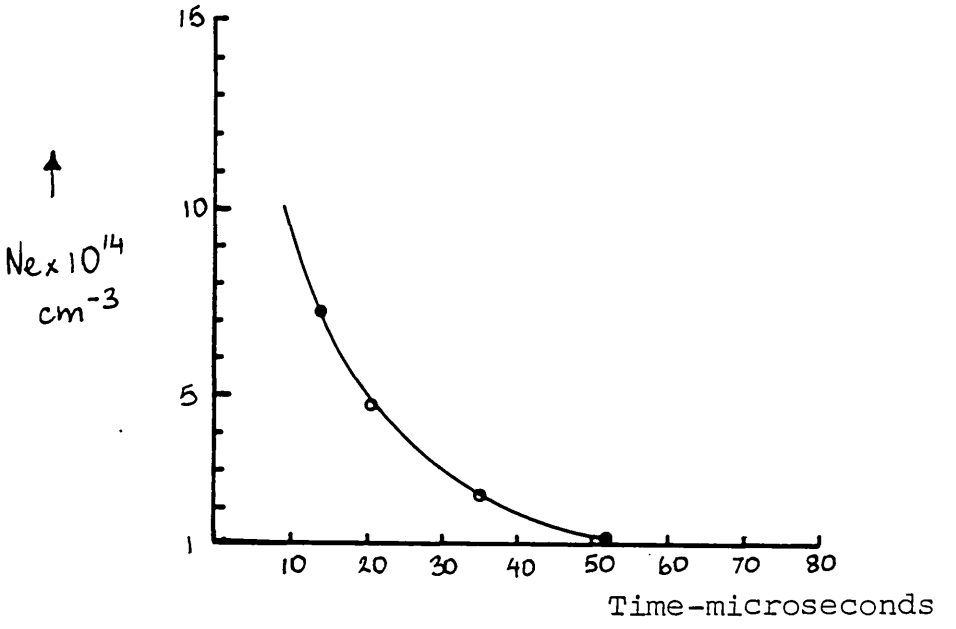

Fig. 3.4

ELECTRON DENSITY in HELIUM

AFTERGLOW PLASMA

Conditions were 20 KV charging voltage.

Pressure was 0.1 Torr

3.1.3. ELECTRON TEMPERATURE - HYDROGEN

The electron temperatures were measured by Thomson Scattering. This work was performed by Mark Nicholson, to whom I am extremely grateful. The experimental method is detailed in the thesis of M.Nicholson (1983) Fig. 3.5 shows a plot of electron temperature as a function of time after peak current for Hydrogen.

3.1.4. ELECTRON TEMPERATURE - HELIUM

The electron temperature was determined by Thomson Scattering. For the He plasma for a time 18 microseconds after peak current when the electron density was $Ne = 5 \times 10^{14} cm^{-3}$. This temperature was found to be 1,35 eV.

However, this Thomson Scattering measurement was not performed until after the publication of the results of the collision rate measurements by Kolbe, Huang and Burgess (1982). For thepurposes of that publication, the temperature was derived by determining the He II level populations for n=3,4,6,7,8, and 9, by calibrated emission measurements.

A He II collisional radiative model (described in Appx 1) was then run, varying the temperature in an iterative manner, to give the best agreement between theoretical and experimental level populations. For a temperature of 4.3eV the predicted level populations agreed with those measured, to within a factor of two.

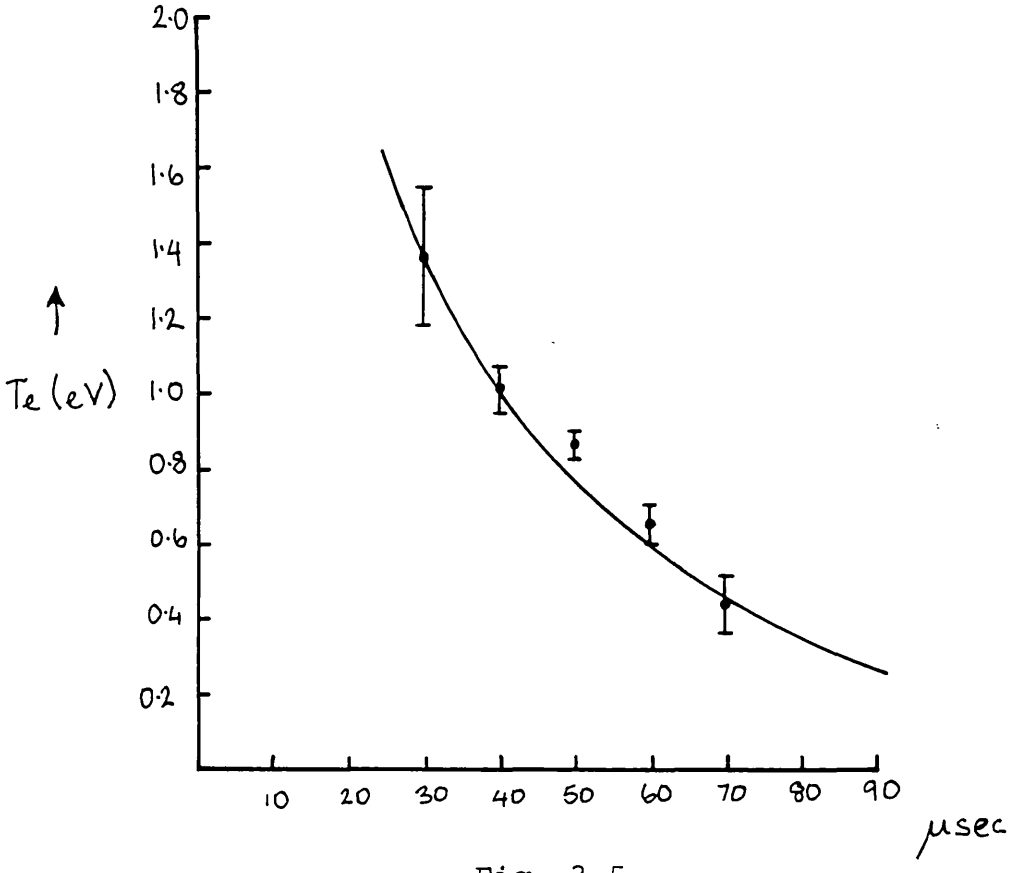

Fig. 3.5

ELECTRON TEMPERATURE of HYDROGEN

AFTERGLOW PLASMA

Obtained by Thomson Scattering for a charging voltage of 20 KV and a filling pressure of 0.45 Torr .

An exponential fit to the data (solid line) gives

$$Te = (3.16 \pm 0.03)\exp - (t/36.4 \pm 2.7)\,eV$$

3.1.5. COAXIAL FLASHLAMP LASER SYSTEM

The coaxial flashlamp pumped lasers used, were based on a de-mountable design, described in the thesis of C.H. Skinner (1974). The differences between the present laser system and that of Skinner being ones of detail, making the present laser system more reliable.

The electrical circuit of the laser is shown in Fig. 3.6. It consists of a rapid discharge, low inductance, 0.5 microfarad, 30 K.V. capacitor; whose charge is switched into the lamp via a low inductance, mid plane type spark gap, developed by S.J.Fielding and J.Wheaton. (A'mid plane' spark gap is one where the trigger electrode is placed equidistant from the two main electrodes and is biased to a voltage equal to half the bank voltage)

3.1.6. THE COAXIAL LASER TRIGGERING SYSTEM

The spark gap of the Skinner laser was triggered by switching a 250 volt pulse into a 1:100 pulse transformer. The 25 K.V. pulse generated, took about 20 microseconds to rise. In consequence, it proved difficult to obtain jitter times of less than a microsecond for the laser output.

Since the laser pulse was only 300 nsec long, it was a problem to try and synchronize the laser pulse to any other short time event, such as another laser pulse, or to use a Pockels cell to switch out part of the laser pulse and give it a fast leading or trailing edge. This

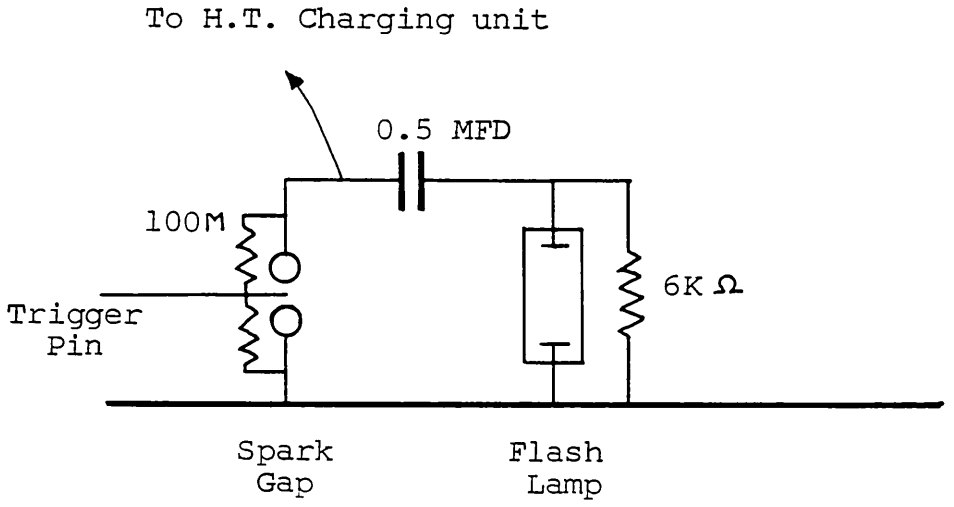

Fig. 3.6

ELECTRICAL LAYOUT for COAXIAL

FLASHLAMP PUMPED DYE LASER

problem was solved by building a system, first developed at Culham Laboratory, for the fast switching of spark gaps This syatem consisted of a Thyratron trigger unit, which discharged a 1000 p.f. capacitor charged to 10 K.V.into a 50 ohm cable. At its other end, the cable was attached to the trigger pin of the spark gap via an isolating 1000p.f. capacitor - the cable side of which was grounded via a 2.7K resistor, see Fig. 3.7. There was thus an impedence missmatch at this point of the cable, resulting in a doubling of the voltage pulse to 20 K.V.

If the electrode separation in the spark gap, (about 3mm) and the spark gap pressure, (about 3lb per sq. in.) were adjusted to give a gap breakdown voltage some 500 volts higher than the bank charging voltage, (about 20 K.V.); then the jitter time, using the thyratron trigger unit, was about 10 n.sec. (These trigger units are now marketed by Chelsea Instruments.) The circuit diagram of the trigger unit is shown in Fig. 3.8.

Given the small jitter time in triggering the laser flashlamps, it became possible to use two flashlamps in conjunction, as an oscillator-amplifier combination.

Fig. 3.9 shows the complete optical layout of the oscillator-amplifier combination. The oscillator was tuned using two Fabry Perot etalons. A limiting aperture was placed between the oscillator and the amplifier. This served to prevent, so called, 'whispering' modes, that is, off axis high divergence radiation being re-

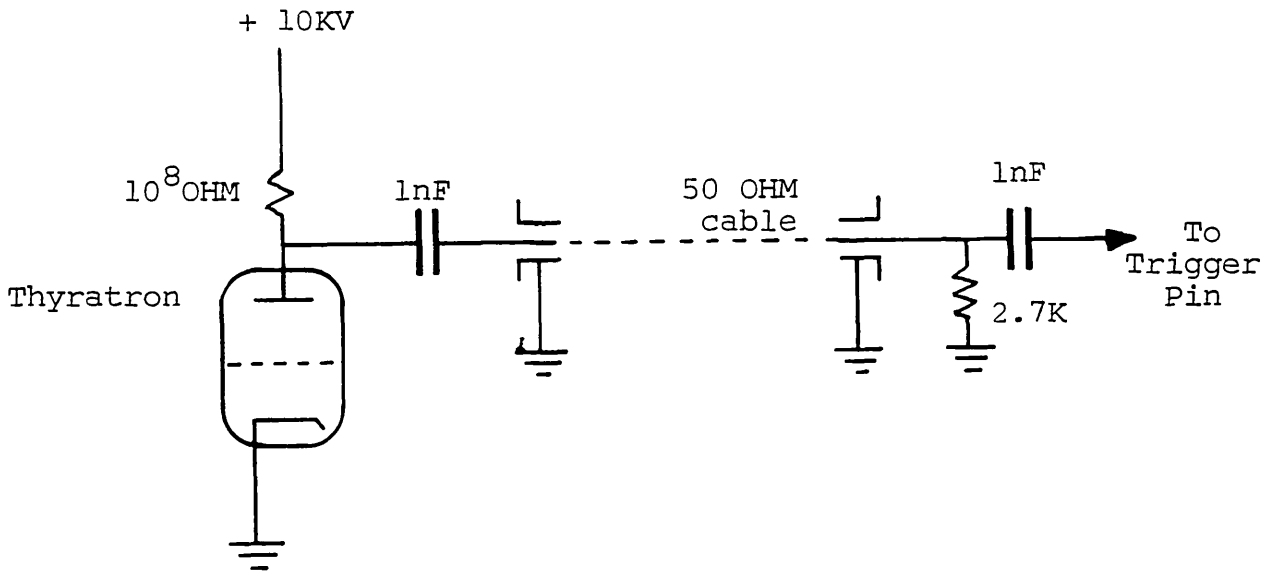

Fig. 3.7

SCHEMATIC of TRIGGERING SYSTEM

for FLASHLAMP LASER

A 1nF capacitor charged to 10KV is discharged into a 50 ohm transition line by a Thyratron. The large impedence mis match at the other end of the cable caused voltage doubling, so creating a 20KV pulse rising in 10nsec to trigger the laser spark gap.

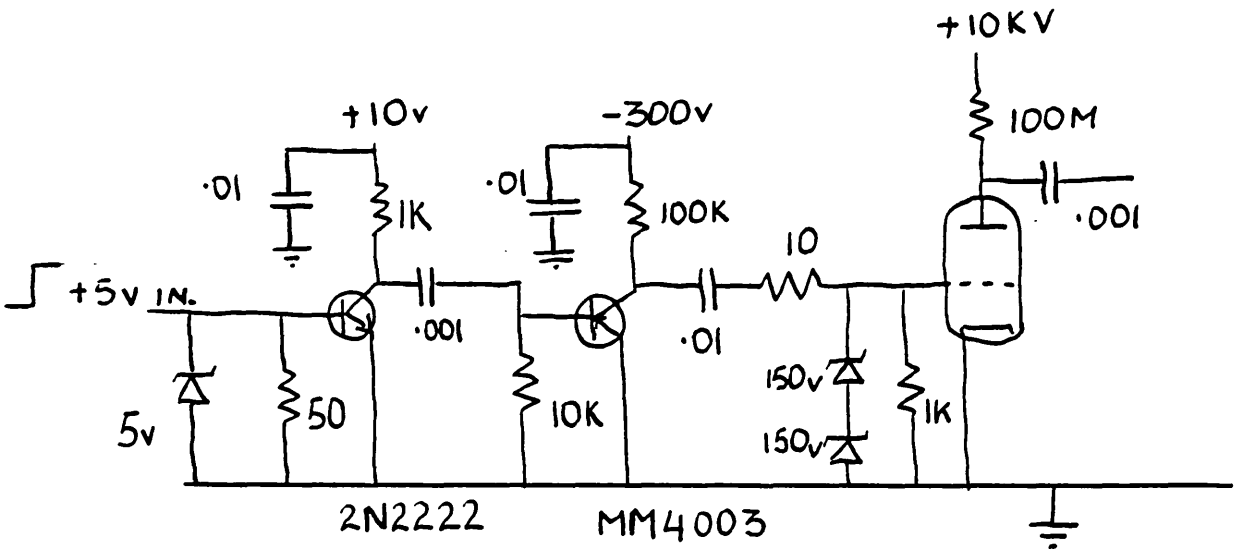

Fig. 3.8

ELECTRICAL CIRCUIT for TRIGGERING the THYRATRON of Fig. 3.7

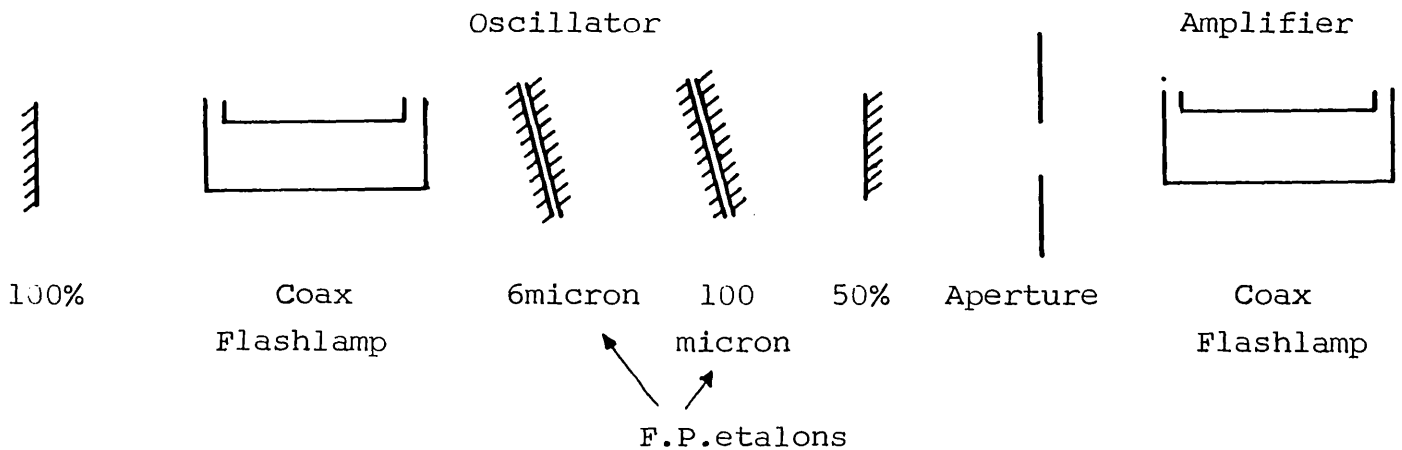

Fig 3.9

LAYOUT of OPTICAL COMPONENTS for

OSCILLATOR - AMPLIFIER COAXIAL FLASHLAMP

PUMPED DYE LASER.

flected at grazing incidence, off the walls of the dye tube in the amplifier.

Using one 6 micron gap etalon in the oscillator cavity, gave bandwidths of the order of 5Å. Adding a 100 micron gap etalon, reduced the bandwidth to about 0.3Å. The powers available, using the tuned oscillator-amplifier system, were about 600 K.W. The divergence was measured to be about 2 m.radians F.W.H.M.

3.1.7. THE NITROGEN LASER

The principles of operation of the Nitrogen Laser has been well described by Cherrington (1979). In this section, only the relevant details of the laser used, will be given.

The laser was built following a lumped Blumlein voltage doubler design, described by C.L.Sam (1976). Fig. 3.10 shows a schematic diagram of the laser. The cavity was 30cm long and had a 100% Aluminium coated rear mirror and a quartz parallel flat was used as the output mirror. The 2mm radiused copper electrodes were set 25mm apart. The capacitor bank consisted of twenty 1000p.f.Barium Titanate capacitors, ten of which were placed along each electrode. The switch was an English Electric CX1571 thyratron, which was especially designed for use with pulsed lasers of this sort, as it will still work in a glow discharge mode regardless of whether the 'anode' polarity is positive or negative. This is of importance since voltage reversals can take place on failure of the

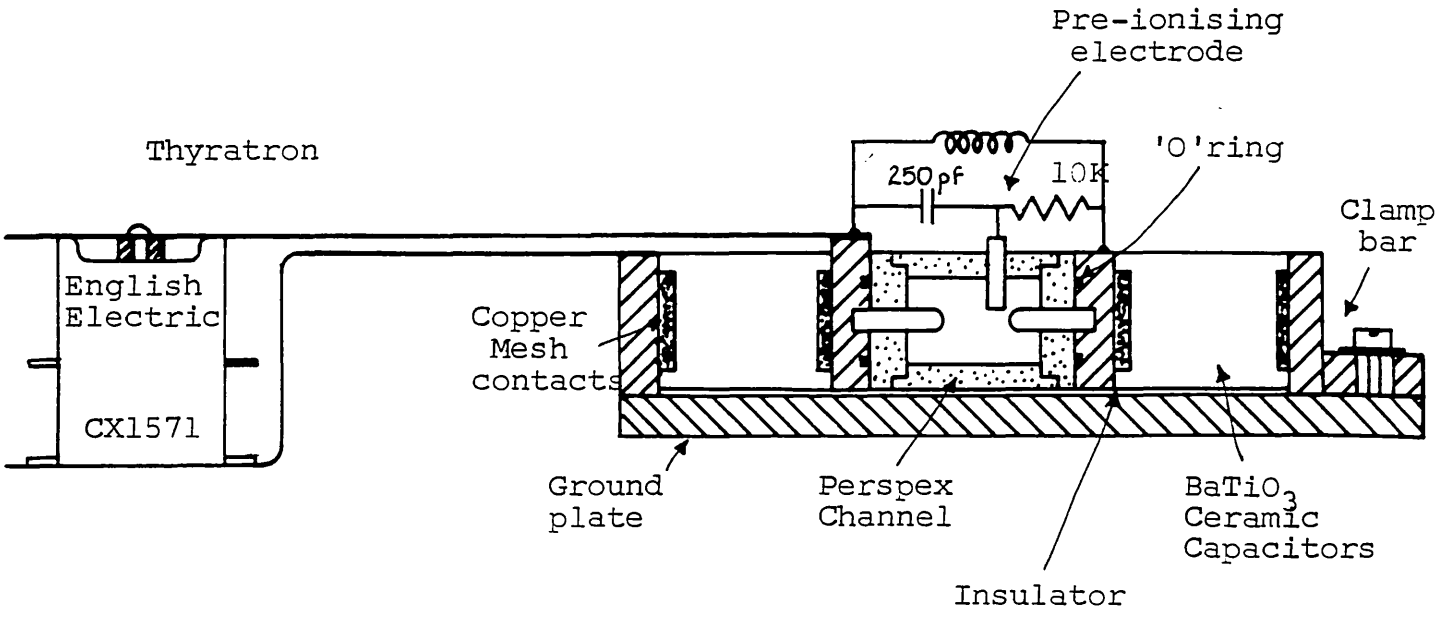

Fig. 3.10

CROSS SECTION VIEW of N_2 LASER.

The gap between the main electrodes is 2.5cm and their length is 30cm.

The laser is held together by a sliding clamp fixed by five screws.

The main electrodes project through the perspex channel which is rendered vacuum tight by two large 'O' rings surrounding the electrodes.

discharge channel to break down, so causing ordinary thyratrons to break down in a spark discharge mode. Repeated spark discharges would quickly destroy the thyratron, resulting in very short thyratron life.

To promote reliable breakdown and uniform discharge in the discharge channel, a varient of the Lambert and Pearson type preioniser circuit was constructed. This consisted of a series of 4 electrodes placed equally above the unswitched electrode, as shown in Fig 3.10. Due to the much smaller gap, the preioniser circuit will breakdown marginally before the main discharge. The ions and U.V. radiation produced in the preioniser discharge will help seed the main discharge and promote a uniform breakdown along the channel.

The performance of this Nitrogen Laser is summarised in Table 3.1. The circuit used to trigger the thyratron is shown in Fig. 3.11.

The entire laser plus power supplies was placed in a 16 gauge steel box to prevent radiation of electrical noise. The layout of the laser is shown in Fig. 3.12.

NITROGEN LASER PERFORMANCE - TABLE 3.1

Pulse delay = 500n sec after input pulse

Jitter time = 10 n sec

Pulse width = 3 n sec F.W.H.M.

Optical output energy = 0.5 m.J.

Efficiency : $\frac{\text{Optical output energy}}{\text{Stored electrical energy}} = 3 \times 10^{-4}$

Bank voltage for all measurements was 13 K.V.

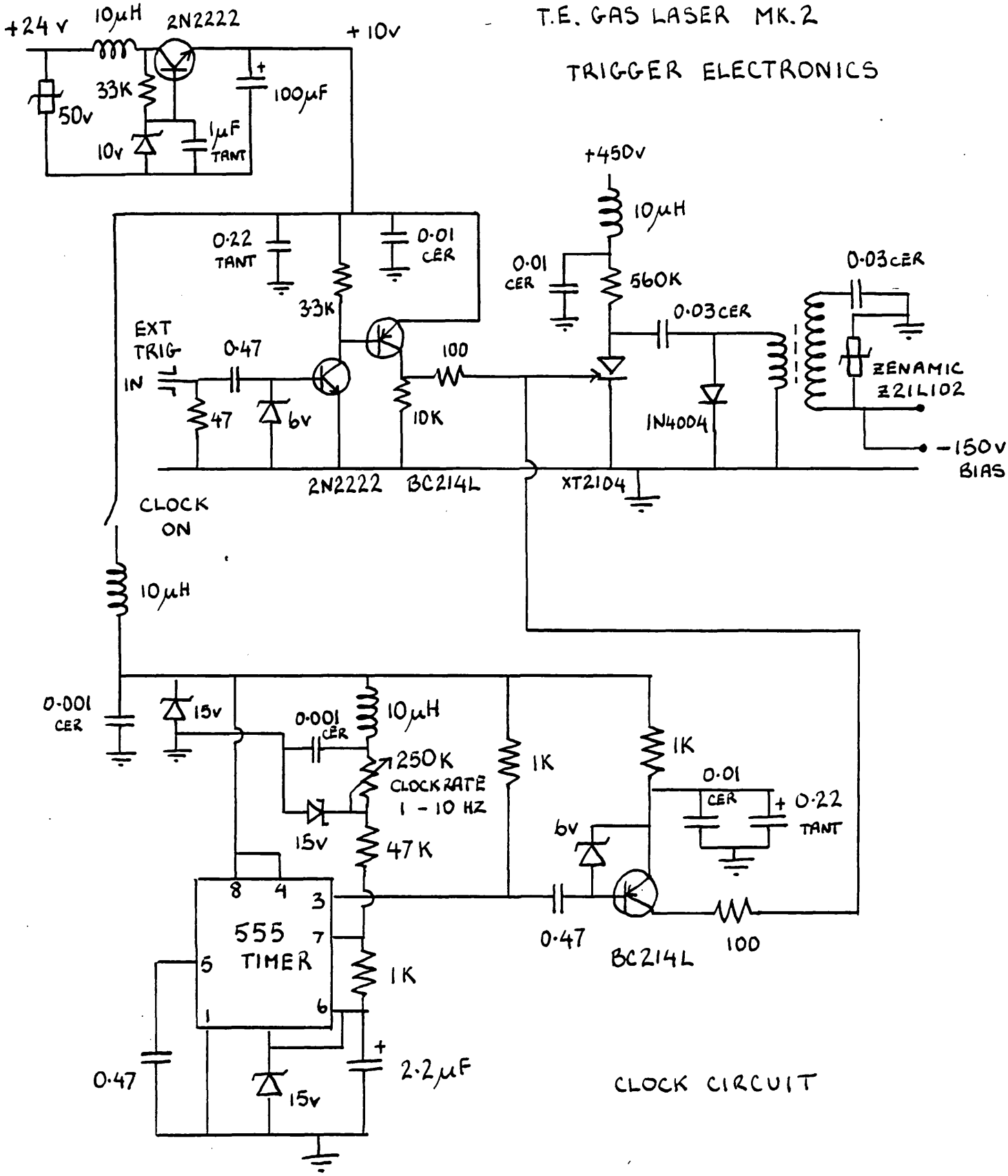

Fig. 3.11

CIRCUIT DIAGRAM of TRIGGER CIRCUIT

for THYRATRON of N_2 LASER

Fig. 3.12

A PHOTOGRAPH of the NITROGEN LASER

(See overleaf)

In the foreground is the circuitboard containing the thyratron trigger circuitry (Fig.3.11) Behind that is seen the thyratron itself which is connected to the discharge channel via a flat plate transmission line. On the top of the perspex discharge channel can be seen the capacitor resistor networks serving the four pre-ionizing electrodes. On the far side of the discharge channel can be seen 10 of the $BaTiO_3$ capacitors held in place by the clamp bar.

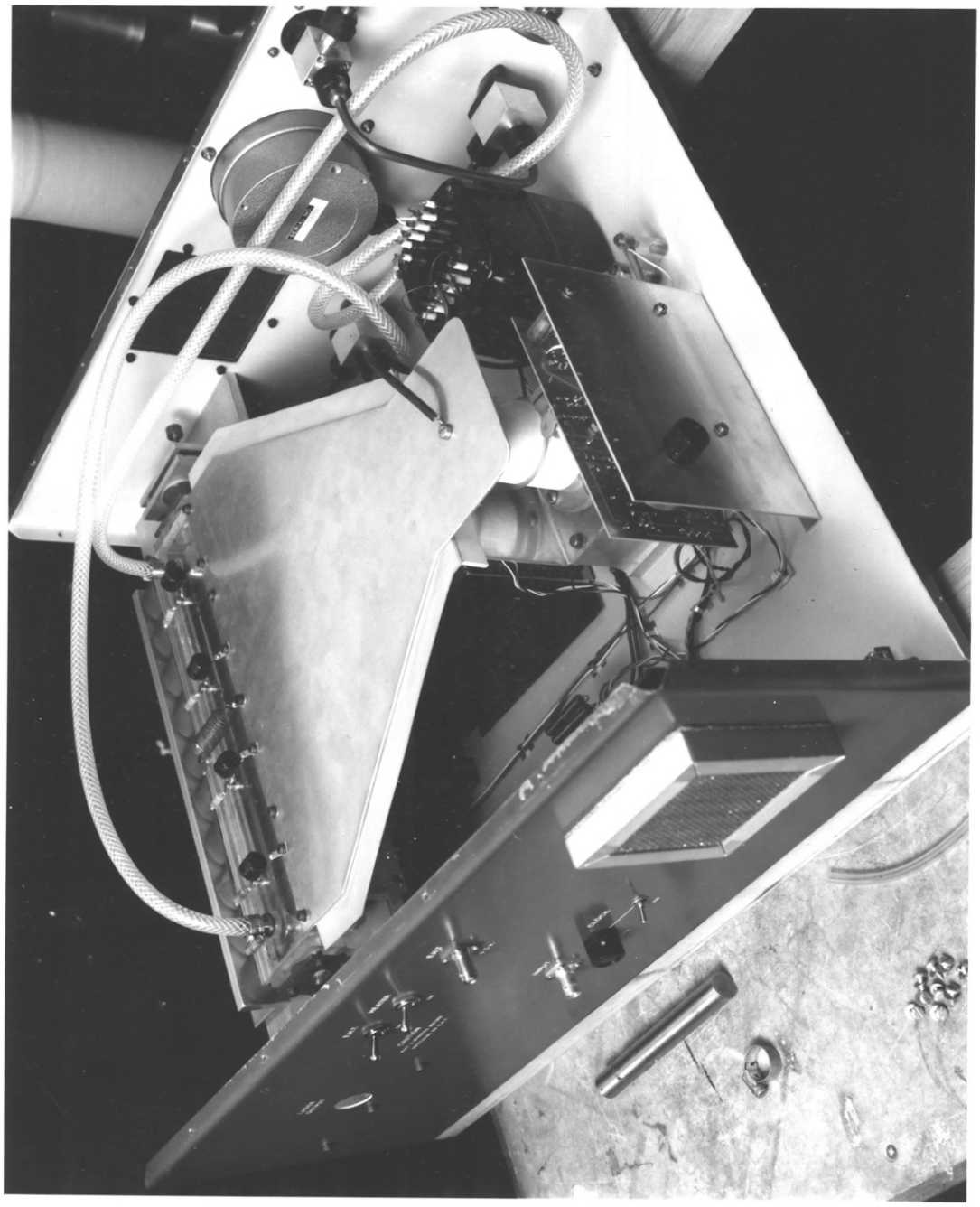

3.1.8. LASER PUMPED DYE LASER

Various forms of intra-cavity beam expansion systems have been published for use in transverse laser pumped lasers. Having tested the telescope beam expander, (Hansch, 1972), The prism beam expander, (Hanna, Karkkainen and Wyatt, 1975) and the grating beam expander, (Shoshan, Danon and Oppenheim, 1977), it was decided to use the grating beam expander system on the grounds of relative cheapness, ease of allignment and low bandwidth. A detailed comparison of these various arrangements can be found in a paper by Trebino, Roller and Siegman (1982)

Fig. 3.13 shows a schematic diagram of the laser, using the grating as the beam expander. The grating is used at grazing incidence which gives it high dispersion. The output is taken from the zero order reflection off the grating.

Fig. 3.14 shows the final layout of the constructed dye laser. The tuning mirror mount has fine and coarse adjustment. The coarse adjustment micrometer acts directly on the mirror mount which swings on bearings attached to the fine adjustment arm. The coarse adjustment micrometer is mounted on the fine adjustment arm. The fine tuning is affected by means of a large diameter, 2 micron per division, micrometer acting upon a spring loaded one degree wedge. The sloping edge of the stainless steel wedge acts against a graphite loaded teflon ball set in to the fine adjustment arm. The datum side of the wedge slides against a stainless steel flat.

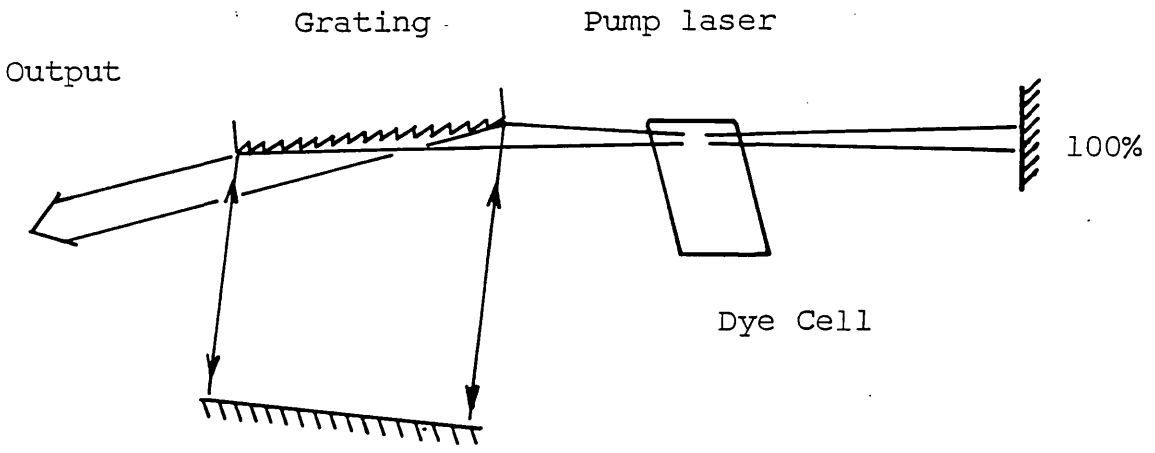

Fig. 3.13

LAYOUT of GRATING BEAM EXPANDER

TRANSVERSE PUMPED DYE LASER.

Fig.3.14

A PHOTOGRAPH of the DYE LASER
(See overlesf)

In the right foreground is seen the 100% rear mirror mount. Behind that is seen the dye cell which is held in place with a magnet in a precisely relocatable corner mount. Behind the dye cell is the grating mount which allowed rotation about the two mirror axes and lateral movement (left ↔ right as viewed).

To the left is the tuning mirror assembly. The actual mirror mount, with its vertical adjustment screw, is hung by pin bearings on the fine control arm.

The fine control arm is itself hung by pin bearings on a post attached to the base plate. Coarse tuning is effected by the small micrometer, which moves the mirror mount with reference to the fine tuning arm. Fine tuning is effected by the large micrometer moving a one degree wedge against a graphite loaded teflon ball set into the fine tuning arm.

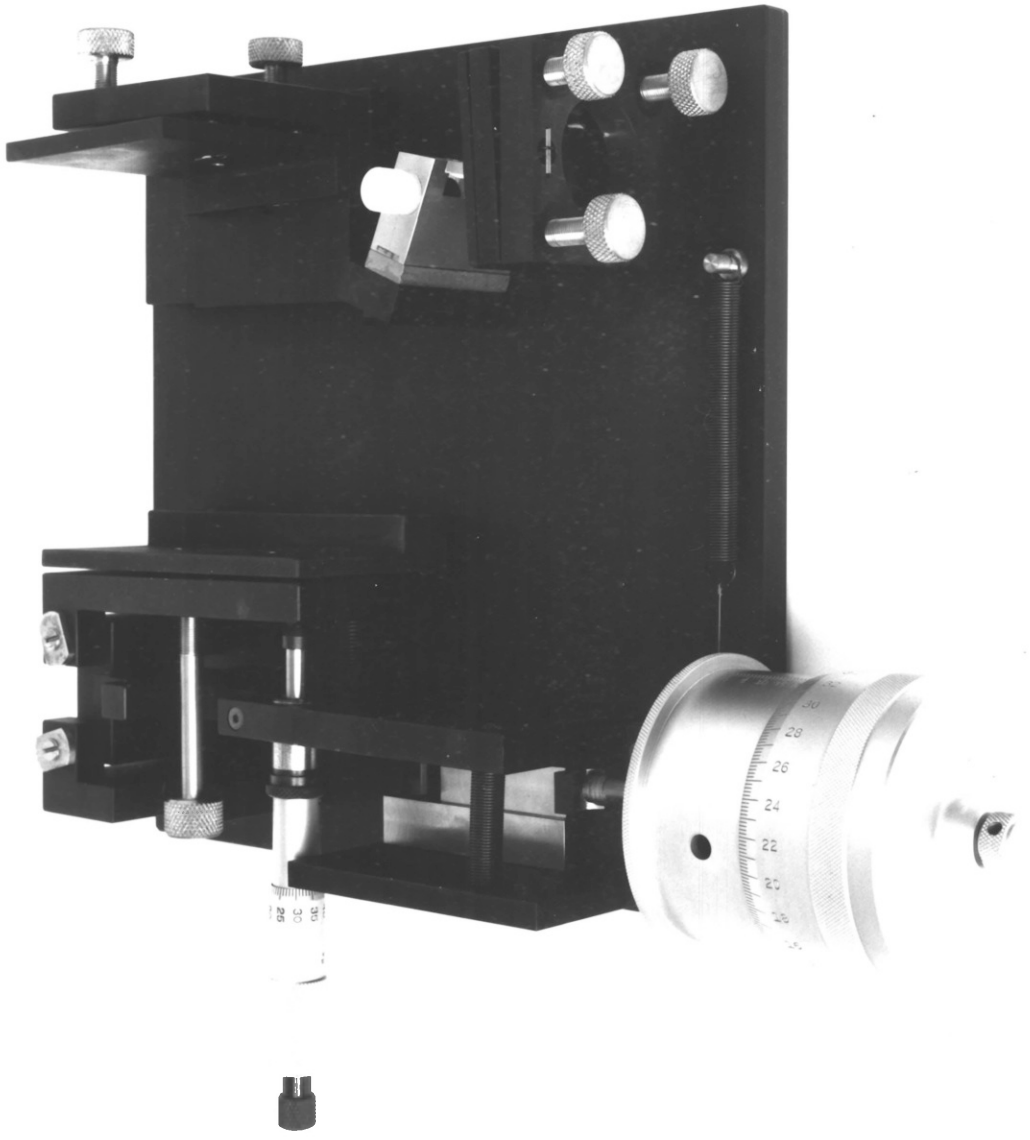
30
28
26
24
22
20

The performance of this laser is summarised in Table 3.2. A 1200 line per m.m. holographic grating was used. The angle of incidence at which the grating was set was about 89^{o}.

LASER PUMPED DYE LASER

Coarse tuning rate	=	About 100Å per mm of micrometer throw.
Fine tuning rate	=	About 0.75Å per mm of micrometer throw.
Conversion efficiency	=	$\frac{\text{Pumplaser energy}}{\text{Dye laser output energy}} = 0.1$
Laser bandwidth	=	About 0.01Å.
Laser divergence	=	2 m. radians F.W.H.M.

TABLE 3.2

SECTION 2

3.2.1. EXPERIMENTAL LAYOUT for He II COLLISION RATE EXPERIMENT

Initially, an attempt was made to determine the collision rates out of $n=4$ in He II, by observing the transient behaviour of the $n=4$ population as the $n=3$ to $n=4$ transition, 4686Å, was pumped with a coaxial flashlamp pumped dye laser - much in the manner of Burgess et al (1980), who used this technique to determine the collision rates out of $n=3$ in Hydrogen, by pumping Balmer Alpha with a high power dye laser. The apparatus layout is shown in Fig. 3.15.

The dye laser tuned to 4686Å was directed down the axis of the plasma. The fluorescence at 4686Å was monitored at 90° to the laser beam using an f/10 1 meter 'Monospec 1000' monochromator with an R.C.A. 4836 photomultiplier mounted on the exit slit.

The signal was displayed on a Tektronix 7904 oscilloscope and photographed. No transient leading edge or 'spike' was seen, however, and the failure of this experiment was thought to be due to three factors.

1. The signals were very noisy, having a signal to noise ratio of about 2:1. The signals observed by Burgess and Skinner when observing H-Alpha, using essentially an identical set of apparatus were much cleaner. This is accounted for by noting that the predicted $n=4$ He II population was about three orders of magnitude lower than

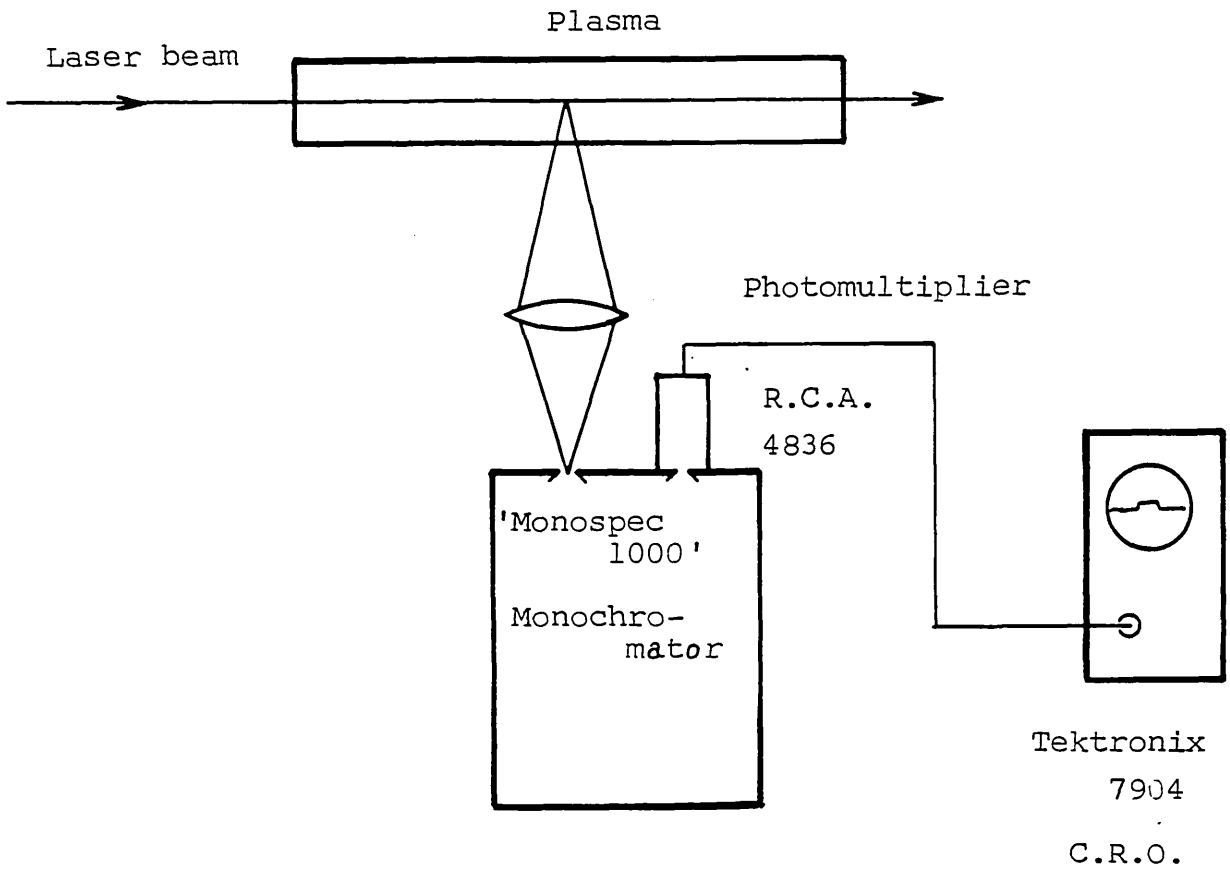

Fig. 3.15

ORIGINAL LAYOUT for He II 4686Å

LASER FLUORESCENCE EXPERIMENT

Both the laser and the plasma were tuned to 4686Å. The laser fluorescence was focussed onto the entrance slit of the monochromator. The signal from the Photomultiplier was displayed on the C.R.O. screen and photographed.

the $n=3$ hydrogen populations observed by Burgess et-al.

2. The predicted rates out of $n=4$, He II, were about an order of magnitude higher than the rates observed out of $n=3$ in Hydrogen for the same electron density and temperature conditions. It would therefore require much higher laser powers to saturate the He II, 4686Å transition than to saturate H-Alpha. (For $Ne = 5 \times 10^{14}$, this meant power densities greater than $10^6 W/cm^{-2}$ were required)

3. Electrical noise generated by the laser was comparable to the small signal levels that were being observed.

In an attempt to rectify these deficiencies, the apparatus was modified, as shown in Fig. 3.16.

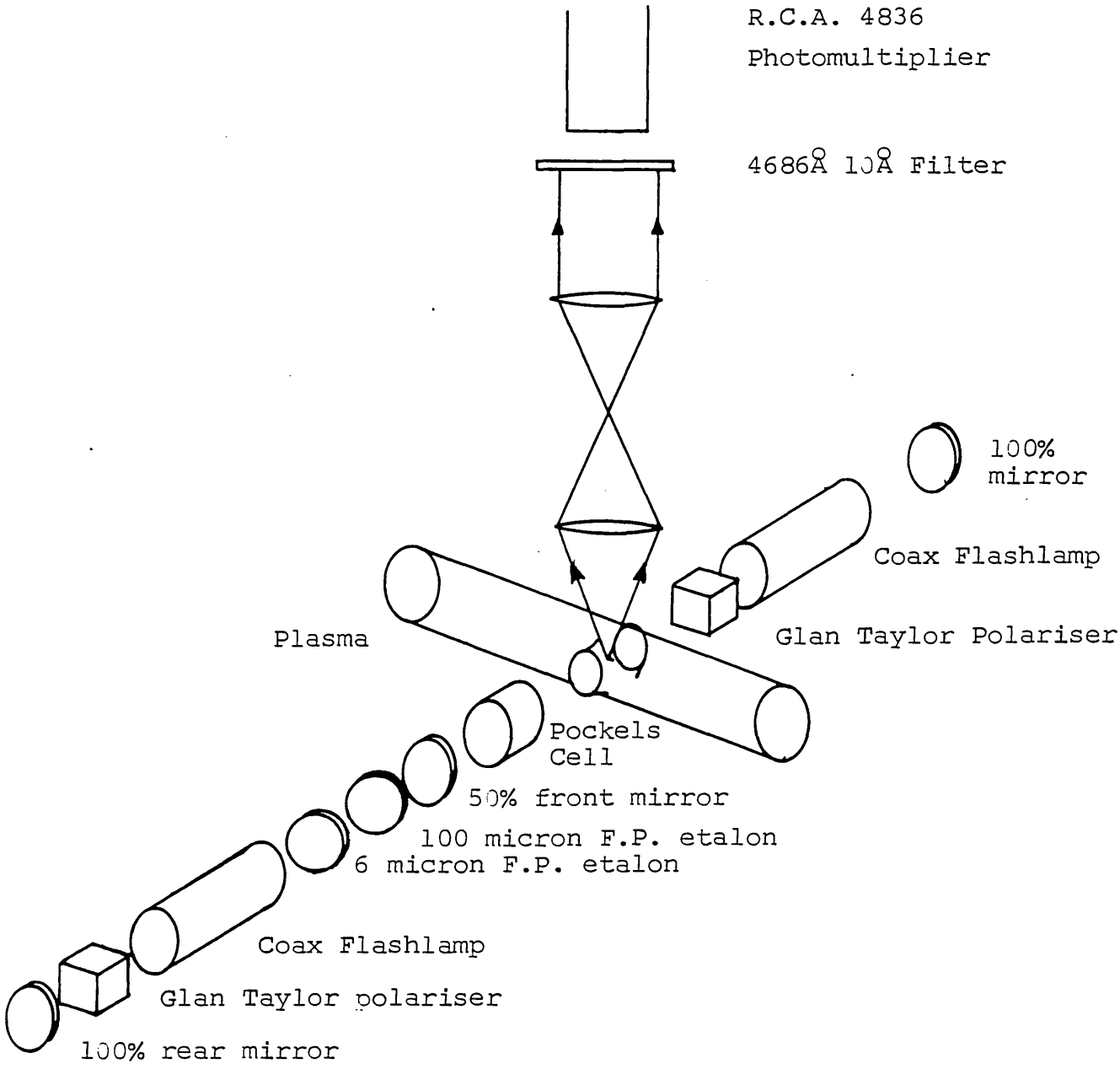

Fig. 3.16

MODIFIED LAYOUT for He II 4686Å

LASER FLUORESCENCE EXPERIMENT

This layout was an attempt to produce maximum laser power with minimum laser risetime in the plasma.
The detection system now used a lens train and interference filter to obtain more light grasp.

The purpose of the layout, was to maximise the laser power within the test volume of the plasma. To this end the pyrex tube of the plasma vessel was modified, by putting four side arms on the tube at its midpoint. Two of the side arms had optically flat windows placed on them to allow a laser beam to pass through the plasma without degradation of its optical quality. A viewing port, with an optically flat window and a Rayleigh horn viewing dump, were placed orthoganal to the laser ports.

The flashlamp dye laser oscillator was now placed on one side of the plasma vessel and the amplifier was placed on the other side of the vessel. A 100% mirror, M_3, placed after the amplifier to be used in a multipass arrangement. However, the mirror M_3 was adjusted, so that the amplifier did not lase broadband of its own accord between mirrors M_2 and M_3. The amplifier could then be described as a regenerative amplifier.

The photomultiplier detector, a R.C.A. 4836 type, was placed behind a 10Å passband interference filter centred at 4686Å. The optical collection system was arranged as in Fig.3.16 and had an f number of 5. The collection system was now about five times faster than the monochromator shown in Fig.3.15.

The photomultiplier was placed within a 16 gauge aluminium box to prevent pickup of electrical noise from the laser. Similarly, the attendant signal and power leads to the photomultiplier, were placed within a copper tube. The consequent shielding of the photomultiplier and attendant leads was tested by placing a small 145 MHz oscillator

within the aluminium box and using a calibrated reciever to measure the signal reduction as the lid was placed on the box. There was found to be a 45db. reduction in radiated signal. The noise pickup now seen at the oscilloscope when the laser fired was reduced from a peak of about 200mv, to negligible levels - this for a signal voltage of about 100mv.

Despite these modifications, no transient leading edge to the fluorescence was observed. Problems due to stray laser light were also encountered, which proved difficult to eliminate entirely.

Consequently, it was decided to use the three level technique, described in Chapter 2 and attempt to gain information regarding the rates out of $n=4$ in the He II by using $n=4$ as the lower level of a laser pumped transition.

The apparatus was then modified, as shown in Fig. 3.17, in that the Pockels cell and polariser were removed and provision was made to monitor the laser intensity.
The wavelength at which the laser lased, was also changed. Firstly to 4859Å, $n=4$ to $n=8$, and then to 6560Å, $n=4$ to $n=6$. The dye fill was the same for pumping 4859Å as for 4686Å - 30mg of coumarin 480 to 1 litre of Methanol. This was changed for pumping 6560Å, to 30mg of Rhodamin 6G and 16mg of Cresyl Violet Perchlorate to 1 litre of Methanol.

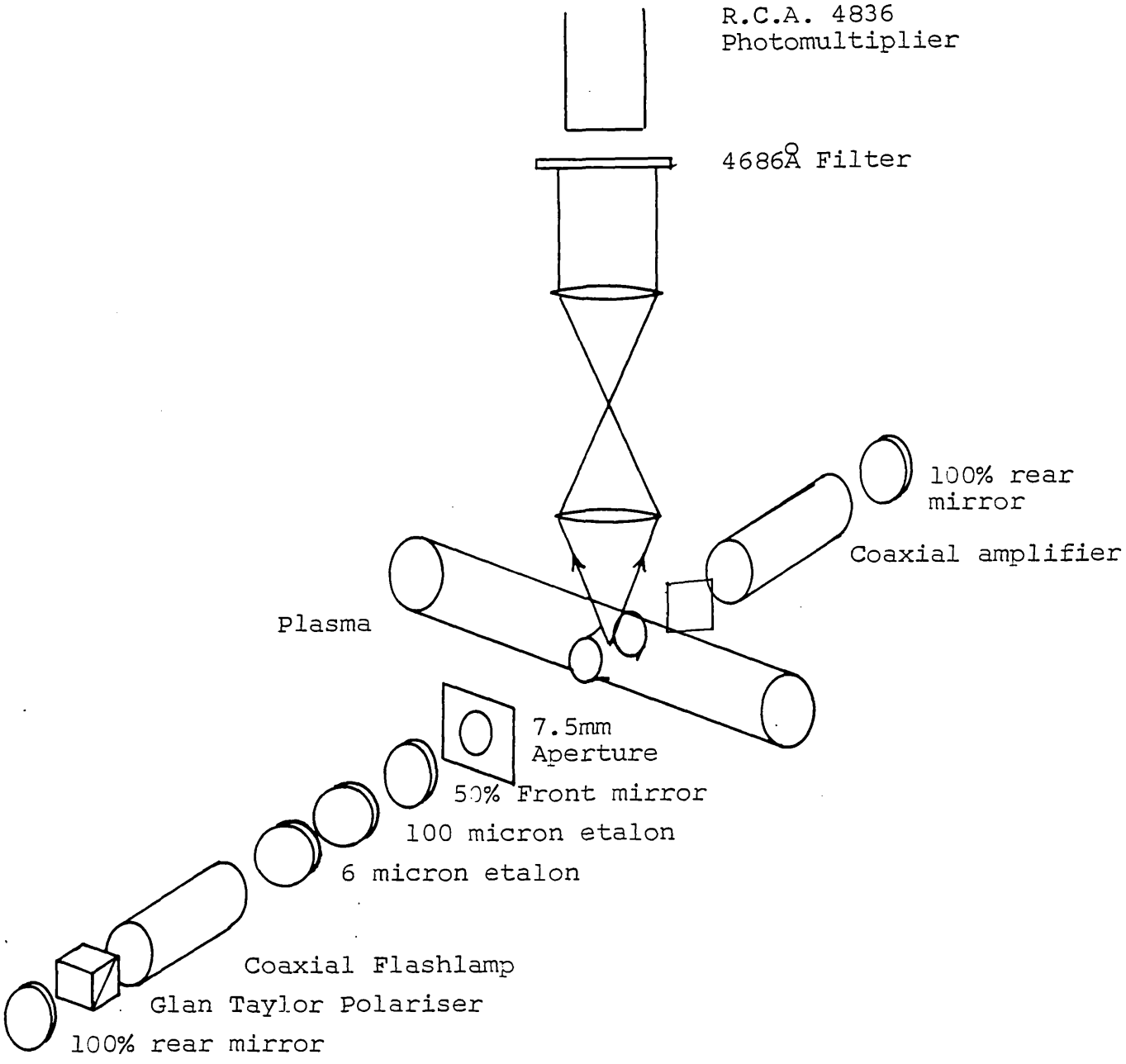

Fig. 3.17

FINAL LAYOUT for He II n=4

COLLISION RATE EXPERIMENT

The Pockels cell and one of the Glan Taylor Polarisers of Fig. 3.16 are removed. The polariser in the oscillator cavity was left in so as not to disturb the alignment.

3.2.2. DETERMINATION of the LASER POWER DENSITY in the PLASMA for the He II COLLISION RATE EXPERIMENT

The laser power density within the plasma test volume was obtained from a knowledge of the beam diameter, the time history of the laser pulse and the laser energy which was measured for every shot.

The beam diameter was determined by placing a 7.5mmaperture after the oscillator, as shown in Fig. 3.17.

The laser energy was measured in two ways, depending on whether the amplifier was being used or not. If the amplifier was being used, as it was when pumping $n=4$ to $n=8$, 4859Å, then a glass slide beam splitter was put between the Z pinch and the amplifier, as shown in Fig. 3.17. This split off 16% of the amplified laser beam as it entered the plasma and directed it to a calorimeter which measured the energy. Measurements taken off the other side of the glass slide beam splitter were about 50% of those taken off the side shown in Fig. 3.17. The true value of the energy passing through the test volume, could be determined by multiplying the measured value by

$$\frac{1}{1.5 \times 0.16} = 4.17$$

The time history of the laser pulse was measured after the experimental runs by replacing the calorimeter with a photodiode, displaying the temporal history of the laser on a C.R.O. screen and photographing it. This was done for the various laser bank voltages used during the experimental run.

The laser power was varied, by either varying the laser bank voltage or placing neutral density filters between the oscillator and the plasma.

If the amplifier was not used, the calorimeter was put between the Z pinch and the amplifier in place of the beam splitter and the energy was measured directly.

SECTION 3

THREE LEVEL LINESHAPE OF H-BETA

3.3.1. GENERAL EXPERIMENTAL LAYOUT

The general layout of the apparatus used, is shown in Fig. 3.18. The H-Beta probe laser was the N_2 pumped dye laser described in section 3.1.8. This laser was directed down the axis of the Z pinch via a 4% beam splitter (i.e. one surface of a non parallel glass slide). The H-Alpha pump laser was the coaxial flashlamp pumped laser, described in section 3.1.6. This laser passed through the beam splitter coaxial with the H-Beta probe laser down the axis of the plasma vessel.

On passing through the plasma, the H-Alpha beam was filtered out, using a combination of a Carbon Disulphide liquid prism and a dichroic filter in front of the signal photodiode.

A second photodiode monitored 8% of the H-Beta probe laser which is split off before going into the pinch. This serves as a monitor of the input intensity of the H-Beta probe laser.

The signals from the two photodiodes were then recorded, using two Tektronix transient digitizers, type 7912AD and R7912, signals were then stored on floppy disc.
A detailed description of the experimental layout now follows.

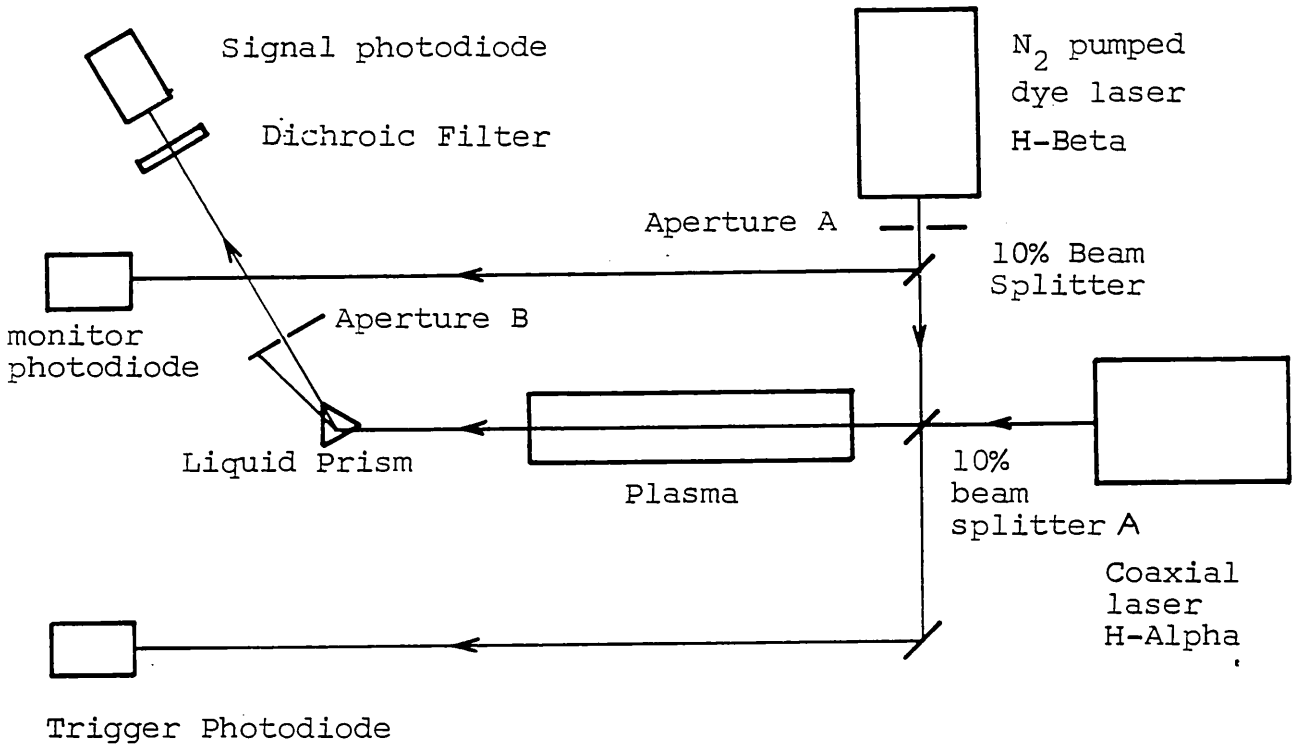

Fig. 3.18

LAYOUT of APPARATUS for H-BETA

THREE LEVEL LINESHAPE EXPERIMENT

At Beam Splitter A, the H-Alpha pump laser and 10% of the H-Beta probe laser combine to pass coaxially down the plasma column. Having passed through, the H-Alpha laser is blocked by a combination of a liquid prism, aperture B and a dichroic filter, Aperture A ensures the H-Beta probe laser is of smaller diameter than the H-Alpha pump laser, so that only plasma pumped by the H-Alpha laser is probed.

3.3.2. THE COAXIAL H-ALPHA LASER

The coaxial laser oscillator amplifier system has been described earlier. In this instance it was run, using a single 6 micron Fabry Perot tuning element, so giving a linewidth of about 5 angstroms.

3.3.3. ELECTRICAL SCREENING OF THE LASER

It was necessary, however, to reduce the electrical noise generated by the laser and picked up by the signal cables running to the digitizers, to a minimum, so a screening box was built around the entire laser system - that is, flashlamps, spark gaps, capacitors, charging unit and trigger units. This was built of 20gauge aluminium sheet on a wooden frame. The doors were of $\frac{1}{2}$inch plywood with 16 gauge steel backings. Electrical contact, from the rest of the box to the steel backing, was made by the hinges on one side and by copper fingers on the other three sides. The mains power entered the box via an isolation transformer and a mains filter.

The efficiency of the screening was tested at 145 MHz using an oscillator and a calibrated receiver. The oscillator was placed on an insulating wooden block, inside the box. The receiver then measured the power radiated, with the doors open and shut. The ratio of the two powers was about 45db. So this was the effective screening effeciency at 145 MHz .

3.3.4. BEAM STEERER

On exciting the box, the laser was steered down the axis of the Z pinch, using a cell filled with methanol, whose end windows were adjustable. The windows were mounted on the cell, using brass rings to press the window against an 'O' ring. The four screws, retaining the brass ring at equal intervals around the brass ring, could be inter-dependently tightened, so slightly altering the angle of the window in any chosen direction.
In this way, an infinitely adjustable liquid prism was used to steer the beam in the required direction.

3.3.5. THE N_2 PUMPED H-BETA PROBE LASER

Since it is required to measure the H-Beta optical depth whilst the H-Alpha laser is on, it is necessary that the H-Beta laser have a shorter pulse length. This is easily satisfied, since the H-Alpha laser pulse length was 300 nsec and the H-Beta laser pulse length was 3 nsec.

Since there was effectively no spectral filtering in front of the photodiodes, it was necesssry to filter off the amplified spontaneous emission (A.S.E.) at the laser. This was accomplished by constructing a spectrometer, through which the laser beam passed. See Fig.3.19. This consisted of two 40 cm focal length lens , a constant deviation prism on a prism table and a 200 micron slit.

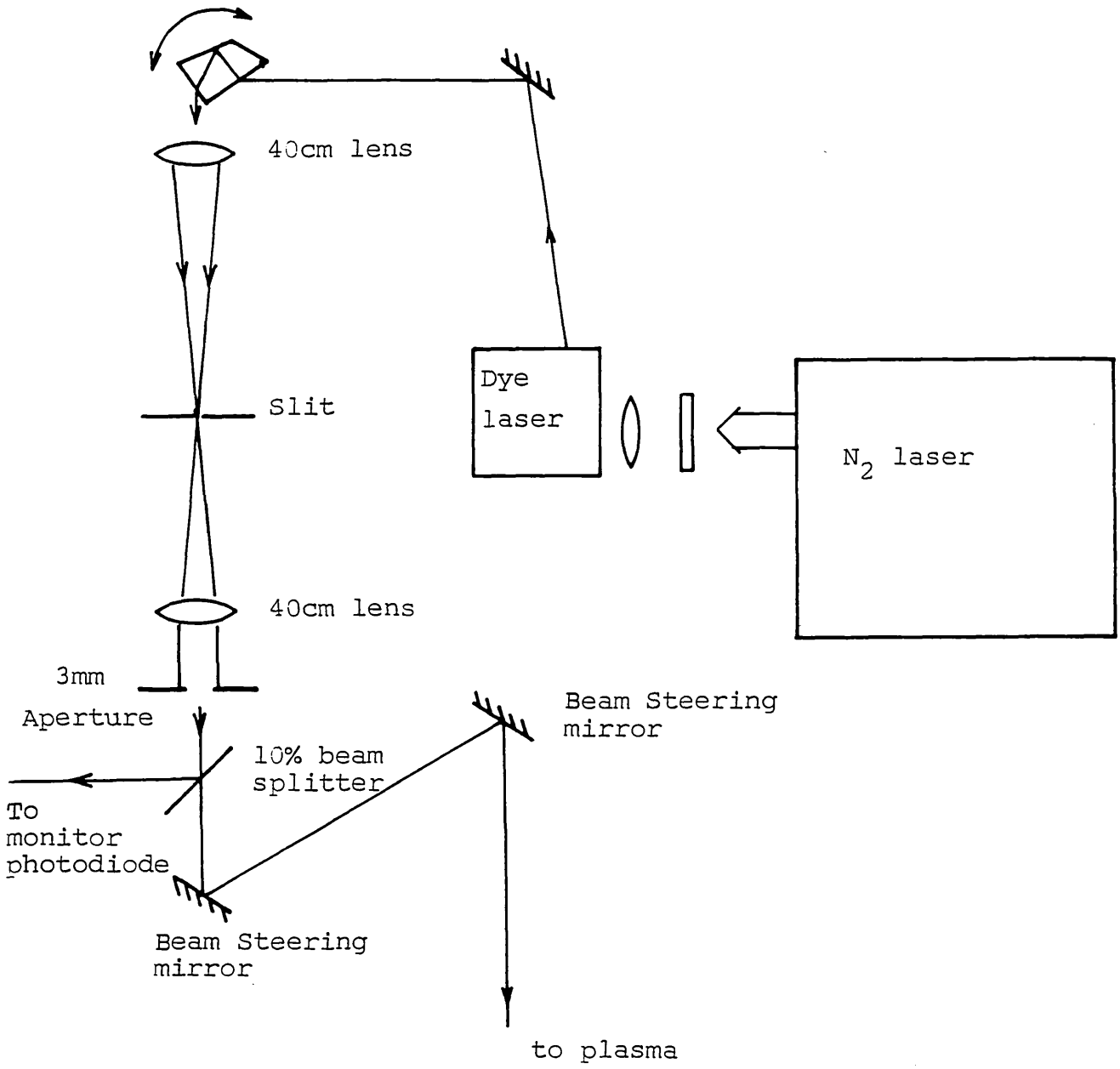

Fig. 3.19

LAYOUT of N_2 PUMPED DYE LASER

with A.S.E. FILTER

By using a constant deviation prism mounted on a rotating prism table, adjustment could easily be made to keep the tuned radiation passing through the slit, as the laser was tuned through the H-Beta line.

In addition, two steering mirrors were used to ensure the laser output passed coaxially down the Z pinch, after coming off the 4% beam splitter. A further beam splitter, placed further back in the beam, split off 8% for the 'input intensity' photodiode monitor. These optical components were positioned on a wooden table, covered in 16 gauge sheet steel and were held in place using home-made magnetic bases.

This A.S.E. filter proved very effective in removing any observable trace of A.S.E. A 5mm aperture, placed in the beam, ensured that the H-Beta beam was of smaller diameter than the H-Alpha pump laser beam. So ensuring that the H-Beta laser only probed the H-Alpha irradiated plasma.

3.3.6. PHOTODIODES

The photodiodes used, were made by Centronic, type OSD - 2HSA. These had an active area of $1mm^2$ and a rise time of 1 nsec. The photodiodes were mounted in boxes as shown in Fig. 3.20. The beam was slightly focused onto a diffusing screen, behind which was mounted the photodiode. It had been found that it was necessary to destroy any spatial coherence of the laser beam, so that every part of the photodiode active surface

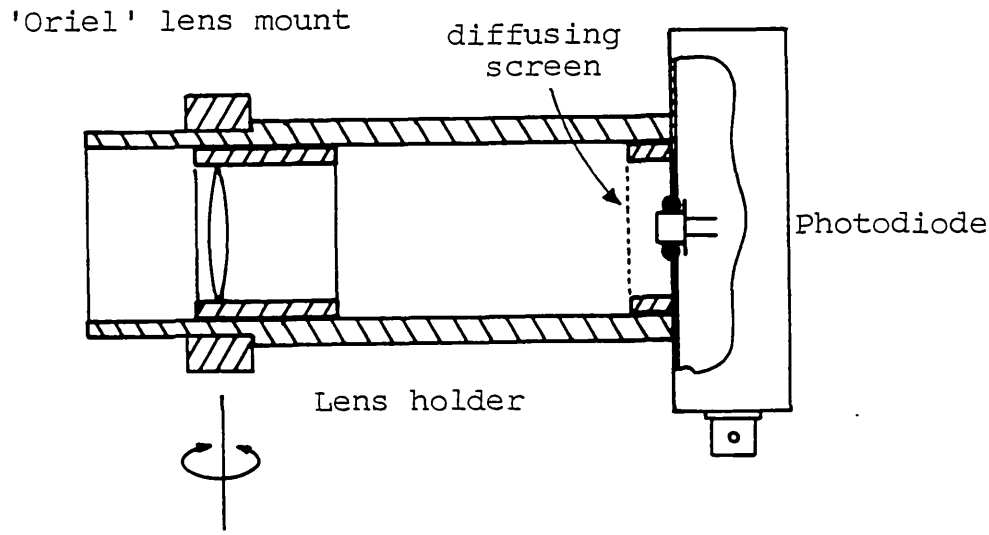

Fig. 3.20

THE CONSTRUCTION of the PHOTODIODE DETECTOR

The lens provides a soft focus for the incoming light onto the diffusing screen.
The whole photodiode detector is held in an 'Oriel' 2 inch mirror mount which rotates the detector about two orthogonal axes through the plane of the lens - so aligning the detector.

monitored equally the light from all parts of the laser beam cross section. Unless this precaution was taken, it was not possible to get the signals from the two diodes to agree to better than $\pm$ 10%, but using the diffusers, it was possible to attain tracking accuracies of better than 1%.

The diodes were reverse biased, using batteries to a voltage of 70 volts. Two decoupling capacitors, of value 1 m.f.d. and 0.001 m.f.d. were placed across the batteries The signal cables, coming from the photodiodes, passed into a 1 inch copper tube, earthed to the diode boxes, to prevent pickup of electrical noise.

As mentioned above, an H-Alpha blocking filter was placed in front of the signal diode to prevent any H-Alpha laser radiation scattered from the liquid prism, being detected. Such a filter was not necessary on the monitor diode.

It should be noted, that due to the precaution taken in screening the signal cables, the coaxial laser and the N_2 laser, there was absolutely no problem experienced, due to noise pickup.

3.3.7. TRIGGERING AND TIMING

The firing of the Z pinch and the two lasers, was synchronised by a 5 channel delay unit, built by Chelsea Instruments, to a design by the author. The delay units were connected to the pinch and the two lasers via optical fibre links, to prevent the delay units being affected by electrical noise.

The N_2 laser had to be fired three or four times before the data taking shot. This was to preionise the laser cavity sufficiently so that the data taking shot would be reliable and fairly reproducible. Since it was required that the digitizers, (armed and ready) did not fire on these preionizing shots and did fire on the data taking shots, it was necessary to devise an AND gate device, which only allowed the trigger pulse through on the data taking shot. This AND gate was opened, using a pulse from the Delay box. Fig. 3.21 shows the distribution and generation of the trigger pulses.

3.3.8. OPTICAL FIBRE LINKS

These links used 200μ 'Radio Spares' glass optical fibre. An infra red light emitting diode and photodiode, also made by Radio Spares, and having special screw coupling attachments to the optical fibre, were used as the active optical elements. The circuit diagram for the transmitter is shown in Fig. 3.22.

It consists of an NPN transistor, which is switched on by the input pulse (5 volts into 50Ω). This, in turn, switches on a PNP transistor which has the L.E.D. in its collector circuit. A 47 ohm resistor is placed in parallel with the L.E.D. to speed up the rise time of the pulse across the L.E.D. The input is protected with a 15 volt Zener diode.

At the other end of the cable, the receiving photodiode is reverse biased. On reception of the optical pulse from the transmitter, it gives out a one multi volt

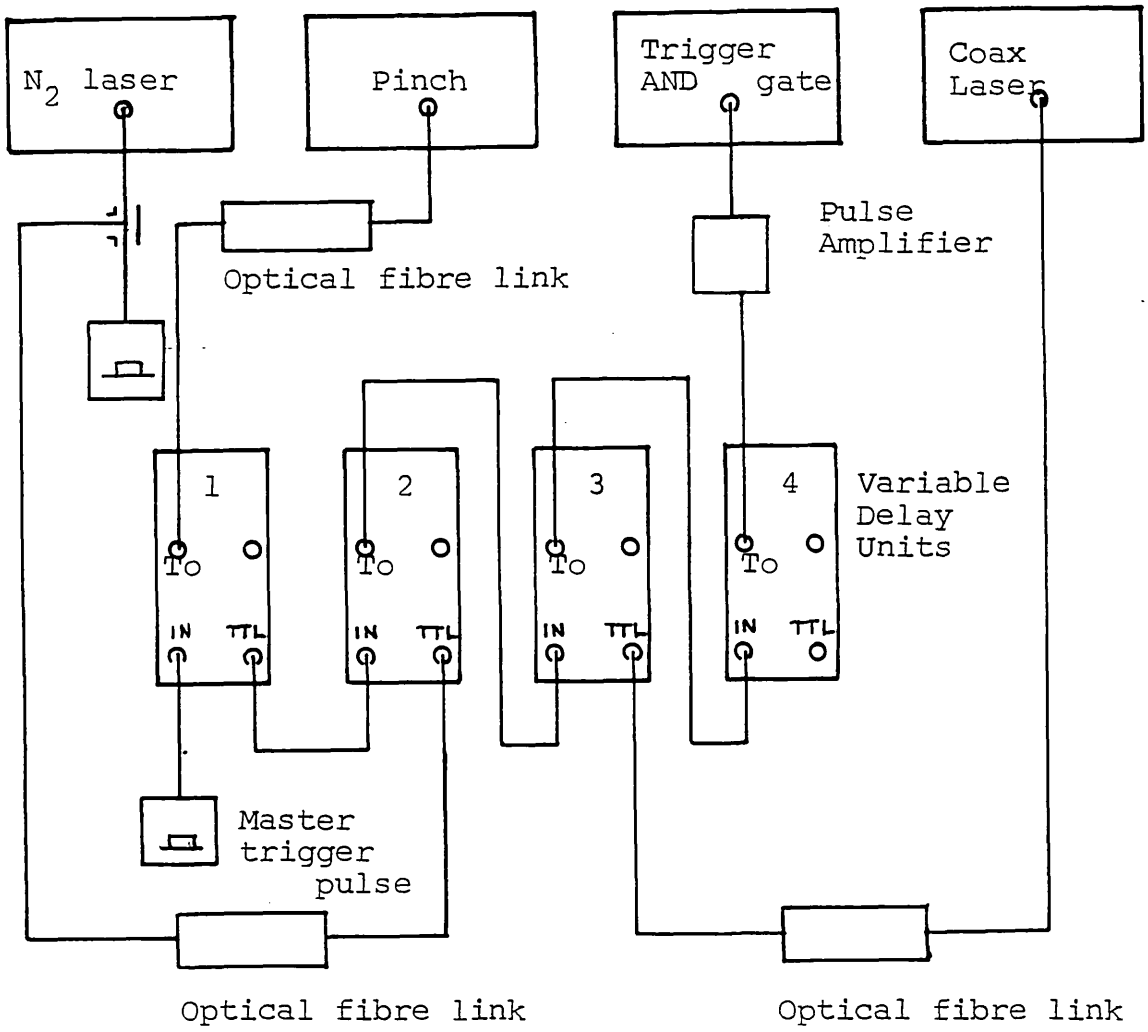

Fig. 3.21

TRIGGERING LOGISTICS

Delay unit 1 is 10 to 110 microseconds (adjustable) and determines the time in the afterglow at which the lasers fire.

Delay units 2,3 and 4 ensure the N_2 laser fires 100 nsec after the start of the Coax dye laser pulse, and that the AND gate is opened to allow the digitizers to be triggered.

A To pulse is one which is initialised by the input pulse and then lasts the duration of the set delay time.

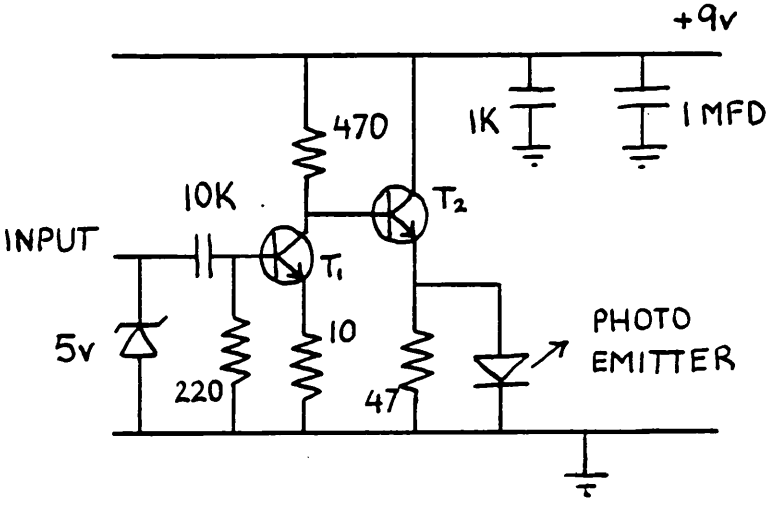

Fig. 3.22

CIRCUIT of TRANSMITTER for OPTICAL FIBRE LINK

Transistor T_1 is 2N2222

T_2 is BC214L

All capacitors are ceramic, except the 1MFD which is Polyester.

pulse, which needs to be amplified. The circuit for the receiver is shown in Fig. 3.23. It consists of a reverse biased photodiode capacitance coupled to three shunt feedback stages, in tandem, each having a gain of 12. This gives a linear gain of 1200, so turning the 1 millivolt signal into a 1.2 volt pulse. This pulse is now sufficient to turn on the transistor T7 and then T8, which drives the 50 ohm output line. Because T7 and T8 are biased in class C, they are non-linear in the way they amplify the rising edge of the pulse. This has the effect of shortening the risetime of the output pulse. This is necessary because the optical fibre is a multimode one and so tends to integrate the pulse shape (having the effect of an RC circuit).

If the transmitter launches a light pulse, having a risetime of less than 10 nanoseconds down a 50m length of optical fibre, the risetime at the other end will be 50 nanoseconds.

The 'non-linear' amplifier, formed by T7 and T8, will reduce the pulse risetime from 50 nsec. to 10 nsec. The linear amplifier formed by T1 to T6 is, however, very fast, having a bandwidth of 100 MHz. The 100 ohm resistor in the 9 volt supply line is to prevent instability.

Both the optical fibre transmitter and receiver are built inside die cast boxes and are battery operated to reduce susceptibility to electrical noise. These devices were found to be very successful.

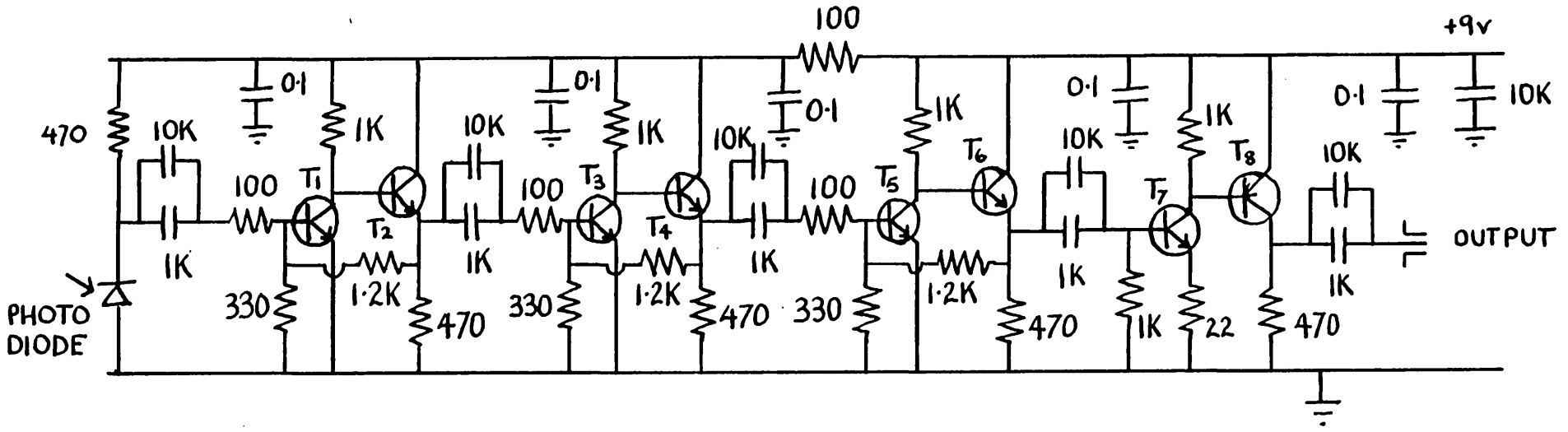

Fig. 3.23

CIRCUIT for RECEIVER for OPTICAL FIBRE LINK

All transistors are 2N2222 except T_8 which is a BC214L.

Total propagation rime of a pulse through the transmitter and receiver (excluding optical fibre) is 70 nsec.

Propagation velocity down optical fibre is 5.5 nsec m^{-1}.

3.3.10. DIGITIZER TRIGGER AND GATE

As explained above, the N_2 laser needed several 'preionising' shots to seed the laser cavity for a reliable data taking shot. As shown in Fig. 3.21, this was achieved by having a separate trigger line in parallel with the line from the Delay box, to trigger to the N_2 laser for these preionising shots.

To ensure that the Digitizers were only triggered by the data taking shot, an AND gate was put in the trigger line to the digitizers. This allowed only the trigger pulse through, provided the gate was open, due to a pulse derived form the Delay box.

The circuit for the gate is shown in Fig. 3.24. The power for the photodiode comes via the transistor T1. This transistor becomes conducting, when there is a positive voltage on the base of the transistor. The voltage on the photodiode will be 0.7 volts lower than the applied gate voltage - so there is no gain in the circuit and it is unaffected by electrical noise. A manual switch across the transistor allows the digitizers to be triggered in the absence of the delay unit.

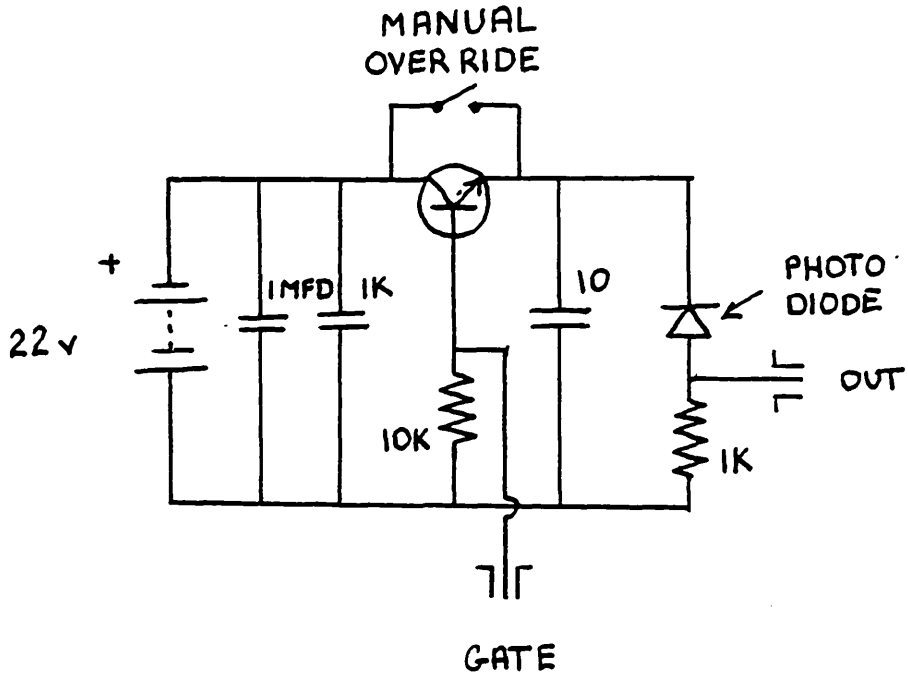

Fig. 3.24

CIRCUIT of TRIGGER PHOTODIODE

The AND Gate for only allowing the digitizers to be triggered when a data shot was being taken.
The N_2 laser had to be triggered several times before the data taking shot, in order to pre-ionise the discharge channel.
The gate of the AND gate is opened by a To pulse from the delay unit. Since the voltage applied to the diode, when the transistor is turned on, is 0.7v lower than the applied voltage at the gate, an amplifier boosts the 2 volt To pulse up to 20 volts.

3.3.11. THE DIGITIZED SIGNAL

The signal from the photodiodes was digitized and stored on floppy disc. The area under laser pulse signal was integrated and this number was stored on the disc with the signals. The programmes for storing the data were written by David Spirit, for which I am most grateful.

Having obtained the waveforms of the H-Beta laser pulse it would have been possible to derive an optical depth by comparing the peak height of the signal, (If we assume the intensity of the H-Beta probe laser is well below saturation, then the waveforms of the signal and probe beams will have the same shape - in theory) or to compare the areas under the waveforms. It was thought better to compare areas under the waveforms for one basic reason.

Any noise, e.g. shot noise, digital noise or electrical noise from the lasers, will tend to fluctuate about the mean signal voltage. This noise would be a source of error, if taking a peak height reading, but will tend to cancel on integration over the entire pulse.

3.3.12. TREATMENT OF DATA

The N_2 pumped dye laser was tuned in steps of about 0.1Å. The procedure was to take two shots of just the N_2 dye laser, without pinch or H-Alpha laser, to establish the input laser flux. These two shots were averaged. Then two shots were taken of the N_2 dye laser, with the plasma present and their average taken. Using this laser flux the optical depth τ for that wavelength could now be obtained.

The average of two shots of the N_2 dye laser, with both pinch and H-Alpha pump laser, was then taken. So a new optical depth τ_L could be obtained. τ and τ_L were plotted as a function of wavelength and so a line profile of H-Beta was built up for the two conditions - with and without the H-Alpha pump laser.

REFERENCES

Ashby D.E.T.F.,Jephcott D.F., Appl.Phys.Lett. 3,13,(1963)

Burgess D.D.,Cairns C.J., J.Phys.B. 4, 1364,(1971) and 3, L67, (1970)

Burgess D.D., Mahon R., J.Phys.B., 5, 1756, (1972)

Burgess D.D., Myerscough V.P., Skinner C.H., Ward J.M. J.Phys.B., 13, 1675, (1980)

Cherrington B.E., 'Gaseous Electronics and Gas Lasers' Pub. Pergammon Press. Oxford.(1979)

Hanna D.C.,Karkkainen P.A.,Wyatt R., Opt.Quant.Elec. 7, 115,(1975)

Hansch T.W., Applied Optics. 11, 895, (1972)

Kolbe G.,Huang Y.W.,BurgessD.D., J.Phys.B.15,4283,(1982)

Mahon R., Ph.D. Thesis.,University of London.(1973)

Nicholson M., Ph.D.Thesis.,University of London.(1983)

Sam C.L., App.Phys.Lett. 8, 29,(1976)

Shoshan I.,Danon N.N.,Oppenheim V.P., J.Ap.Phys. 48, 4495, (1977)

Skinner C.H. Ph.D.Thesis. University of London. (1974)

Trebino R.,Roller J.P.,Siegman A.E., I.E.E.E. J.Quant.Elec. 18, 1208, (1982)

CHAPTER 4

He II COLLISION RATE EXPERIMENT

- RESULTS and ANALYSIS -

4.1 INTRODUCTION

In this chapter the results of an experiment to determine the rate coefficient out of the n=4 level of He II in a plasma will be presented and analysed. At the time of writing, this was the *only* laser based measurement of the rates out of an excited level of an ion in a plasma.

The experimental method is described in Section 2 of Chapter 3. It consisted of observing the change in the n=4 population density, (monitored by looking at emission from n=4 to n=3, λ =4686Å) whilst using a laser tuned to a transition having n=4 as its lower level to deplete the n=4 population. The consequent relation between the the rates out of n=4, the population of n=4 and the laser power density, was described in Section 2.6 of Chapter 2.

The experiment was performed twice. Once, with the pump laser tuned to the n=4 to n=6 transition, λ = 6560Å, and again with the laser tuned to the n=4 to n=8 transition, λ = 4859Å. Performing the experiment twice in this manner, would largely eliminate systematic errors due to possible, unexpected laser induced rates, provided the two sets of measurements were self-consistent. This is because the pumping wavelengths are well separated from each other and the powers needed at 4859Å, were about 6 times higher for an equivalent depletion than at 6560Å.

The measurements were taken 18 microseconds into the after-

glow phase of the plasma, where Ne = 5 x $10^{14}cm^{-3}$ and Te = 1.35eV

4.2 EXPERIMENTAL RESULTS

Figure 4.1 shows a typical experimental result. The emission on 4686Å is depleted during the period of the laser pulse. However, experimentally, the whole of observed volume of plasma was not irradiated. See Fig. 3.1b.

Initially then it was assumed that the He II plasma filled the plasma vessel homogeneously, so that the diameter of the He II plasma was 45mm. (The diameter of the plasma vessel) The observed relative depletion of the 4686Å emission was then adjusted by the ratio of the pinch diameter to the laser beam diameter(45/7.5), to give the relative depletion of n=4 in the irradiated volume.

Figures 4.2a and 4.2b show the experimental results for the relative depletion of the n=4 level against laser power density. Figure 4.2a shows the results obtained whilst pumping n=4 to n=8, λ = 4859Å and Figure 4.2b, the results obtained whilst pumping n=4 to n=6, λ =6560Å. This data is plotted, assuming the He II plasma is homogeneous and fills the plasma vessel.

Tables of the Data points are also given in Tables 4.1a and b.

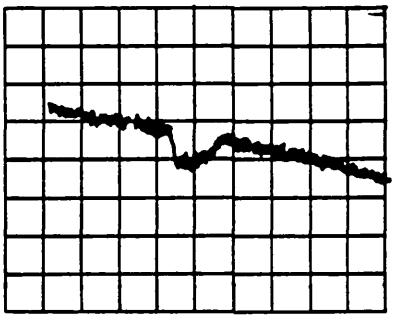

1 microsecond/div.

Fig. 4.1

Depletion of 4686Å emission due to laser pumping of 6559Å, n = 4 to n = 6.

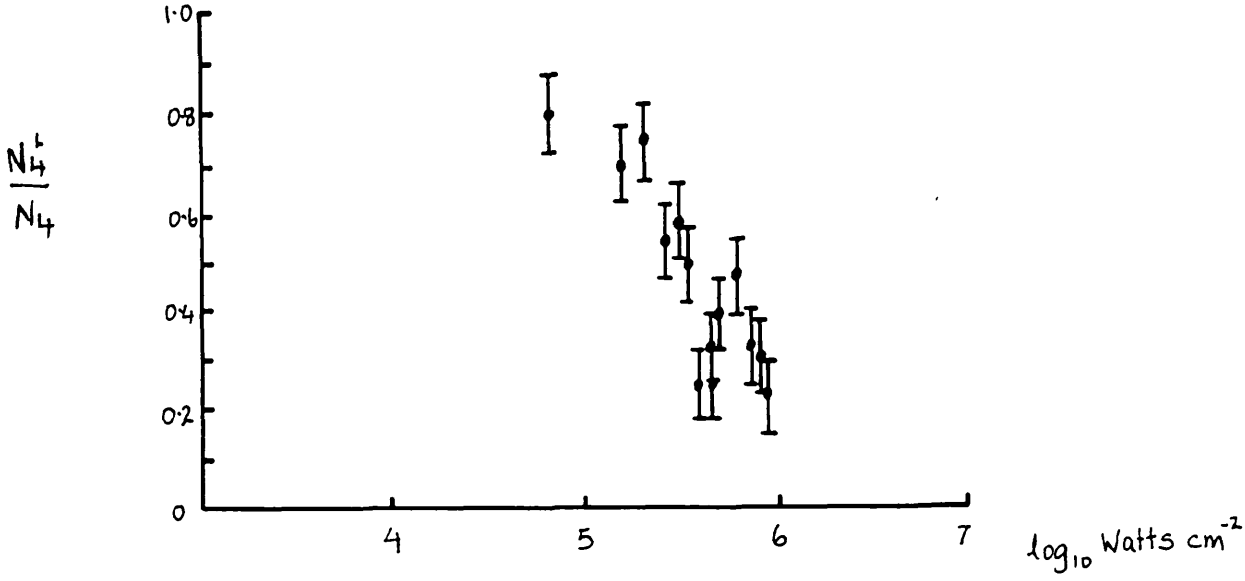

Fig.4.2a

Depletion of n=4 due to pumping n=4 to n=8, 4859Å.

He II plasma diameter assumed to be 45mm.

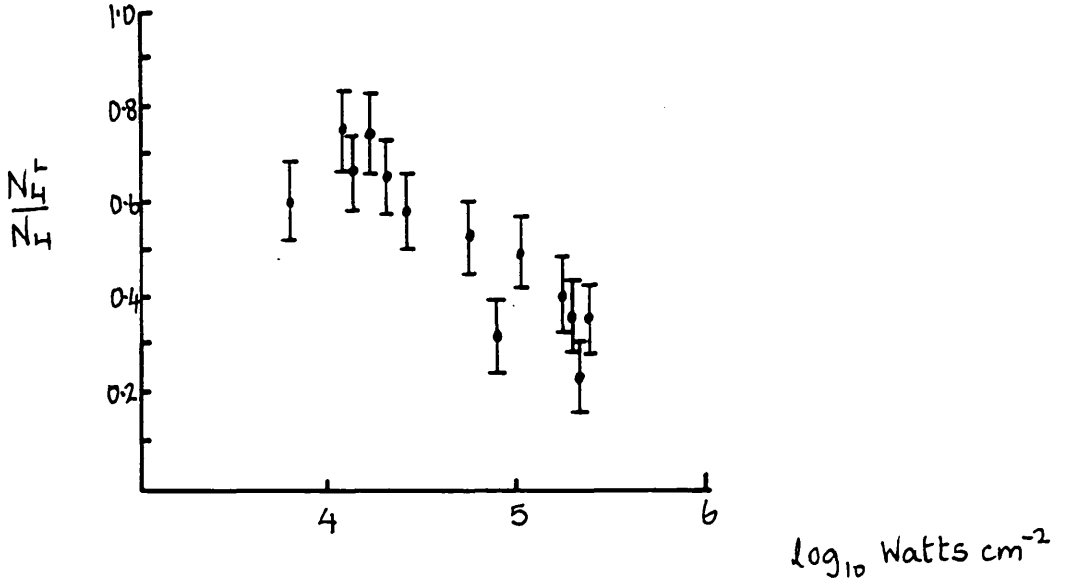

Fig. 4.2b

Depletion of n = 4 due to pumping n = 4 to n = 6, 6559Å.

He II plasma diameter assumed to be 45mm.

TABLE 4.1a

$N4^L/N4$	$P \times 10^6$ cm^{-2}
0.8	0.08
0.72	0.15
0.785	0.22
0.55	0.29
0.6	0.335
0.51	0.36
0.28	0.36
0.28	0.4
0.34	0.4
0.41	0.49
0.5	0.55
0.35	0.7
0.32	0.7
0.23	0.88

Table showing the data points for Fig. 4.2a

TABLE 4.1b

$N4^L/N4$	$P \times 10^5 cm^{-2}$
0.6	0.075
0.74	0.13
0.67	0.14
0.75	0.18
0.65	0.21
0.57	0.3
0.54	0.6
0.32	0.69
0.52	1.02
0.5	1.41
0.4	1.89
0.34	2.04
0.21	2.22
0.34	2.34

Table showing data points for Fig. 4.2b

4.3 ANALYSIS of the DATA

In this section a first attempt will be made to deduce the rates out of n=4 from the data shown in Fig. 4.2. To this end, the two level model, represented by equations 2.39a and 2.39b, will be fitted to the data by a least squares method.

Having achieved values for the parameters $\frac{N4^{L}(Sat)}{N4}$ and K from eqn. 2.39a, all that is then required, finally to obtain the rate D4 out of n=4 from eqn2.39b, is a value for $\Delta\nu$. This was obtained experimentally by obtaining emission profiles for the 6560Å and 4859Å transitions. For 4859Å, the data was noisy and unreliable, so a width was estimated, using the data for 6560Å and the theory of Griem (1960)

Finally, the effects on the depletion of n=4 due to the diameter of the He $\overline{\text{II}}$ plasma being smaller than that assumed, (i.e. the diameter of the plasma vessel), are considered.

An estimate of the rate out of n=4, D4, was obtained using eqns 2.39 and 2.40 on the data shown in Fig. 4.2.

In each case, a value of K was obtained by fitting eqn. 2.39 to the data, using a least squares fitting routine on a computer. It was assumed, in this procedure, that the principal error was in the estimation of the relative depletion and that the associated experimental power density was comparativly well determined.

The fitting procedure was as follows:

The function to which the data was fitted, was eqn 2.39a where level a was level 4 for He II

$$\frac{N_a^{\downarrow}}{N_a} = \left[\frac{N_a^{\downarrow}(Sat)}{N_a}\right]\left(P+K\right) \Big/ \left[P+K\left(\frac{N_a^{\downarrow}(Sat)}{N_a}\right)\right]$$

For further analysis this eqn is simplified, letting

$$\frac{N_4^{\downarrow}}{N_4} = Y \quad \text{and} \quad \frac{N_4^{\downarrow}(Sat)}{N_4} = a$$

then

$$Y = \frac{a(P+K)}{P+aK} \qquad 4.1$$

Following the usual principles of least squares fitting, the error on the nth data pair Y_n, P_n is given by

$$\left(Y_n - \frac{a(P_n+K)}{P_n+aK}\right)^2 \qquad 4.2$$

The best fit being obtained, when the total sum of errors for all data points S is minimised, where

$$S = \sum_n \left(Y_n - \frac{a(P_n+K)}{P_n+aK}\right)^2 \qquad 4.3$$

S must be minimised with respect to the two adjustable constants a and K and in principle this can be done uniquely by solving the pair of simultaneous equations

$$\frac{\partial S}{\partial K} = \sum_n 2\left[\frac{aP_n(1-a)}{(P_n+aK)^2}\right]\left[\frac{Y_n - a(P_n+K)}{P_n-aK}\right] = 0 \qquad 4.4$$

$$\frac{\partial S}{\partial a} = \sum_n 2\left[\frac{P_n(P_n+K)}{(P_n+aK)^2}\right]\left[\frac{Y_n - a(P_n+K)}{P_n-aK}\right] = 0 \qquad 4.5$$

In practice the eqn 4.4 was minimised on a computer, by itteratively varying K. The term a was held as a constant estimated from the data. The quality or goodness of the fit of eqn 2.39, to the data, was estimated by looking at $\bar{S}$, the average error of the data, where

$$\bar{S} = \frac{\sum_n \left[y_n - \frac{a(P_n+K)}{P_n+aK} \right]^2}{\sum_n n} \qquad 4.6$$

The term a was then varied by inspection to minimise $\bar{S}$.

Table 4.2 shows the results of fitting eqn 2.39 to the data shown in Fig. 4.2. Table 4.2a shows the parameters obtained for fits to Fig. 4.2a and Table 4.2b for fits to Fig. 4.2b. Eqn 2.40 shows that it is the product of K and a, (or K and $N4^L$(Sat)/N4), that is required to determine D4. So this product is also listed.

TABLE 4.2a

a	K x 10^6	$\bar{S}$ x 10^{-3}	aK x 10^6
0.01	35.8	4.9	0.35
0.05	6.2	5.0	0.31
0.1	2.9	5.5	0.29
0.2	0.96	7.2	0.19

TABLE 4.2b

a	K x 10^5	$\bar{S}$ x 10^{-3}	aK x 10^5
0.1	4.8	9.4	0.48
0.2	1.4	6.2	0.28
0.3	0.72	4.5	0.21
0.4	0.29	5.6	0.12

It can be seen from Tables 4.2 that, in fact, the product aK is not very sensitive to initial choices of a, so showing that the trial and error determination of the term a, is sufficiently accurate.

Figures 4.3 show fits of eqn 2.39 to the data shown in Figures 4.2. From Tables 4.2 and Figures 4.3, the results for the product term aK, can be stated as follows:-

From Table 4.2a and Fig. 4.3a, where n=4 was being pumped to n=8, then

$$aK = 0.32 \times 10^6$$

From Table 4.2b and Fig. 4.3b, where n=4 was being pumped to n=6, then

$$aK = 0.21 \times 10^5$$

All that is now required for an estimate of D4 is a determination of $\Delta\nu$ in each case.

Firstly, emission profiles were taken of the 4859Å and 6560Å transitions. These spectra were taken from the side of the plasma using a 'Monospec 1000' one meter monochrometer having a resolution of 0.2Å.

The signals from the photomultiplier, placed at the exit slit, was displayed on an oscilloscope and photographed. The results are shown in Figs 4.4a and 4.4b. Both profiles are seen sitting on the wings of the H-Beta and H-Alpha profiles respectively. (Hydrogen was present as an impurity in the plasma)

The 4859Å Data is very noisy and the profile of 4859Å is difficult to discern. The 6560Å transition is seen to

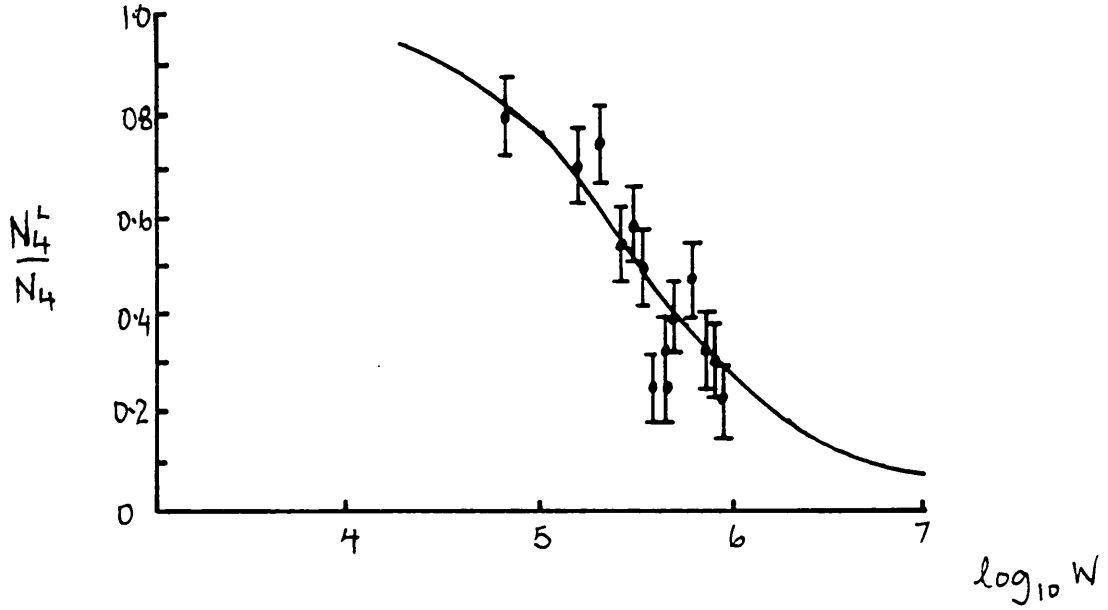

Fig. 4.3a

Two level model fit to data shown in Fig. 4.2a.

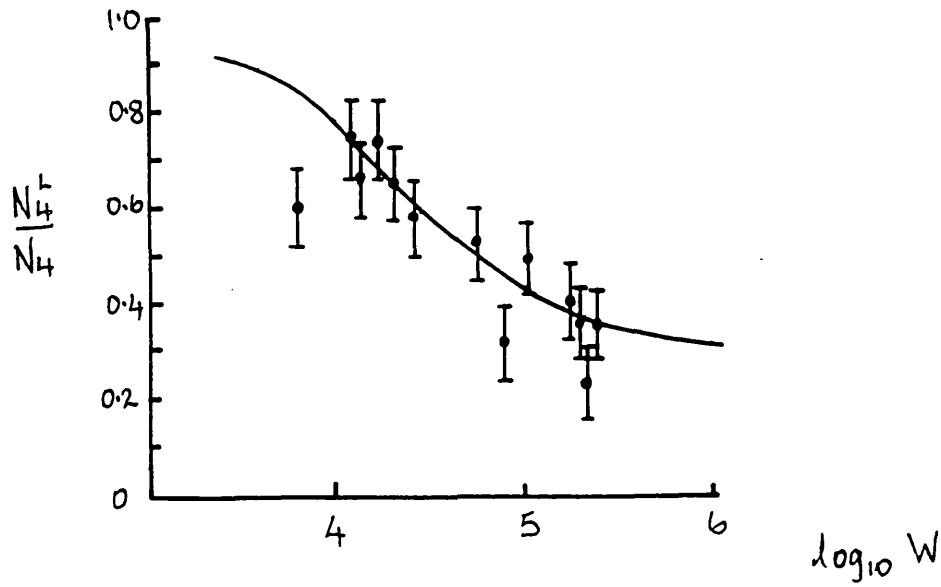

Fig. 4.3b

Two level model fit to data shown in Fig.4.2b

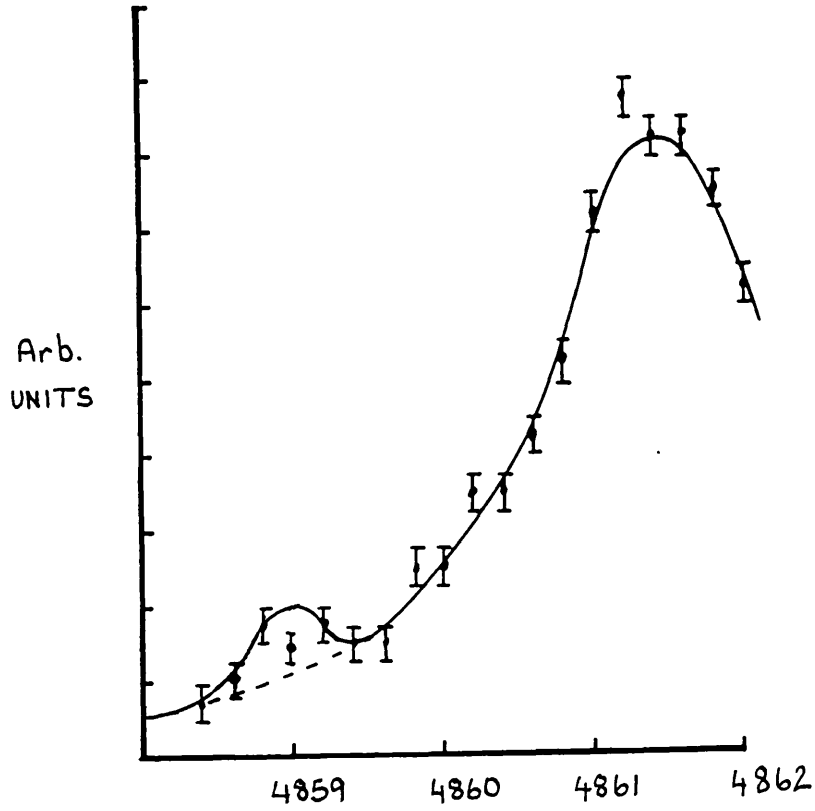

Fig. 4.4a.

Emission lineshape profile, n = 8 to n = 4, 4859Å.

He II 4859Å emission lineshape seen on the wing of the H-Beta profile due to residual hydrogen in the Helium gas. The extrapolated H-Beta profile is shown under the 4859Å He II profile. Data taken 18 microseconds after pinch phase when Ne = $5 \times 10^{14} cm^{-3}$ and Te = 1.35eV.

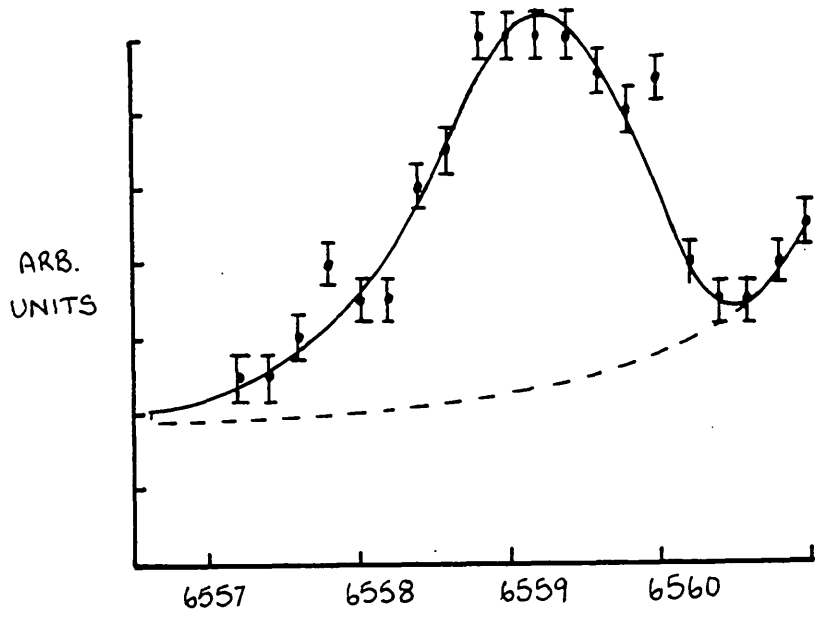

Fig. 4.4b.

Emission lineshape profile, n = 6 to n = 4, 6559Å.

He II 6559Å emission lineshape seen on the wing of H-Alpha profile due to the residual Hydrogen in the Helium gas. The extrapolated H-Alpha profile is shown under the 6559Å He II profile.
Ne = 5 x 10^{14} cm^{-3} and Te = 1.35eV.

have a half-width of 1.6Å and the 4859Å transition about 0.5Å. The linewidths of transitions should increase up a series, roughly as

$$\Delta\lambda \propto (ab)^4 / (b^2 - a^2)$$

(where a is the lower level and b is the upper level, Griem, 1960), due to the increased cross section of higher lyihg levels, so the 4859Å data looks to be untrustworthy. Griem also gives approximate formulae for the lineshapes of hydrogenic transitions, which, for $Ne = 5 \times 10^{14} cm^{-3}$ and Te = 1.35eV, show halfwidths of:-

For 4859Å transition F.W.H.M. = 4Å

For 6559Å transition F.W.H.M. = 3.2Å

These are considerably broader than those measured, however, the same formulae give a halfwidth for neutral Hydrogen H-Beta of 3.2Å, when $Ne = 10^{15} cm^{-3}$ and Te = 1eV.

For these conditions, it is now well known from many experimental and recent theoretical results, that the F.W.H.M. of H-Beta, at $Ne = 10^{15} cm^{-3}$, should be 2·2Å. Though the halfwidths may be wrong, the ratio of halfwidths of 4869Å to 6559Å should be reasonable, so for the experimental linewidth of 4859Å, a width of 2·0Å* was used. For convenience at this point, eqn 2.40 was converted to units of wavelength and the Einstein B coefficient converted to the A value. Then

$$D_a = \frac{K A_{ba} g_b \lambda^5}{8\pi h c^2 g_a \Delta\lambda} \left[\frac{N_a^2 (Sat)}{Na} \right] \qquad 4.7$$

The 'equivalent width' $\Delta\lambda$ was estimated, using Fig. 2.1 and the measured halfwidth of the laser of 0.5Å.
The summary of the results is given below.

* See, for example, Burgess and Mahon (1972) and Esrom and Helbig (1981). Full references at the end of Chapter 1.

LINEWIDTH MEASURED	LINEWIDTH RE-ESTIMATED	$\Delta\lambda$	D_4
4859Å 0.5Å	2.0Å	2.1Å	3.16×10^9
6559Å 1.6Å	1.6Å	1.7Å	2.7×10^9

It has been assumed in the discussion above, that the He II plasma was homogeneous and filled the plasma vessel. In fact, there will be radial temperature and electron density gradients in the plasma and the population density of He II is very sensitive to temperature. (See Cox and Tucker 1969).

Thus the He II plasma could be confined to a small hot cylinder of undetermined radius, around the central axis of the plasma. If this were the case, it would result in the experimental points being placed too low, commensurate with the error in estimating the diameter of the He II emitting region. Fig. 4.5 shows how the experimental results, as represented by eqn 2.39, would be plotted, if in fact the plasma was represented by a two temperature model where the He II was confined to a hot volume of given radius around the central axis. This model assumes the boundary is sharp, which is not unreasonable, given the sensitivity of the He II n=4 population density with temperature.

The effect can be seen to be similar to the lowering of both Na^L(Sat) and K, so leading to a lower value of Da. From the data and the fits to the data shown in Fig. 4.3, it can be seen that the effect is not drastic enough to be noticable from the data itself. That is to say, the data

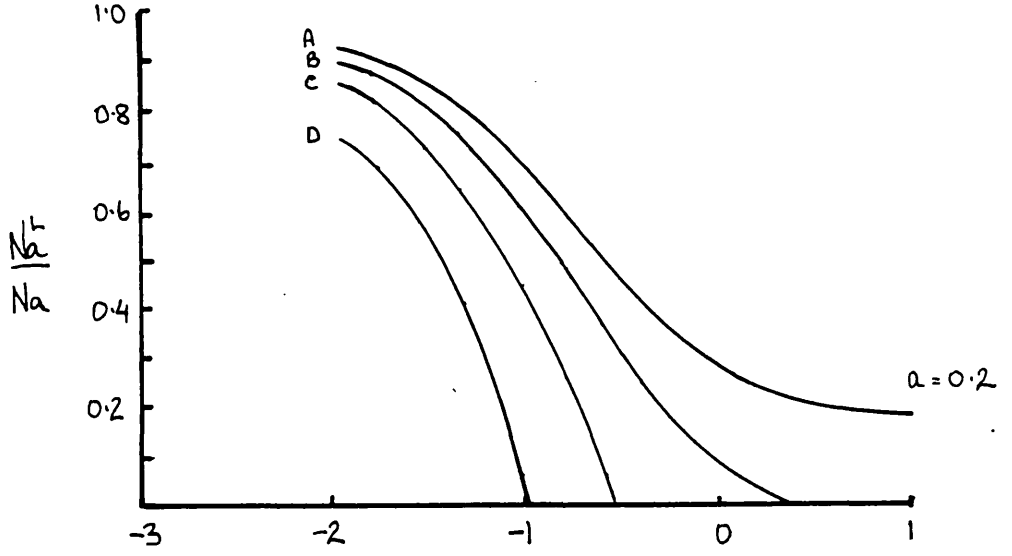

Fig. 4.5

The effect of over-estimating the He II plasma Diameter

A. Expected results if He II plasma was estimated correctly.

B. He II plasma 20% smaller

C. He II plasma 50% smaller

D. He II plasma 70% smaller (only 30% of that estimated)

do not appear to be tending to go below the axis.

However, the values of D4 arrived at above, may be considered to be lower limits.

4.4 COMPARISON of the DATA with a He II COLLISIONAL RADIATIVE MODEL and FINAL RESULTS

In this section, the experimental data will be compared to the predictions of a Collisional Radiative Model for He II. The model will be used to correct the assumed diameter of the He II plasma. The data in Fig, 4.2, will then be re-plotted, using the new plasma diameter and the two level model will again be used to deduce new revised rate out of n=4.

The errors in the experiment, both random and systematic, will then be analysed.

A Collisional Radiative Model (C.R.M.) for He II is described in Appendix 1. Using this model, it is in principle, possible to compare theory with experiment without any approximations being made. For the C.R.M. used here however, the assumption was made that the plasma relaxed slowly enough so that all the populations of the excited states were in equilibrium with each other.

However, when running the model for Te = 1.35eV and $Ne = 5 \times 10^{14} cm^{-3}$, the model predicted virtually zero population densities for the excited states. For temperatures below about 10eV, the He III population density is too low for recombination from the continuum to be sig-

nificant, in comparison to excitation from the ground state, in populating the He II excited states. See Cox and Tucker (1969). With the first excited state 41eV above the ground state, the collisional excitation rate for a 1.35eV plasma from the ground state to the excited states will be very small.

Experimental measurements of the He II excited state population densities however, showed quite reasonable densities. Table 4.3,

As mentioned above, it was assumed that all states of the system would be in dynamic equilibrium, but Roberts (1973) showed that for a Helium plasma, decaying in a similar time scale to the present one, the comparatively slow recombination rate of He III to He II, could lead to He III densities 12 orders of magnitude higher than the steady state equilibrium values.

It was found that by setting the He III population to a value of $2 \times 10^{13} cm^{-3}$, the predicted C.R.M. populations could be made to agree with the experimental excited state populations to within a factor of 2 for n=4. See Table 4.3.

Given the temporal history of Ne and Te in the plasma, it is possible to construct a rate equation for the He III population density, N(III) , and use this to plot the evolution of the He III population density from some known value. Unfortunately, there is only one time for which Te is known and the He III population density is not known at any time.

POPULATIONS of EXCITED STATES of He II

n	C.R.M.THEORY	EXPERIMENT
1	5×10^{14} cm^{-3}	
2	2.7×10^{9} cm^{-3}	
3	3×10^{7} cm^{-3}	
4	8.2×10^{5} cm^{-3}	1.14×10^{6}
5	3.8×10^{5} cm^{-3}	
6	2.1×10^{5} cm^{-3}	4.2×10^{5}
7	1.3×10^{5} cm^{-3}	1.6×10^{5}
8	8.6×10^{4} cm^{-3}	10^{5}
9	5.8×10^{4} cm^{-3}	10^{5}
10	4.3×10^{4} cm^{-3}	

TABLE 4.3

C.R.M. assumes a value of N(III) = 2×10^{13}cm^{-3} and the experimental values of Te = 1.35eV, Ne = 5×10^{14}cm^{-3}. The experimental populations were measured by a calibrated absolute emission experiment. The detection system, a 'Monospec 1000' monochromator with an R.C.A. 4836 photo-multiplier attached to the exit slit, was calibrated in terms of photo-multiplier current against photon flux into the input slit for the wavelengths of the transitions of interest (the levels shown above to n=4). A standard lamp, itself calibrated for blackbody temperature against lamp current, at the National Physical Laboratory, was used. For the actual emission experiment the layout was as for Fig.3.15, except that the lens was focussed at infinity, to simplify the computation of the observed plasma volume and the subsequent photon flux for a given number density in that volume.

However, it is possible to fit the Ne data to a curve, where

$$Ne = 1.48 \times 10^{15} \exp -4891\, t \quad cm^{-3} \qquad 4.9$$

The projected electron density for a time, just after the pinch phase, will be Ne = 1.48 x $10^{15} cm^{-3}$. If it is assumed N($\overline{111}$) is in equilibrium at this time, then a temperature of 4eV is required to produce N($\overline{111}$) = 2 x $10^{13} cm^{-3}$. Assuming then that the temperature decays linearly thereafter the temporal history of the temperature will follow.

$$Te = 45000 - 15 \times 10^{8} t \quad {}^{o}K \qquad 4.10$$

Now, writing down the rate equation for N($\overline{111}$)

$$\frac{dN(III)}{dt} = C_{II\,III}\, N(II)\, Ne - Ne^{2} N(III)\, D_{III\,II} \qquad 4.11$$

The total ionization coefficients $C_{II\,III}$ and recombination coefficient $D_{III\,II}$ are given in Appendix 1. N($\overline{11}$) is assumed equal to Ne as N($\overline{111}$) $\ll$ Ne at all times of interest. $C_{II\,III}$ and $D_{III\,II}$ are functions of Te, but become functions of t, by substituting eqn 4.10.

Eqn 4.11 is now solved numerically, where

$$\Delta N(III) = \left(C_{II\,III}\, N(II)\, Ne - Ne^{2} N(III)\, D_{III\,II} \right) \Delta t \qquad 4.12$$

and

$$N(III)(t + \Delta t) = N(III)(t) + \Delta N(III) \qquad 4.13$$

POPULATION DENSITIES of He $\overline{\text{III}}$

t microseconds after pinch	N($\overline{\text{III}}$) Steady State	N($\overline{\text{III}}$) Model
0	2.02×10^{13}	2.02×10^{13}
2	5.68×10^{12}	" "
4	1.34×10^{12}	" "
6	2.5×10^{11}	" "
8	3.7×10^{10}	" "
10	3.7×10^{9}	" "
12	2.4×10^{8}	" "
14	8.4×10^{6}	" "
16	2.2×10^{5}	" "
18	4.6×10^{2}	" "
20	2×10^{-1}	2.015×10^{13}

TABLE 4.4

Table 4.4 shows the results for the first 2.0 microseconds for the values of N($\overline{\text{III}}$), both assuming eqiulibrium, i.e.

$$N(\text{III}) = \frac{C_{\text{II III}}\, N(\text{II})\, Ne}{N_e^2\, D_{\text{III II}}} \qquad 4.14$$

and then by solving eqns 4.12 and 4.13.

It can be seen from Table 4.4 that N($\overline{\text{III}}$) has hardly departed from its t=o value of $2.02 \times 10^{13} cm^3$. Whilst this should not be considered an accurate prediction of N($\overline{\text{III}}$), since eqn 4.10 is assumed and the value of N($\overline{\text{III}}$) at t=o is not known, the general trend, that N($\overline{\text{III}}$) will, in fact, remain unchanged from an earlier epoch, is seen to be valid.

Figs 4.6 shows plots of the theoretical C.R.M. predictions for the relative depletion of N4 against laser power density. The collisional rate coefficients used, were those due to Bates, Kingston and McWhirter (1962) from cross section calculations, due to Seaton (1962).

It can be seen that, in general, the fits of both curves are reasonable, but also, that the experimental points appear to lie above the theoretical curve for the low depletion points, (i.e. points at low laser powers, where Na^L / Na is high) and below the curve for the high depletion points. This would seem to indicate that the experimental rate out of N=4 was slightly higher than that predicted by the C.R.M. code - which would bring the theory curve to the right, so fitting the low depletion points better, and also the He II plasma did not in fact, fill the vessel, which would lead to the high depletion points lying too low, as shown in Figs 4.6.

As explained in Chapter 2, section 2.6c, it is only really possible to comment on the general correctness of the model, by judging how well it predicts the experimental data. The C.R.M. curves were produced using the predicted total rate coefficient of $2.9 \times 10^9 sec^{-1}$ out of n=4. The rate coefficients predicted, using the two level model, agree with this to about 20%. However, the values of $(N4^L(Sat)/N4)$ produced by the C.R.M. will depend on the ratios of the rates between the various levels, rather than the absolute rates.

The ratios of the steady state populations (without laser irradiation, Table 4.3) of the various excited states,

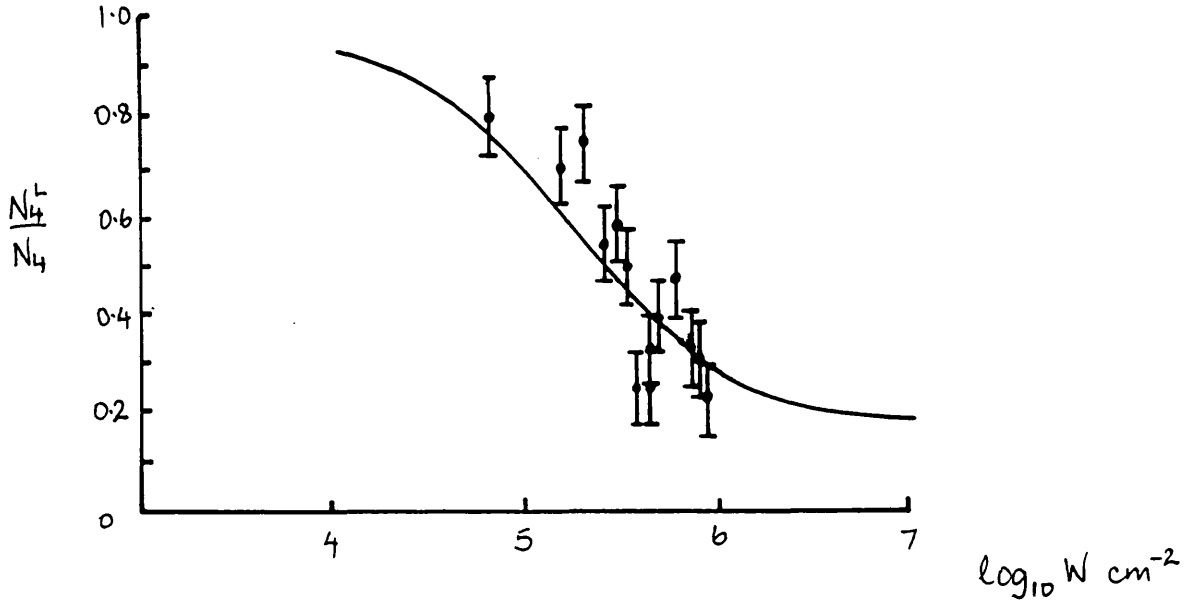

Fig. 4.6a

C.R.M. Prediction shown with data for laser pumping n = 4 to n = 8, (from Fig.4.2a)

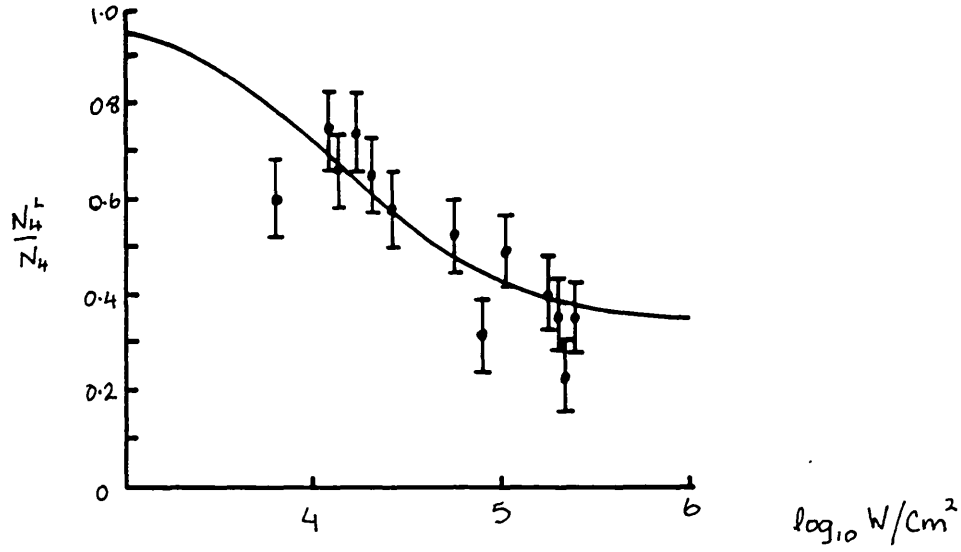

Fig. 4.6b

C.R.M.Prediction shown with data for laser pumping n = 4 to n = 6, (from Fig.4.2b).

one to another, will also depend on the ratio of the rates, into and out of, the levels in question, rather than the absolute rates. Table 4.3 shows that, experimentally, the populations of n=4 and n=8 have a similar ratio to theory (11.4 and 9.5), though ratios of populations for n=4 and n=6 are not quite so good (2.71 and 3.9). However, there is some justification for assuming the ratios of rates, for the experiments are similar to the ones used in the C.R.M. theory and that therefore the higher values of ($N4^{L}$(Sat)/N4) predicted by the C.R.M. are indicative that the He II plasma diameter was, in fact, smaller than assumed in plotting Fig. 4.2.

To estimate the actual plasma diameter then, the assumption will be made, that the values of (N4(Sat)/N4) produced by the C.R.M., are in fact correct. The plasma diameter will now be

$$45 \times \left[\frac{1 - \text{C.R.M.}(N_4^L(\text{Sat})/N_4)}{1 - \text{EXP.}(N_4^L(\text{Sat})/N_4)} \right] \quad \text{mm}$$

For the two experiments the new estimated He II plasma diameter will be

He II PLASMA DIAMETER

Pumping n=4 to n=8. - - New He II plasma Dia. = 39mm

Pumping n=4 to n=6. - - New He II plasma Dia. = 42mm

Now, using the average Diameter of 40.5mm, the data of Tables 4.4 are replotted in Figs 4.7 and Tables 4.5. To obtain a value for D4, eqn 4.1 is now fitted to the data as before and the resulting values of a and K are shown in Table 4.6.

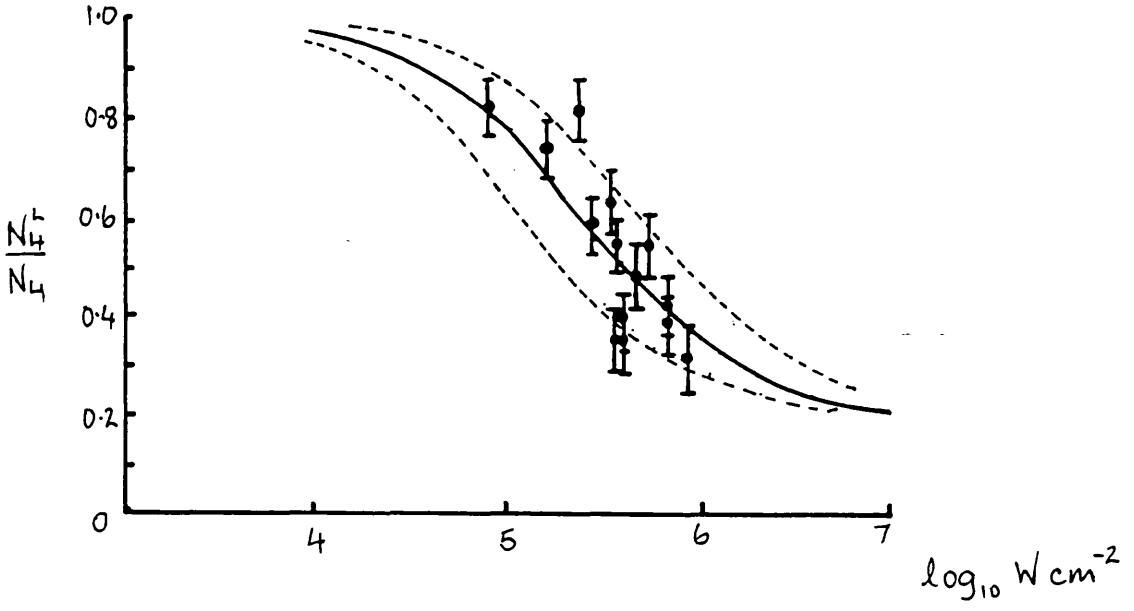

Fig. 4.7a

Data from Fig.4.2a (laser pumping n=4to n=8) replotted for He II plasma diameter 40.5mm. Also subsequent two level model fit. (Full curve). The dotted curves are generated by the two level model with K increased and decreased by a factor of 2.

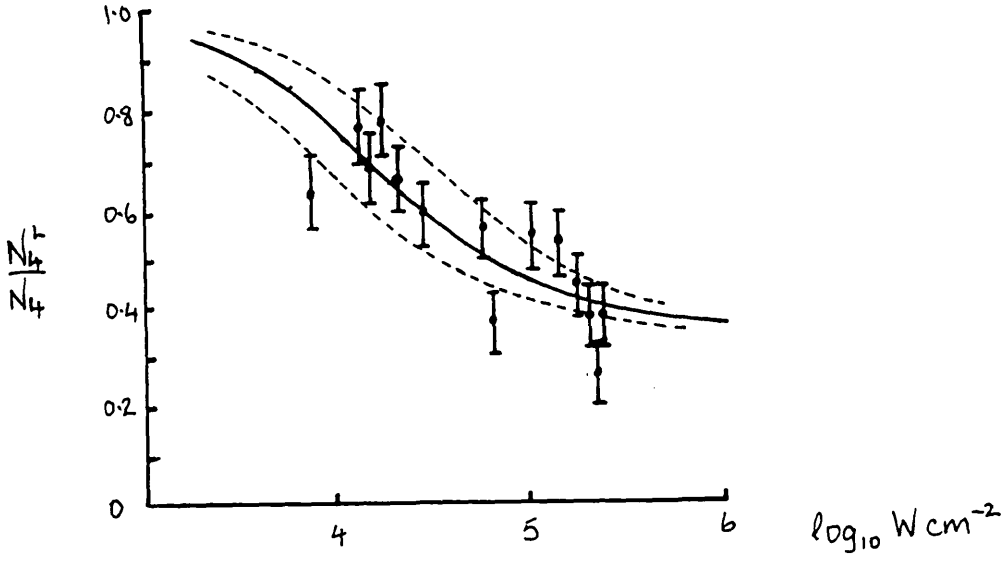

Fig.4.7b

Data from Fig.4.2b (laser pumping n=4 to n=6) replotted for He II plasma diameter 40.5mm. Also a subsequent two level model fit. (Full curve). The dotted curves are generated by the two level model with K increased and decreased by a factor of 2.

Pumping on 4859Å, n=4 to n=8.

a	K	$\bar{S} \times 10^{-3}$	$aK \times 10^{6}$
0.3	0.42	10	0.13
0.25	0.61	7.4	0.15
0.19 C.R.M.	0.98	4.1	0.19
0.15	1.38	2.5	0.17
0.1	2.37	1.3	0.24

Pumping on 6560Å, n=4 to n=8.

a	K	$\bar{S} \times 10^{-3}$	$aK \times 10^{6}$
0.4	0.34	2.8	0.14
0.35	0.55	3	0.19
0.3	0.77	3	0.23
0.25	1.18	2.1	0.3

TABLE 4.6

Values for a and K when fitting two level Model to data, replotted for plasma Diameter 40.5mm.

	$N4^L/N4$	$P \times 10^6 cm^{-2}$
1.	.82	0.08
2.	.75	0.15
3.	.81	0.22
4.	.6	0.29
5.	.64	0.335
6.	.56	0.36
7.	.35	0.36
8.	.35	0.4
9.	.41	0.4
10.	.47	0.49
11.	.55	0.55
12.	.42	0.7
13.	.39	0.7
14.	.31	0.88

TABLE 4.5a

Relative depletion of n=4 against laser power for HeII plasma diameter 4.05cm. Laser pumping at 4859Å, n=4 to n=8.

	$N4^L/N4$	$P \times 10^5 cm^{-2}$
1.	0.63	0.075
2.	0.76	0.13
3.	0.69	0.14
4.	0.77	0.18
5.	0.67	0.21
6.	0.60	0.3
7.	0.57	0.6
8.	0.37	0.69
9.	0.55	1.02
10.	0.53	1.41
11.	0.44	1.89
12.	0.38	2.04
13.	0.26	2.22
14.	0.38	2.34

TABLE 4.5b

Relative depletion of n=4 against laser power density for He II plasma diameter 4.05cm. Laser at 6560Å, pumping n=4 to n=6.

Taking the values of a, obtained from C.R.M., it can be seen that the 6560Å data minimises well for $\bar{S}$ at that value (0.35), whilst the 4859Å data, would seem to minimise at a lower value than 0.19. Also shown on Fig. 4.7, are plots generated using the two level model, using the C.R.M. values of a and the consequent best fit values of K. Also shown, are plots for values of K that vary from the best fit value, by a factor of 2. Using eqn 2.40, the values of D4 obtained using these plots is given.

VALUE for D4

	a	K	D4
4859Å	0.19	0.98×10^{6}	3.3×10^{9}
6560Å	0.35	0.55×10^{5}	2.8×10^{9}

As can be seen from Figs 4.7,

4.5 ANALYSIS of ERRORS and FINAL RESULT.

There are several sources of error in this experiment, some of which are random and some of which are syatematic.

RANDOM ERRORS

These are the errors in measuring the actual depletion data from the photographs and was due to the shot noise on the data (see Fig. 4.1). The error bars plotted on the data in Fig. 4.2 and 4.7 are due to this. Generally, the error on $N4^{L}/N4$ is about $\pm$ 0.08.

The dotted curves Fig. 4.7 show the effect of changing the values of K (and hence D4) by a factor of 2. The full curve is obviously a much better fit than the dotted curves. so that errors of + 50% or -20% would seem reasonable.

SYSTEMATIC ERRORS

One major weakness of this particular experiment was the failure to secure an experimental value of $N4^{L}$(Sat)N4. Much effort was spent in trying to get an accurate figure for this, compounded by the fact that the He $\underline{\underline{II}}$ plasma diameter was unknown. From Table 4.6, it can be seen that the product aK (and hence D4) will have an error approximately equivalent to the error in $N4^{L}$(Sat)/N4.

The He $\underline{\underline{II}}$ plasma diameter determined from the C.R.M. predictions, was about 12% smaller than that which the actual plasma vessel diameter actually used. An error of $\pm$ 10% on $N4^{4}$(Sat)/N4 and hence D4, due to this source, would seem reasonable.

Non-uniformity in the power density across the laser beam, would cause a systematic error, which would result in the data points being placed too high (see Fig. 2.6), particularly where $P \simeq K \times N4^{L}(Sat)/N^{4}$. This error was also seen to be a function of $N4^{L}(Sat)/N4$, but for the values used and for a power density variation of 30%, this would cause a maximum error of 2%, which is much smaller than the Random error due to noise on the data. This error source can be discounted.

In the final analysis, the values of $N4^{L}(Sat)/N4$ generated by the C.R.M. were used in the two level model to finally derive a value for D4. It is worth checking how well the two level model agrees with the C.R.M. theory for the same value of D4 and $N4^{L}(Sat)/N4$. Accordingly the two level model was fitted to the C.R.M. curves for the C.R.M. values of $N4^{L}(Sat)/N4$. With the optimised values of K determined, the two curves agreed to within 2% at all points. The values of D4 obtained from eqn 4.7 using these values of K and $N4^{L}(Sat)/N4$ were

Laser pumping on 4859Å, D4 = $3.0 \times 10^{9} sec^{-1}$
Laser pumping on 6560Å, D4 = $2.7 \times 10^{9} sec^{-1}$

This shows the Two Level Model is a fair approximation and should give results to within 5% of the true figure.

The final error on the data would appear to be dominated by the error in measuring the depletion, so that the final results for the measured de-excitation rate out of n=4 are

Pumping 4859Å, D4 = $3.3\ (+1.6 - 0.85) \times 10^{9} sec^{-1}$
Pumping 6560Å, D4 = $2.8\ (+1.4 - 0.7) \times 10^{9} sec^{-1}$

These results agree well with the C.R.M. perdicted value of 2.9 x 10sec^{-1}. Seaton (1962) quoted accuracy of a factor of 2 for his cross sections which were used in the collision rate coefficient formulae of Bates et al (1962) used in the C.R.M.

From the C.R.M. The de-excitation rate out of n=4 is dominated by collision rates to n=5 and n=3, which are respectively, 5.2 x 10^8 and 1.82 x 10^9, the remainder of the total being radiative and collision rates to other levels.

4.6 CONCLUSIONS

To sum up, the data obtained for the depletion of He II n=4, whilst pumping on two transitions having n=4 as the lower level, was fitted to a two level model, described in Chapter 2. Initially the He II plasma diameter was considered to be the same as that of the plasma vessel. Theoretical curves for depletion of n=4 against laser power, was generated using a Collisional Radiative Model for He II.

These curves, when compared to the data, indicated that the He II plasma diameter was probably smaller than that originally estimated and on the basis of a crude two temperature model of the plasma, the data was replotted for the re-estimated plasma diameter. The two level model was again fitted to the new data and estimates of the rate out of n=4 obtained.

The results are in good agreement with the rates predicted by the C.R.M. and are also internally consistant.

The assumption that the linewidth of the 4859Å transition and using of widths, predicted by Griem (1960), was probably correct, considering the subsequent agreement of the 4859Å data with the 6560Å data. This shows the ratios of linewidths predicted by Griem (1960) are probably good though the absolute linewidths are not.

The general agreement of these results with each other, considering a difference in laser power of about 6 (and a difference in laser frequency) for the two experiments, shows there was probably no hidden laser induced rates (from any He molecular species, for example) into n=4.

The experimental method could have been improved by viewing only plasma which had been irradiated by the laser. Fig. 4.8 give a possible arrangement by which this may be achieved. This method has the advantage in that the observed relative depletion would then be the actual relative depletion, without any corrections being needed. Also, only one viewing port into the plasma is required, making the technique far more flexible on what plasma machine it can be used.

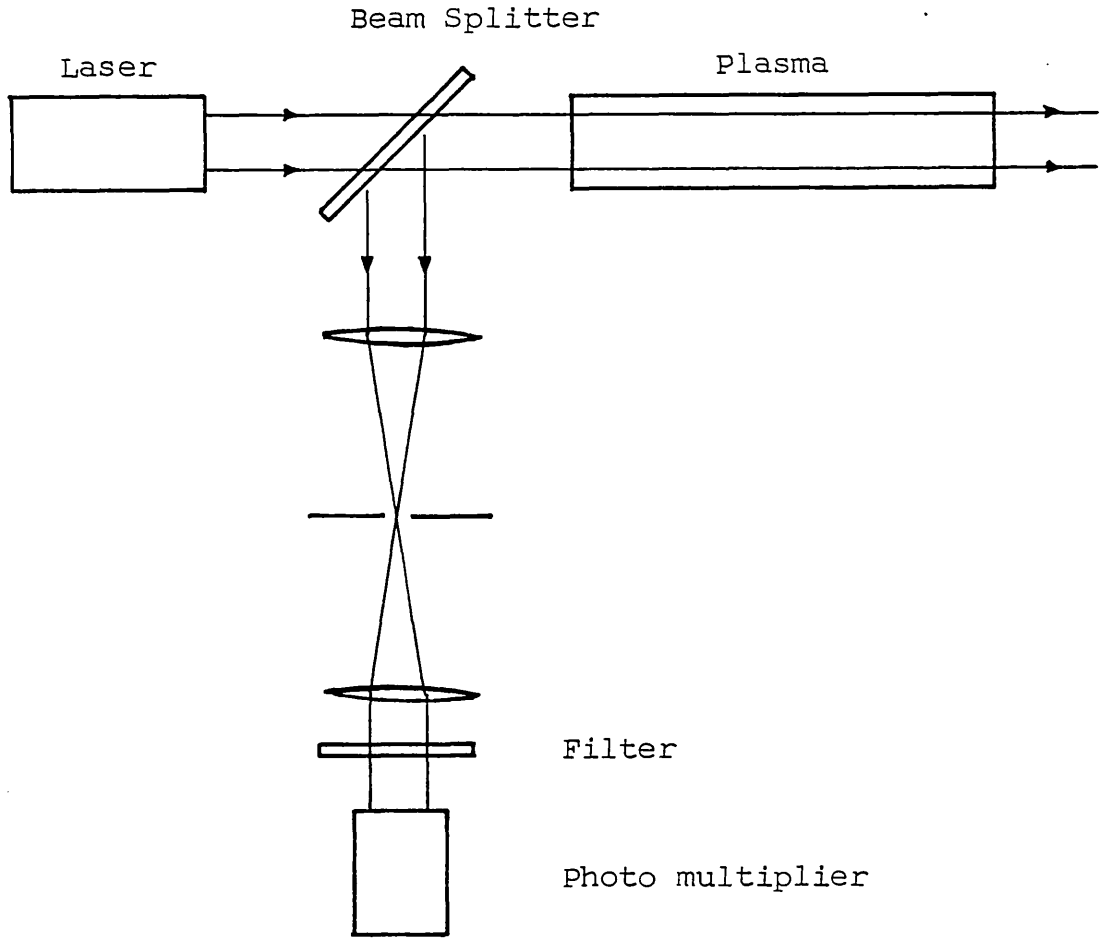

Fig. 4.8

IMPROVED EXPERIMENTAL LAYOUT

for

THREE LEVEL COLLISION RATE EXPERIMENT

In this arrangement the observed plasma is all pumped by the pump laser so removing any uncertainty regarding the ratio of pumped to unpumped plasma.

The observed depletion will now be the actual depletion of the level of interest.

REFERENCES

Bates D.R., Kingston A.E., McWhirter R.W.P., Proc.Roy. Soc. 267, 297, (1962)

Cox D., Tucker W., Ap.J. 157, 1157. (1969)

Griem H.R.,Ap.J. 883, (1960)

Roberts D.E., J.Phys.B. 6, 929, (1973)

Seaton M.J., 'Atomic and Molecular Processes'. Ed. D.Bates, Pub. Academic. New York. (1962).

CHAPTER 5

H-BETA LINESHAPE EXPERIMENT - RESULTS and ANALYSIS

5.1 SUMMARY

A three level technique, discussed in Chapter 2, was used to measure the lineshape profile of H-Beta for an electron density of Ne = $10^{15}cm^{-3}$. The purpose of this experiment was to investigate if, in a plasma substantially similar to that of Burgess and Mahon, (1973), the central dip of the H-Beta was being filled in by an impurity contribution. No measurable impurity contribution to the line core was found.

Also investigated, was a feature observed on the red wing of the H-Beta profile at an electron density of $5 \times 10^{14}cm^{-3}$ This feature was found to be an impurity, but its origin could not be determined with any certainty. That the feature may have been an H_2 molecular transition, was investigated by looking for absorption at the wavelength of the strong H_2 molecular transition at 4856·55Å. No absorption at this wavelength, over that due to the H-Beta line wing, was observed.

The population density of the $n=2$ hydrogen level was measured for the first 90 microseconds of the afterglow phase of the Z pinch. It was also found that during the period that the experiments were being performed, the $n=2$ populations, for any particular time in the afterglow, appeared to have fallen by 25 %. No explanation for this is forthcoming.

5.2. ABSORPTION PROFILE of H-BETA for $Ne=10^{15}cm^{-3}$

The experimental technique used to deduce whether of not there was any impurity contribution to the core of H-Beta was the Saturated Three Level Absorption Spectroscopy (S.T.L.A.S.) technique, described in Chapter 2. The detailed experimental method employed is described in Chapter 3. The plasma used, was the afterglow of a Z pinch device, also described in Chapter 3. From Fig.3.3 it can be seen that the electron density was $10^{15}cm^{-3}$ at a time 30 microseconds into the afterglow. Accordingly, the lasers were fired at this time, scanning the profile (with the probe laser) on a shot to shot basis. Fig. 5.1 shows the final experimental results- both with and without the pump laser. The straight absorption profile, Fig. 5.1a, shows no evidence of any dip greater than 3% at the line core, corroborating the results of Burgess and Mahon (1972) and Fleurier et al (1980).

Fig. 5.1b shows the results when the absorption profile was taken again, but this time the lower level of the H-Beta transition, n=2, was simultaneously depleted by saturating the H-Alpha transition with a flashlamp pumped dye laser. This resulted in an absorption profile, whose optical depth, due to H-Beta at any given wavelength was an order of magnitude lower than that for Fig. 5.1a

In the absence of any impurity, the lineshapes should be the same in both cases. It is immediately obvious from an inspection of Figs 5.1a and 5.1b that any impurity contribution to the line core will be no more than a few percent of the H-Beta line strength at that point.

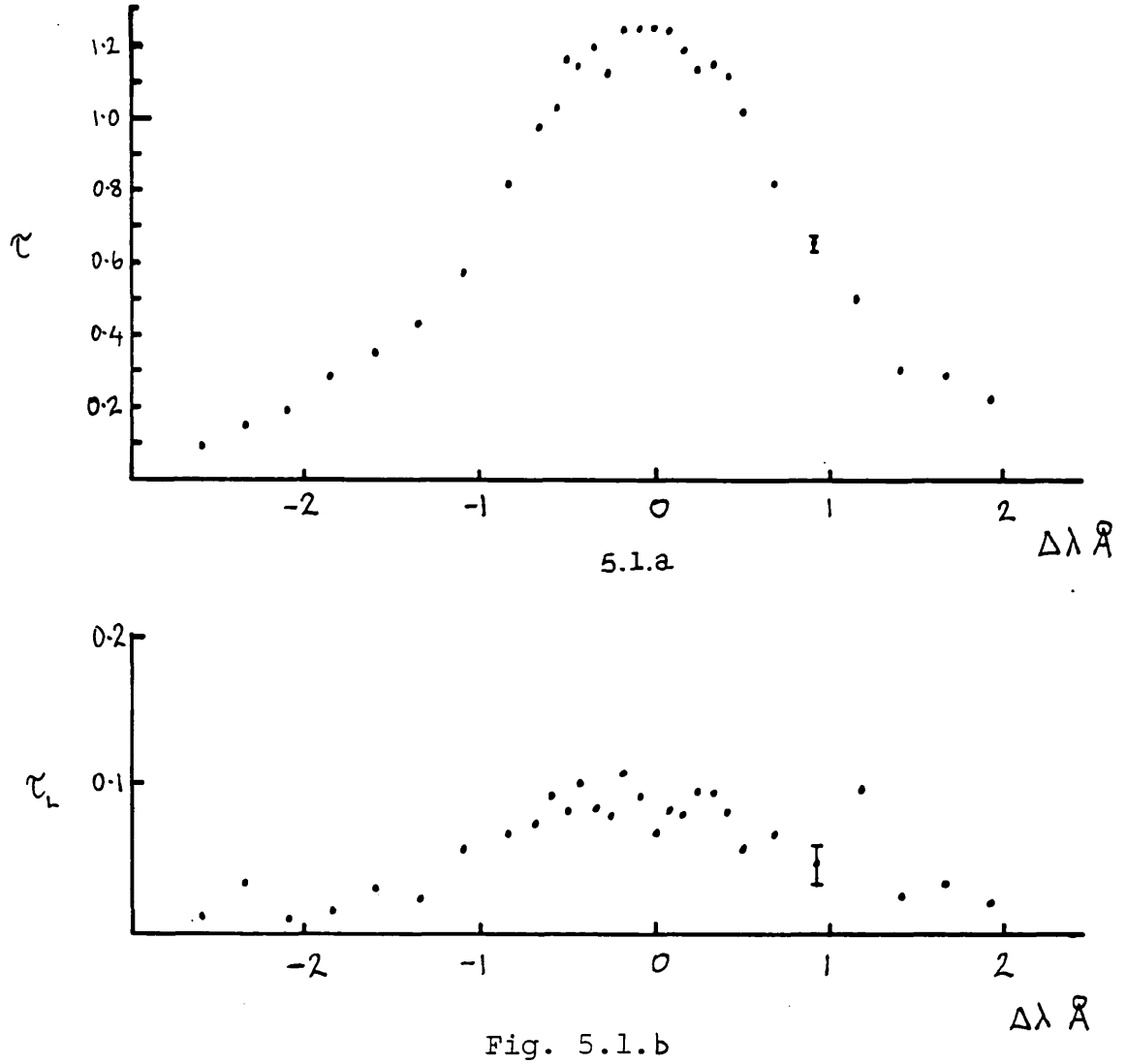

Fig. 5.1.b

Absorption Profiles of H-Beta - with and without H-Alpha pumping.

The top profile shows an absorption profile of H-Beta Ne = $10^{15} cm^{-3}$ and Te = 1·4 eV
The bottom figure shows the same profile for the same conditions, except H-Alpha is being irradiated by laser radiation.

However, the limits of any impurity contribution may be determined by area normalising the two profiles, so that at any wavelength

$$\Delta\tau(\lambda) = F\tau(\lambda) - \tau_L(\lambda) \qquad 5.1$$

Where the factor F is the normalising factor of eqn 2.51 and $\tau_L(\lambda)$ is the optical depth when the H-Alpha pump laser is on. The factor F is estimated initially, by drawing a best fit curve through the experimental points of both profiles, $\tau(\lambda)$ and $\tau_L(\lambda)$, and then taking the ratio of the small area to the large area. Fig. 5.2 shows a $\Delta\tau$ plot for Fig 5.1.

If the two profiles have the same lineshape function, then the points plotted in Fig. 5.2 should form a random (Gaussian) distribution around the $\Delta\tau = 0$ line. If the profiles are the same, but the area ratio F is incorrect, the points will lie on a curve, having the same shape as the absorption profiles. The area under the curve will be proportional to the error in F, which can then be adjusted.

If the two profiles are not the same, but the area ratio is correct, the points will lie on a curve which will intersect the $\Delta\tau = 0$ base line, in such a way, that the areas under the curve will be the same above and below the base line. The $\Delta\tau = 0$ line can then be adjusted to lie on the asymptotic limit of the impurity contribution, where the gradient of the curve is zero. The curve under the base line will then be the lineshape of the impurity contribution.

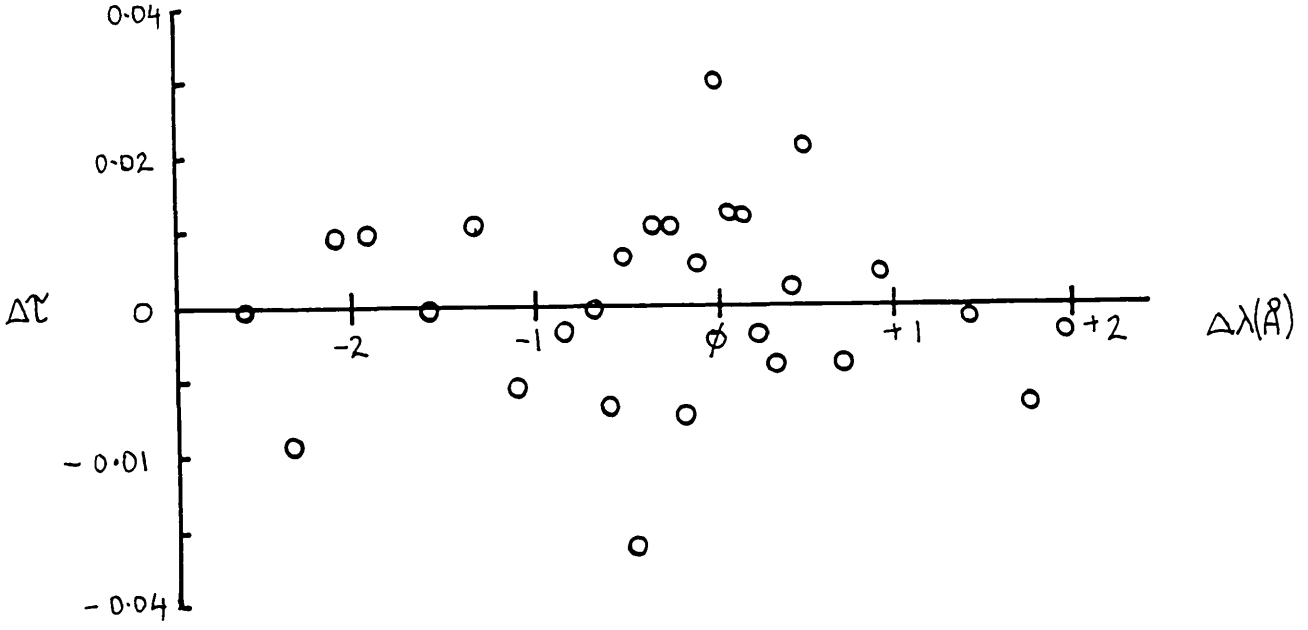

Fig. 5.2.

$\Delta\tau$ plot for H-Beta Ne = $10^{15}cm^{-3}$.

This figure shows a $\Delta\tau$ plot for the data shown in Fig.5.1. $\Delta\tau$ is the normalised value of the optical depth for any given wavelength (obtained by straight forward absorption) minus the optical depth, whilst the H-Alpha laser was on.

An inspection of Fig. 5.2 shows no trend for the points to depart from the $\Delta\tau$ = o base line at any point. However, given that a feature broad enough to fill in the H-Beta dip is being sought, it is reasonable to compare the mean $\Delta\tau$ for the central Ångstrom of Fig. 5.2, (One Ångstrom would be the separation of the peaks of the H-Beta profile, if there were a dip present), to the mean of those points outside the central Ångstrom and so test for the presence of an impurity.

The points for the central Ångstrom in Fig. 5.2 lie about a mean of $\Delta\tau$ = 0.003, whilst the points outside the central Ångstrom have a mean of $\Delta\tau$ = -0.001. In both cases the standard deviation is 0.01.

Fig. 5.3a shows a histogram for the distribution of all the points around $\Delta\tau$ = 0 in Fig. 5.2. It is readily seen, the mean lies on $\Delta\tau$ = 0 and the half-half width of the distribution is 0.01, coresponding to the standard deviation. Figs. 5.3b and 5.3c show histograms for the central Ångstrom and those points outside the central Ångstrom, respectively.

The difference of 0.004 between the two means for the two distributions (the central Ångstrom and those points outside the central Ångstrom) is close enough to the error on the mean ($\sigma/\sqrt{n}$ = 0.003) not to be really significant. In addition, the trend of the points in the central Ångstrom is in the wrong direction to be due to an impurity contribution.

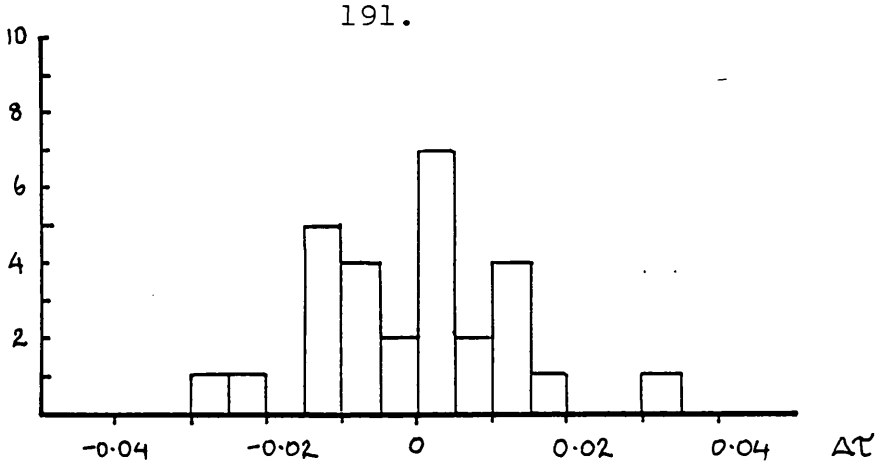

Fig. 5.3a

Histogram of all the points in Fig. 5.2

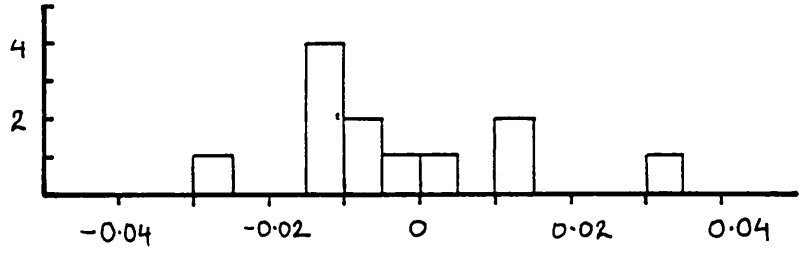

Fig. 5.3b

Histogram of the central $\bar{A}$ of Fig. 5.2

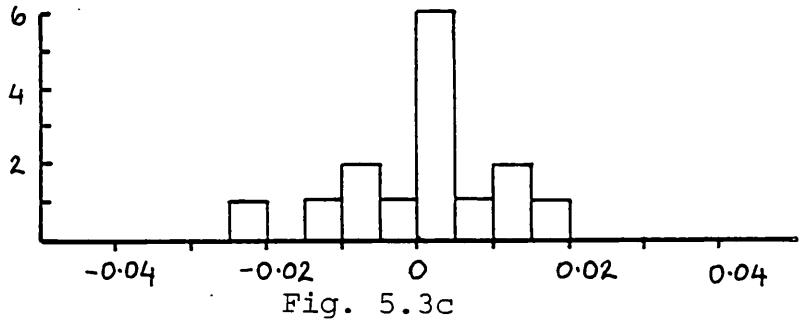

Fig. 5.3c

Histogram of all the points
NOT in the central $\bar{A}$ of Fig. 5.2

HISTOGRAMS OF THE NUMBER OF POINTS
HAVING PARTICULAR VALUES OF $\Delta\tau$

Any impurity having an optical depth greater than 0.01, would have been evident via a statistically significant trend of the points in the central Ångstrom and it is reasonable to conclude therefore, that an impurity contribution having an optical depth greater than 0.01 or 1% of the optical depth at the core of the profile, was not present. No satellites of any sort are otherwise observable on the wings of the profiles in Fig. 5.1.

This experiment does not exclude the possibility that an ion plasma satellite is filling in the line core as suggested by Ramette and Drawin (1976). However, no corresponding electron plasma satellites appear to be observable on the wings of the profile in Fig. 5.1. The only satellite that was observed, occured at an electron density of $Ne = 5 \times 10^{14} cm^{-3}$ and this was shown to be an impurity (see section 5.4). It is unlikely, then, that the line core was being filled in by a plasma satellite.

The H-Beta profile, shown in Fig. 2, is consistent with that of Burgess and Mahon (1972) and Fleurier et al (1980) in that no dip greater than 3% was observed. The electron temperature for this present experiment was somewhat higher than that quoted for the experiments cited above. ($1.5 \times 10^4 K$ as against $10^4 K$) and if the ion temperature can be assumed to be the same as the electron temperature then Mazure et al (1981) show we would not expect to see a dip.

That the ion temperature is the same as the electron temperature, is a reasonable assumption for this plasma,

since the electron - ion equilibr ation time is given by (Spitzer, 1956)

$$T_{eq} = \frac{m_p}{m_e} \frac{0.266\, T_e^{3/2}}{N_e \ln \Lambda} \qquad 5.2$$

Where $\ln \Lambda$ is a slowly varying function of Te and Ne and is given by Spitzer as being about 6, when $N_e = 10^{15} cm^{-3}$ and $Te = 10^4 K$.

Eqn 5.2 then gives $T_{eq} \approx$ 100 nanoseconds, which is very short compared to the γ_e relaxation period for this plasma of 36 microseconds.

5.3 ESTIMATION OF H_2 MOLECULAR DENSITY

It was shown in the previous section, that the electron-ion equilibr ation period should be about 10^{-7}sec for a plasma, where $Te \simeq$ leV and $Ne = 10^{15} cm^{-3}$. The equilibrium time of the atomic and electron temperatures will be about an order of magnitude larger than this, Cairns, (1970), since tha atoms are electrically neutral, so their effective velocity changing cross sections are reduced. Also, atoms have an internal partition function, which allows energy to be transferred, from the electron into exciting the atom internally. Since the electron temperature relaxes on a time scale of 36 microseconds, the atomic, molecular and electron temperatures should be in equilibrium.

The Saha equation for a molecule, consisting of two atoms, A and B, is:-

$$5.3 \qquad \frac{N_A N_B}{N_{AB}} = \left(\frac{2\pi\mu kT}{n^2} \right)^{3/2} \frac{g_A g_B}{g_{AB}} \exp - [E_{AB}/kT]$$

Where - g_A is the partition function of A

E_{AB} is the dis sociation energy

μ is the reduced mass

$$\mu = \frac{m_A m_B}{m_{AB}}$$

For the reaction

$$H_2 \rightleftharpoons H + H$$

we have A = B so that

$$E_{AB} = 4.48 eV$$

$$\mu = \frac{m_H}{2} = 8.4 \times 10^{-28} kg$$

$$g_A = g_B = 2$$

g_{AB} is the partition function for the H_2 molecule which

is obtained from Mayer and Mayer, (1940)

Fig. 5.4 shows a plot of the Mayers' partition function for H_2 against Temperature. This Plot is due to M.P.S.Nightingale.

For the H_2 molecule then, eqn 5.3 goes to

$$N_{H_2} = N_H^2 \times 3.7 \times 10^{-27} \frac{g_{H_2}}{T^{3/2}} \exp\left(5.196 \times 10^4 / T\right) \quad m^{-3} \qquad 5.4$$

For this plasma, when Ne = $10^{15} cm^{-3}$, Te = 1.4ev so g_{AB} = 430 and N_H = 2.8 x $10^{22} m^{-3}$, (N_H is estimated from the filling pressure of 0.45 Torr). we arrive at a value for N_{H_2} = 1.4 x $10^{10} cm^{-3}$.

Comparing this with the measured value for the n = 2 population of 4.5 x 10^{11}, see Fig. 5.8, it is unlikely that H_2 molecules are contributing anything that will be in the least way comparable to the optical depth of H-Beta.

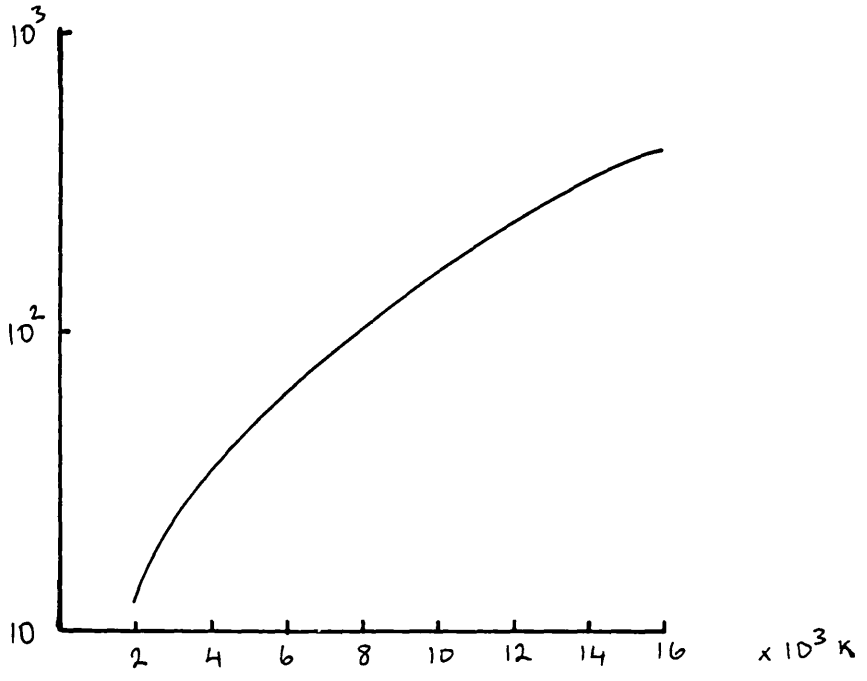

Fig. 5.4

Partition function for H_2 against Temperature.

Plot due to Nightingale. (private communication)

5.4. THE RED WING of H-BETA at Ne = 5 x $10^{14}cm^{-3}$

When initially setting up the apparatus, a trial run was performed at 47 μsec after the pinch phase. This was, because the optical depth at the line centre of H-Beta was highest for this time - which corresponded to an electron density of Ne = 5 x $10^{14}cm^{-3}$. On the red wing profile, two Ångstroms from line centre, there appeared to be several high points. Investigating these points further, a detailed absorption profile of the red wing was performed, shown in Fig. 5.5. The M.I.T. Wavelength Tables (1939) did not list any likely elements having transition at the wavelength of this feature, 4863Å, except an Fe I transition. (The only possible source of Iron was the Pyrex tube of the plasma vessel)

It was then decided to perform a detailed 'three level' investigation of the line around this feature. The results are shown in Fig. 5.6. The straight absorption profile is not as clean as that shown in Fig. 5.5, but the H-Alpha laser pumped profile shows the feature very clearly.

Fig. 5.7 shows a plot of $\Delta\tau$ for this profile where F = 0.1034. The feature now can be seen to have a peak optical depth of about 0.09 and a width of about 0.15Å. Following Drawin (1981) and Piel (1981), it was then thought possible that this feature was of molecular origin.

A strong H_2 molecular transition exists at 4856.5Å, and a scan through the region in straight absorption was tried, but no obvious feature was observed on the wing of H-Beta at that wavelength. See Fig. 5.8.

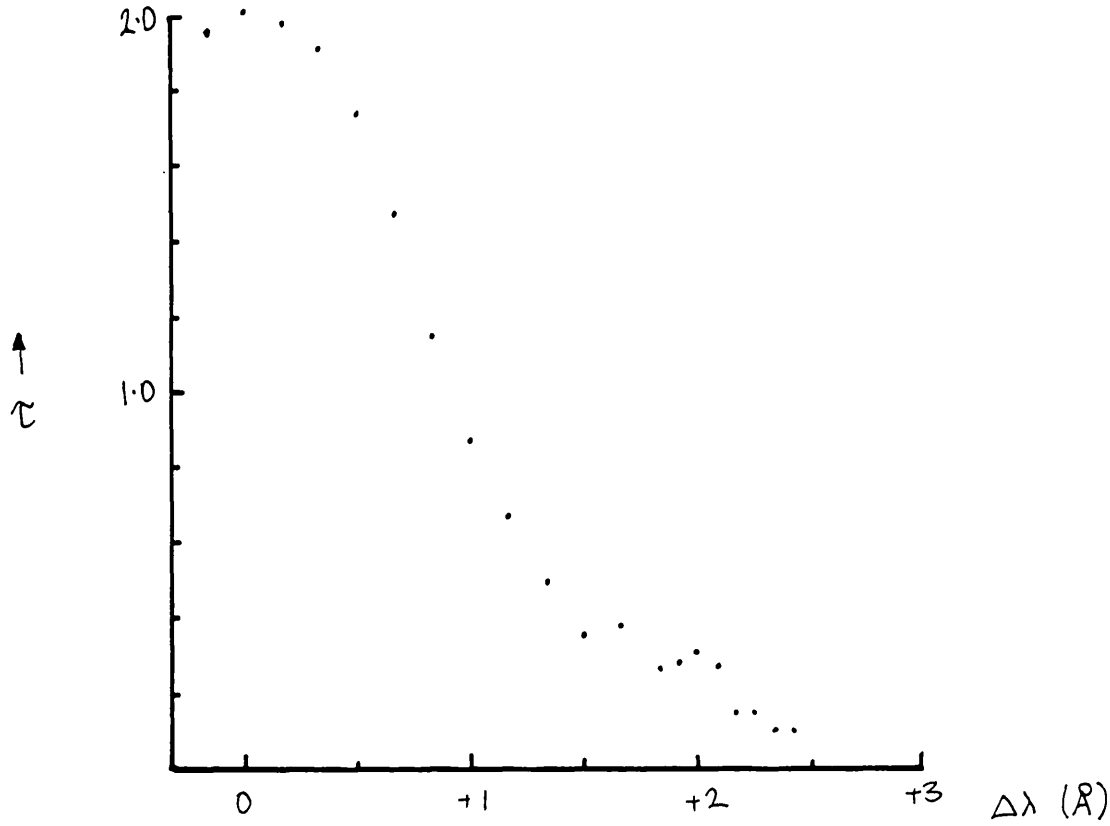

Fig. 5.5

Red wing of H-Beta for Ne = 5 x 10^{14}, Te = 0.8eV.

Note the structure 2Å from line centre.

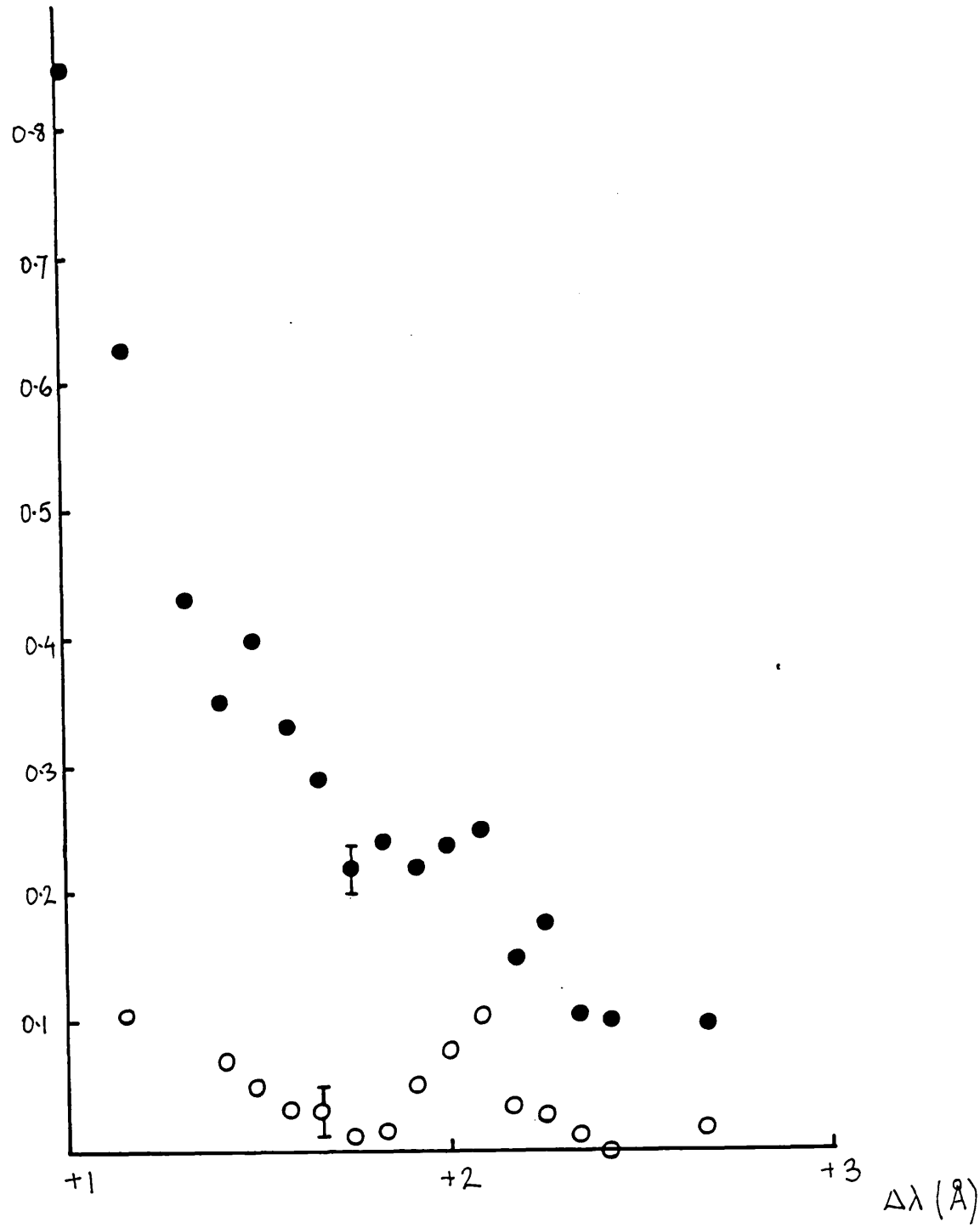

Fig. 5.6

Absorption profiles of red wing of H-Beta, Ne = 5 x 10^{14} cm^{-3} with and without H-Alpha irradiation.

- ● Straight absorption
- o Absorption with H-Alpha laser on.

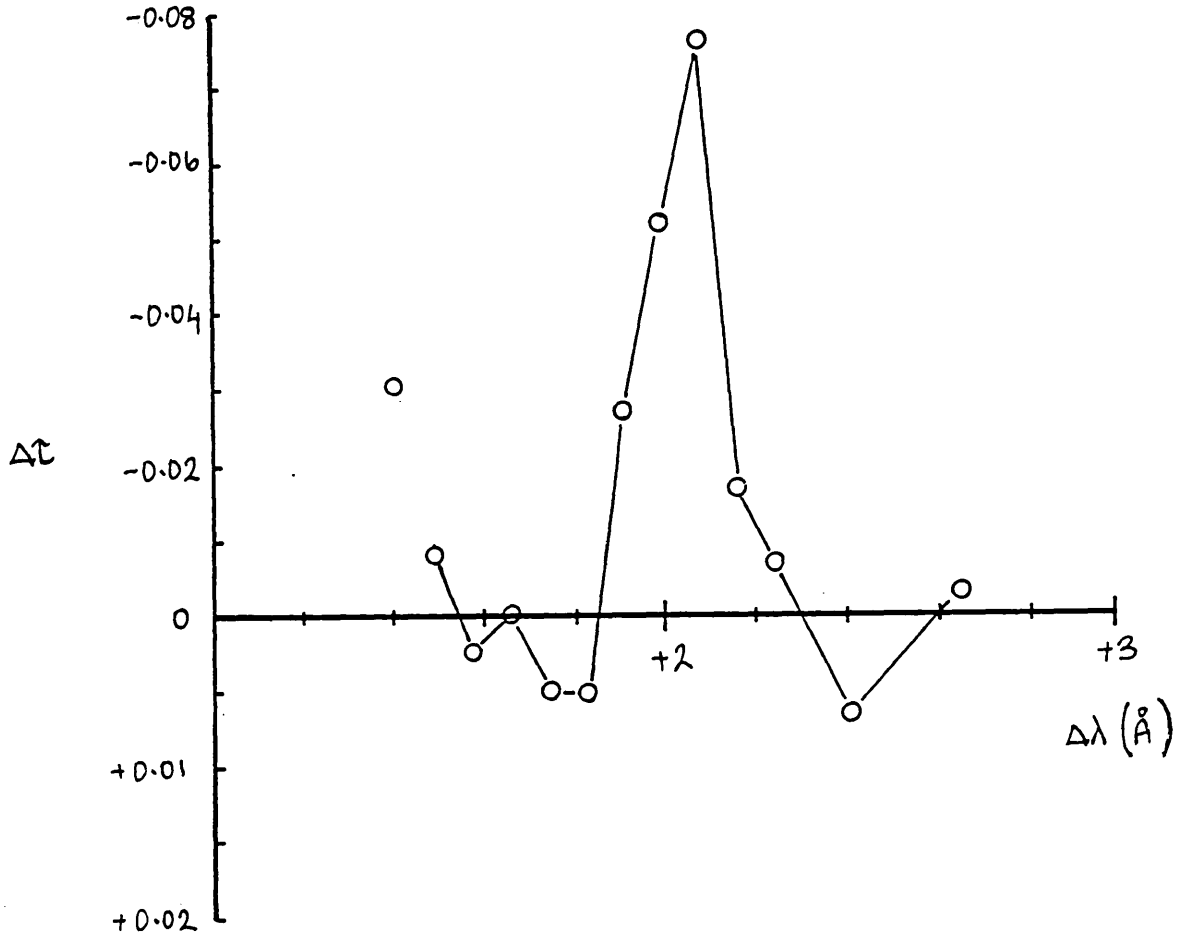

Fig. 5.7.

A $\Delta\tau$ plot of the feature on the red wing of H-Beta

The feature has a line width of about 0.2Å and a line centre opacity of about 4864.4Å.

The plot is inverted to make the line shape look the right way up.

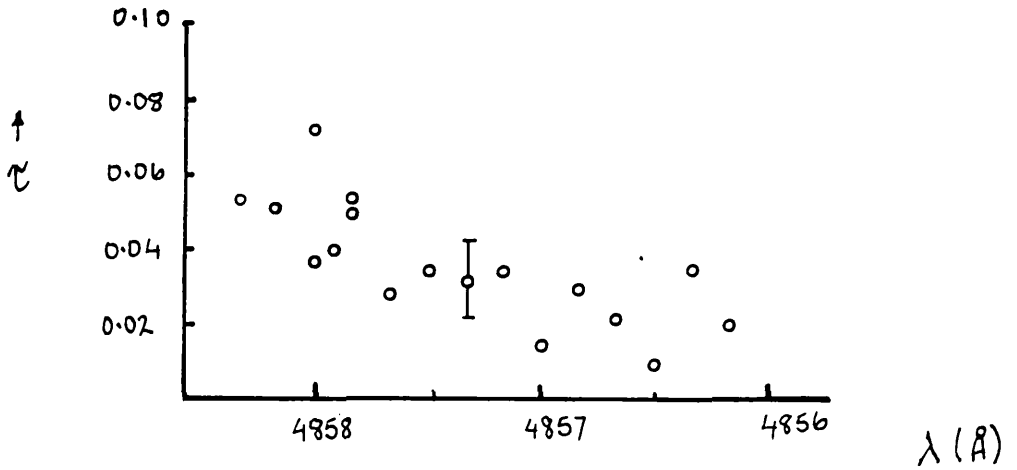

Fig. 5.8

Blue wing of H-Beta Ne = 5 x 10^{14} cm^{-3}.

An attempt to find an H_2 molecular feature at 4856.55Å.

When Ne = 5 x 10^{14}, Te = 0.81eV. The H_2 density can be estimated to be about 8.9 x $10^{10}cm^{-3}$. This again is well below the observed population of n=2 of 4.6 x $10^{11}cm^{-3}$. It is thus unlikely to be molecular Hydrogen forming the feature.

In conclusion then, the feature seen on the red wing of H-Beta, is definitely an impurity, though it cannot be identified with certainty.

5.5 THE POPULATION OF THE N = 2 LEVEL

The population of n=2 as a function of time in the afterglow phase plasma was found by measuring the linecentre optical depth of H-Beta for various times in the afterglow. The population of n=2 was derived, using the expression

$$N_2 = \frac{8\pi c \Delta\lambda g_2 \tau_c}{\lambda^4 A_{42} g_4 L} \qquad 5.4$$

Where τ_c is the line centre optical depth

$\Delta\lambda$ is the equivalent linewidth, such that

$$\Delta\lambda = \frac{1}{\tau_c}\int_\lambda \tau(\lambda)\, d\lambda$$

L is the length of the plasma (0.7m)

g_n is the statistical weight of level n

N_2 is the n=2 population density

Other symbols having their usual meaning.

Using the fact that for N = 10^{15}, $\Delta\lambda$ = 2 Angstroms and that $\Delta\lambda \propto Ne^{2/3}$ (Griem 1964), then

$$\Delta\lambda = 2 \times 10^{-10} Ne^{2/3} \text{ Å}$$

For this plasma, then

$$N_2 = 30\, Ne^{2/3} \tau_c$$

The results are given in Fig. 5.9.

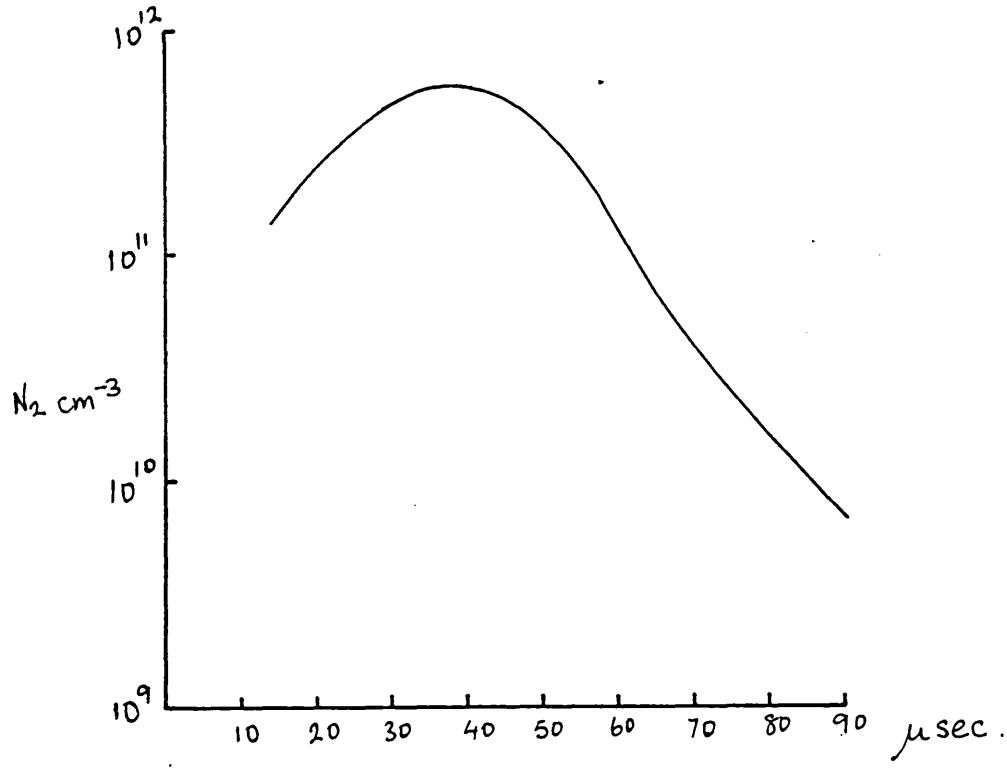

Fig. 5.9.

A plot of the population of N = 2 as a function of time into the afterglow.

obtained by absorption measurements on H-Beta.

5.6. THE LONG TERM CHANGE of the N=2 POPULATION

Fig. 5.10 shows an early H-Beta profile, taken to check the electron density as given by the H-Beta line width, against that given by laser interferometry. This profile was taken on November 30, 1982. The profile shown in Fig. 5.1 was taken on February 22, 1983. While the half width has not changed, (indicating no change in the electron density), the peak optical depth had reduced from τ_c = 1.65 for Fig. 5.10, to τ_c = 1.25 for Fig. 5.1. This indicates a drop in 25% in the number density of n=2 between the dates given above.

The change seemed to occur over a period of days at the beginning of February 1983, when the profile of the red wing of H-Beta for Ne = 5 x 10^{14}cm^{-3}taken. (Fig. 5.6) A few days later, a profile of the blue wing of H-Beta was taken for the same Ne, to see if there were any corresponding satellites to that found on the red wing. This data is shown in Fig. 5.11. Whilst no obvious satellites were observed, note the peak optical depth is 1.85 as against 2.05 for Fig. 5.6.

Checks were made on the gas pressure, charging voltage and general mechanical soundness of the pinch. The elctron density was also re-measured by laser interferometry. No change in any of these parameters could be discerned. Furthermore, no explanation of this anomaly has been forthcoming.

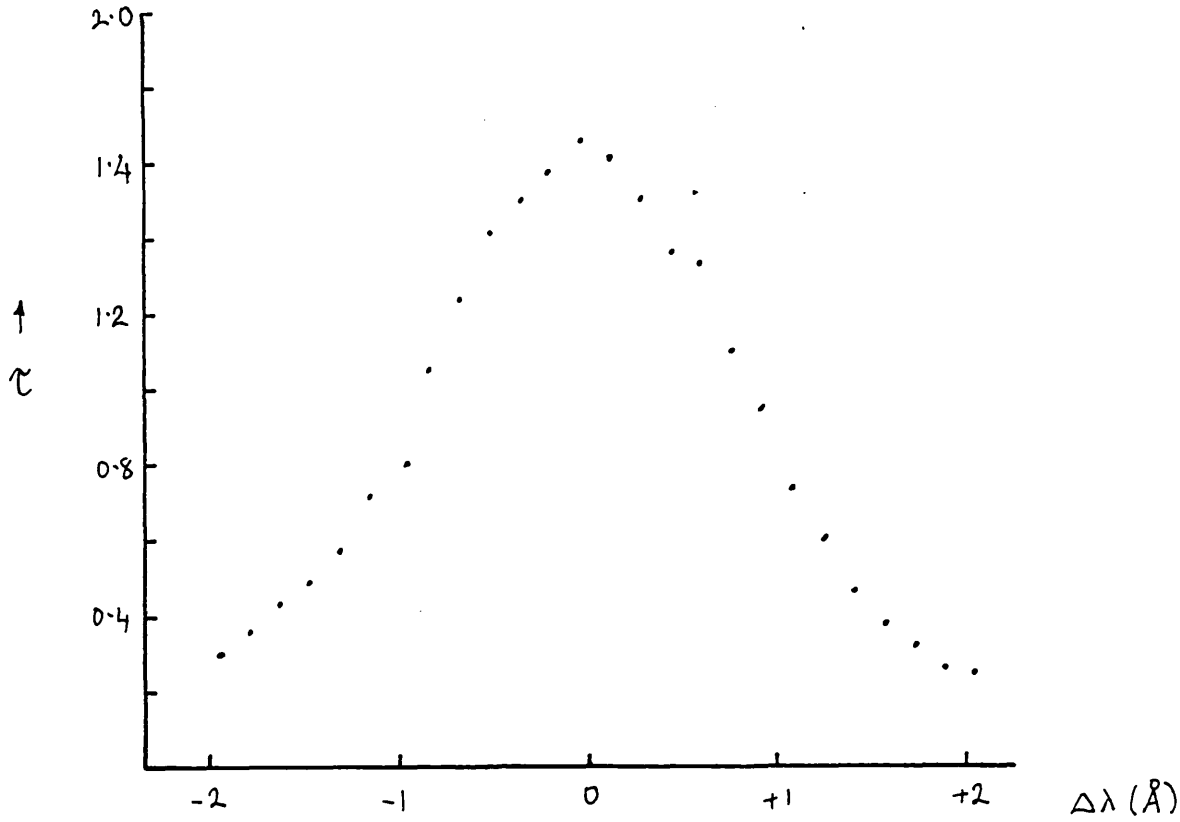

Fig. 5.10.

An early H-Beta profile for Ne = $10^{15}cm^{-3}$.

Note the peak optical depth of 1.65, compared to that of 1.25 for Fig. 5.1., which was taken at a later date.

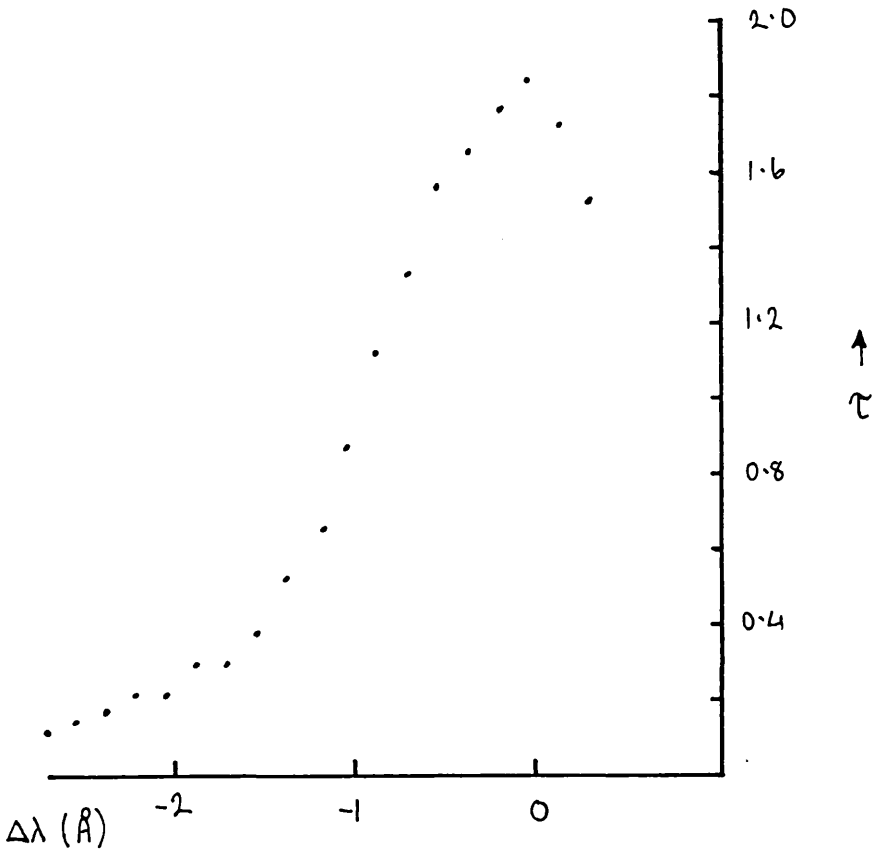

Fig. 5.11.

An absorption profile of the blue wing of H-Beta for Ne = 5 x 10^{14}cm^{-3}.

Note the peak optical depth is only 1.85 compared to 2.05 for Fig. 5.6.

REFERENCES

Burgess D.D.,Mahon R., J.Phys.B. 5, 1756, (1972)

Cairns C.J., Ph.D. Thesis. University of London. (1970)

Drawin H.W., 'Spectral Line Shapes'., p.527. Ed. B.Wende. Pub. W. de Gruyter. New York. (1981)

Fleurier C.,Couland G.,Ranson P., Phys.Rev.A. 21,861, (1980)

Mazure A.,Goldbach C.,Nollez G., (See Esrom H.,and Helbig V. p. 135, 'Spectral Line Shapes'., Ed. B.Wende. Pub. W.de Gruyter. (1981)

Piel A., 'Spectral Line Shapes', p.135. Ed. B.Wende. Pub. W.de Gruyter. (1981)

Ramette J.,Drawin H.W., Z. Naturforsch. 31, 401, (1976)

Spitzer L., 'Physics of Fully Ionized Gases' Pub. Interscience London. (1956).

APPENDIX I

A COLLISIONAL RADIATIVE MODEL for He II

Collisional Radiative Models are well described by Hess and Burrell (1979), so the basic principles of a C.R.M. will not be discussed here. Emphasis will instead be placed on listing the various rate formulae used for this particular model and justifying some of the approximations made. The matrix inversion method will also be described. The code was run on a microcomputer having 16K R.A.M.

ION POPULATIONS

It is necessary at the outset, to compute the densities of the He III ion stage, so that the rates from He III into the various levels of He II may be calculated. Assuming a time stationary system A rates matrix may be written for all the ion stages

$$\begin{pmatrix} -B_{11} & B_{12} & 0 \\ B_{21} & -B_{22} & B_{23} \\ 0 & B_{32} & -B_{33} \end{pmatrix} \begin{pmatrix} N_1 \\ N_2 \\ N_3 \end{pmatrix} = \begin{pmatrix} 0 \\ 0 \\ 0 \end{pmatrix} \qquad \text{A.1}$$

where B_{mn} is the rate coefficient from ion stage m to n and N_m is the population density of ion stage m. As it stands this matrix is overprescribed and a further constraint is needed to give sensible solutions. i.e.

$$N_e = N_1 + 2N_2 \qquad \text{A.2}$$

From A.1 and A.2 the solution for N_3 is

$$N_3 = \left(B_{32}/B_{33}\right)\left(N_e/\left(1 - 2\,B_{32}/B_{33}\right)\right) \qquad A.3$$

B_{32} is the total ionization coefficient from He II to He III and can be obtained from an expression for Hydrogenic ions due to Tucker (1975)

$$B_{32} = 10^{-10} T_e^{1/2} Z^{-4} \exp\left(-Z^2 I_H / KT\right) \quad cm^3 sec^{-1}$$

where $I_H = 13.6eV$ and $Z = 2$

B_{33} is the total recombination coefficient from He III to He II, which may be computed using an expression due to Burbridge et al (1963).

$$B_{33} = 2 \times 10^{-11} Z^2 T_e^{-1/2} \phi(\beta) \quad cm^3 sec^{-1} \qquad A.4$$

$$\text{where } \phi(\beta) = 0.5\left(1.735 + \ln\beta + 1/6\,\beta\right) \qquad A.5$$

$$\text{and } \beta = Z^2 I_H / KT_e$$

For temperatures less than 6eV, the He II ion stage is dominant i.e. $N_2 \gg N_3$, so that setting $N_2 \simeq Ne$ is a good approximation.

COLLISIONAL RATE COEFFICIENTS

For the collision rate between the levels of He II an expression for hydrogenic ions due to Bates, Kingston and McWhirter (1962) was used, which was derived from an expression for collision cross sections for Hydrogenic ions due to Seaton (1962)

$$C_{ij} = 4.75 \times 10^{-5} \frac{j^2 i^2}{j^2 - i^2} \frac{f(ji)}{Z^2 T_e^{1/2}} \exp\left\{\frac{-157890\, Z^2 (j^2 - i^2)}{j^2 i^2 T_e}\right\} \qquad A.6$$

$cm^3 sec^{-1}$

where i is the lower level and f(ij) is the absorption oscillator strength.

Collisional de-excitation rate coefficients may be obtained by invoking detailed balance on eqn A.6, so that

$$C_{ji} = C_{ij}\frac{i^2}{j^2}e^{h\nu/KT_e} = \frac{4.75\times10^{-5}j^4 f(ji)}{(j^2-i^2)z^2T_e^{1/2}} \quad A.7$$

cm^3sec^{-1}

COLLISIONAL IONIZATION

The collisional ionization rate coefficient formula used, was that due to Bates et al (1962) and is a modified form of eqn A.6

$$C_{ic} = \frac{1.4\times10^{-5}i^2}{z^2T_e^{1/2}}\exp\left\{\frac{157890z^2}{i^2T_e}\right\} cm^3sec^{-1} \quad A.8$$

RADIATIVE RECOMBINATION

The radiative recombination rate ceofficients, H_{ci}, were those due to Seaton (1959). Though the expression used is from Johnson (1972)

$$H_{ci} = 5.197\times10^{-14}\left(\frac{\beta}{i^2}\right)^{3/2}\exp\left(\frac{\beta}{i^2}\right)\sum_{n=0}^{2} g_n(i)\,E_{n+1}\left(\frac{\beta}{n^2}\right) cm^6sec^{-1} \quad A.9$$

where $n=0,1,2.$

En is an exponential integral

$$E_n(\beta) = \int_1^\infty e^{-\beta t}t^{-n}dt \quad A.10$$

From Abromowitz and Stegun (1964)

$E_{n+1}(\beta)$ is related to $E_n(\beta)$ for $n \geq 1$ by

$$E_{n+1}(\beta) = \frac{1}{n}\left[e^{-\beta} - \beta E_n(\beta)\right] \qquad A\cdot11$$

The gaunt factors $g_n(i)$ are given by Johnson (1972)

	i=1	i=2	$i \geq 3$
$g_0(i)$	1.1330	1.0785	$0.9935+0.2328i^{-1}-0.1296i^{-2}$
$g_1(i)$	-0.4059	-0.2319	$-i^{-1}(0.6282-0.5598i^{-1}+0.5299i^{-2})$
$g_2(i)$	0.07014	0.02947	$i^{-2}(0.3887-1.181i^{-1}+1.470i^{-2})$

THREE BODY RECOMBINATION

This was obtained by applying detailed balance to the ionization coefficient, C_{ic} . The three body recombination coefficient is then C_{ci} where

$$C_{ci} = \frac{g_i}{g_e g_+} e^{-I_i/KT_e} C_{ic} \quad cm^3\,sec^{-1} \qquad A\cdot12$$

where Ii is the ionization energy out of level i.

The partition function for the electron is

$$g_e = \frac{2}{N_e}\left(\frac{h^2}{2\pi m_e KT_e}\right)^{-3/2} \qquad A\cdot13$$

See Mihalas (1978)

For the He III ion $g_i = 1$ so then

$$C_{ci} = \frac{Ne}{2}\left(\frac{h^2}{2\pi m_e KT}\right)^{3/2} g_i \, e^{I_i/KT_e} C_{ic} \quad cm^3 \, sec^{-1} \qquad A\cdot14$$

$$= \frac{2.87 \times 10^{-27} \, i^4 \, Ne}{z^2 T_e^2} \quad cm^3 \, sec^{-1} \qquad A\cdot15$$

RADIATIVE RATES

The absorption oscillator strength f(ij), for Hydrogenic ions was calculated using an expression due to Kramers (1923)

$$f(i,j) = \frac{32}{3\sqrt{3}\pi} \frac{i^3 j}{(j^2 - i^2)^3} \, g(j,i) \qquad A\cdot16$$

where g(j,i) is a gaunt factor of order unity. Johnson (1972) gives an expression for the gaunt factor which then makes f(i,j) correct to 0.5%.

$$g(i,j) = g_0(i) + g_1(i) j^{-1} + g_2(i) j^{-2} \qquad A\cdot17$$

g_0, g, and g_2 are tabulated for the expression for radiative recombination. The relationship between the B value and the absorption strength is

$$\frac{\pi e^2}{m_e} f(i,j) = B_{ij} \, h\nu$$

Using the Balmer equation

$$h\nu = z^2 I_H \left(\frac{1}{i^2} - \frac{1}{j^2}\right) \qquad A\cdot19$$

and relating the A value to the B value

$$A_{ji} = \frac{g_i \, 8\pi h\nu^3 \, B_{ij}}{g_j \, c^3} \qquad A\cdot20$$

then finally

$$A_{ji} = 8\times10^{9} z^{4}\left[\frac{1}{i^2}-\frac{1}{j^2}\right]^{2}\frac{i^2}{j^2}\times\frac{32}{3\sqrt{3}\pi}\frac{i^3 j}{(j^2-i^2)^3}\,g(i,j) \qquad A\cdot22$$

using these expressions for the A value and the oscillator strength, all the collisional, radiative and laser rates can be computed

MATRIX INVERSION PROCEDURE

When inverting large order matrices, the conventional Cramers-rule procedure is very inefficient and time consuming. Forsythe (1953) points out that inverting a matrix of order n would require about (n+1)! multiplications. So for a matrix of order 26 this would require about 10^{28} multiplications.

In consequence there has been a large body of literature devoted to the invention of more efficient techniques. For the most efficient techniques, Forsythe says, only about $n^3/3$ multiplications are required; say about 6000 for a matrix of order 26. Forsythe gives a number of ways in which matrices may be inverted rapidly. However, a method due to Choleski (Fox et al, 1948), was finally chosen for its simplicity, accuracy and speed.

This method is only suitable for symmetric matrices and so the matrix is first symmetrized, by multi-

plying by its own transpose.

Let $\underline{W}$ be the matrix to be inverted, then let $\underline{W}\,\underline{\tilde{W}} = \underline{M}$, a symmetric matrix. The matrix $\underline{M}$ is then expressed in the form of two triangular matrices; $\underline{L}$, a lower triangular matrix and $\underline{\tilde{L}}$, its transpose and an upper triangular matrix.

So now $\underline{M} = \underline{L}\,\underline{\tilde{L}}$

This is inverted, so that

$$(\underline{M})^{-1} = (\underline{\tilde{L}})^{-1}(\underline{L})^{-1} \qquad A\cdot23$$

$\underline{L}$ and $\underline{\tilde{L}}$ are easily found by back substitution. Then $(\underline{\tilde{L}})^{-1}$ or $(\underline{L})^{-1}$ can be obtained by noting that $(\underline{\tilde{L}})(\underline{\tilde{L}})^{-1} = \underline{I}$, a unitary matrix. $(L)^{-1}$ is simply the transpose of $(\underline{\tilde{L}})^{-1}$; so enabling $(\underline{M})^{-1}$ to be determined.

The inverted matrix $(\underline{W})^{-1}$ may be retrieved by noting that

$$(\underline{W})^{-1} = (\underline{M})^{-1}\,\underline{\tilde{W}} \qquad A\cdot24$$

ACCURACY of MODEL

The model was run to compute the population densities of the first 9 excited states. It was assumed that the system was time stationary and in equilibrium. A further constraint was put upon the model. Which was, that the He II ground state population was equal to the measured electron density. This was justified by two arguments

1. For temperatures Te $\lesssim$ 6eV, the He II population should be much greater than the He III population.

See Tucker (1975).

2. The first excited state is more than 40eV above the ground state, so the excited state populations should be small compared to the ground state for any temperature expected in the plasma.

There being no real way of testing that the code was actually working correctly (i.e. producing the correct numbers) all the collisional ionization and recombination coefficients were replaced by those for neutral Hydrogen, due to Vriens and Smeets (1980). The predicted populations for a given Ne and Te were in close agreement with C.R.M. developed by Gohil (1982) for neutral hydrogen. This showed the code to be working correctly, in principle.

Bates et al (1962), state that their collision rate coefficients agreed, within a factor of 2, with the rate coefficients derived from cross section for He II 1S - 2P, due to Burgess (1961). However, the close coupling calculation of Burke et al(1964) should be superior to the Born approximationcalculation of Burgess, especially near threshold.

As an independent check, the cross sections of Burke et al were fitted to a curve of form of the Born approximation at high energies

$$\sigma = \frac{A}{v^2} \ln Bv \qquad A.25$$

Where v is the electron velocity.
This gave a fit to within 10% for the range of energies given by Burke et al, when $A = 3.67 \times 10^{-8}$ and $B = 3.72 \times 10^{-7}$. See Fig. A.1.

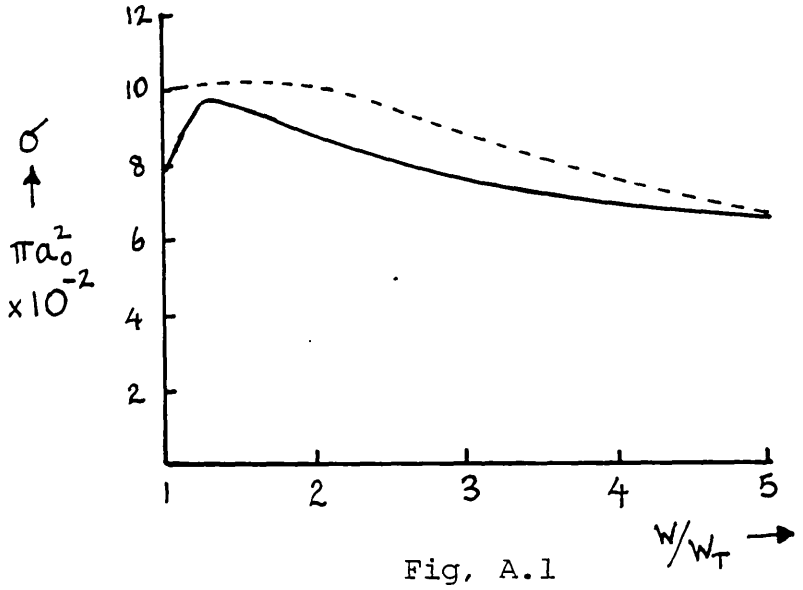

Fig, A.1

CROSS SECTIONS for He II, 1S - 2P.

The continuous line shows the theoretical cross section of Burke et al (1964).

The dotted line is a fit of the form of the Born approximation at high energy. (See text).

W is the energy of the colliding electron,

W_T is the threshold energy.

The fitted curve was made to go through the points

σ = 0.1 at W/W_T = 1

σ = 0.0635 at W/W_T = 5

Eqn A.25 was then converted into a rate coefficient using the formula

$$C_{12} = \int_{v_T}^{\infty} \sigma(v)\, P(v)\, v\, dv \qquad m^3 sec^{-1} \qquad A.26$$

Where v is the electron velocity and v_T is the cut off velocity at threshold.

The Maxwellian electron-velocity distribution is

$$P(v)dv = 4\pi \left(\frac{m_e}{2\pi K T_e}\right)^{3/2} v^2 e^{-m_e v^2/2KT_e} dv$$

$$= 1.35 \times 10^{-11} \frac{v^2}{T^{1.5}} \exp\left(-3.3 \times 10^{-8} \times v^2/T_e\right) \qquad A.27$$

Therefore

$$C_{12} = 4.96 \times 10^{-19} \int_{v_T}^{\infty} \frac{v}{T^{1.5}} \times \ln\left(3.72 \times 10^{-7} \times v\right) \times e^{-3.3 \times 10^{-8} v/T_e} \qquad A.28$$

$$\text{where} \quad v_T = 3.8 \times 10^6 \ m\, sec^{-1}$$

This expression was integrated numerically, where the upper limit of velocity was set at $100V_T$ and the results were compared with those obtained, using eqn A.6. The results are tabulated below for a range of temperatures.

C_{12} (eqn. A·28)	C_{12} (eqn. A·6)	Temperatures
$m^2 sec^{-1}$	$m^2 sec^{-1}$	Kelvin
9.9×10^{-18}	1.28×10^{-17}	6×10^4
2.65×10^{-18}	2.88×10^{-18}	5×10^4
3.42×10^{-19}	$3. \times 10^{-19}$	4×10^4
9.9×10^{-21}	6.73×10^{-21}	3×10^4
6.5×10^{-24}	3.07×10^{-24}	2×10^4
3.55×10^{-27}	1.32×10^{-27}	1.5×10^4

The two equations would appear to be in good agreement for a temperature of 5×10^4. For higher temperatures, the equation of Bates et al, eqn A·6 gives progressively higher rates and the reverse is true for temperatures below 5×10^4. However, the rate coefficient C_{12} would appear to be trustworthy to within a factor of two, as stated by Bates et al.

REFERENCES

Abramowitz M.,Stegun I.A., 'Hand book of Mathematical Functions' N.B.S.: Washington. (1964)

Bates D.R.,Kingston.A.E.,McWhirter R.W.P. Proc.Roy.Soc. 267, 297,(1962).

Burbridge G.,Gould.R.,Pottasch S., Ap.J. 138, 945, (1963)

Burgess A., Mem.Soc.Roy.Sci. Liege. 4, 299.(1961)

Burke P.G.,McVicar D.D.,Smith K. Proc.Phys.Soc. 83, 397, (1964).

Cox D., Tucker W., Ap.J. 157, 1157, (1969).

Forsythe G.E., B. of A.M.S. 59, 299, (1953).

Fox L.,Muskey H.D.,Wilkinson J.W.,Q.J.M.A.P., 1, 149, (1948)

Gohil P., Ph.D. Thesis., Univ. of London. (1982)

Hess R.,Burrell F., J.Q.S.R.T. 21, 23, (1979).

Irons F.E., M.N.R.A.S., 182, 705, (1978)

Johnson L.C., Ap.J. 174, 227, (1972)

Kramers H., Phil.Mag. 46, 836, (1923).

Mihalas D., 'Stellar Atmospheres' p.112. Pub.Freeman: San Francisco. (1978)

Seaton M.J., M.N.R.A.S. 119, 81. (1959)

Seaton M.J., 'Atomic and Molecular Processes'.
Ed. D.Bates. New York. Academic. (1962)

Tucker W., 'Radiation Processes in Astrophysics', p.290,
Pub. MIT Press; Cambridge, Mass. (1975).

Vriens L.,Smeets H.M., Phys.Rev.A. 22, 940, (1980).

THIS THESIS IS DEDICATED TO THOSE WHO FOLLOW ON....